INHIBITORY CIRCUITS GENERATE DISTINCT SPATIOTEMPORAL RECEPTIVE FIELD PROPERTIES IN RETINAL NEURONS

Benjamin L. Murphy-Baum

A DISSERTATION

Presented to the Neuroscience Graduate Program

Vollum Institute

Oregon Health and Science University

School of Medicine

In Partial Fulfillment

of the Requirements for the Degree of

Doctor of Philosophy

February 2017

School of Medicine
Oregon Health & Science University

_____

CERTIFICATE OF APPROVAL

_____

This is certify that the Ph.D. dissertation of

Benjamin L. Murphy-Baum

has been approved

_____
William Rowland Taylor, Ph.D., Advisor

_____
Craig Jahr, Ph.D., Chair

_____
Henrique von Gersdorff, Ph.D.

_____
Laurence Trussell, Ph.D.

_____
Stephen David, Ph.D.

_____
Eric Schnell, Ph.D.

DATE: _____

Table of Contents

LIST OF ABBREVIATIONS

AMPA	α-amino-3-hydroxy-5-methyl- 4-isoxazolepropionic acid
ChAT	choline acetyltransferase
CRT	cathode ray tube
D-AP5	D-(-)-2-amino-5-phosphonopentanoic acid
DIC	differential interference contrast
DS	direction selective
DSGC	direction selective ganglion cell
E_{Cl}	chloride reversal potential
EGTA	ethylene glycol tetraacetic acid
EPSC	excitatory postsynaptic current
GABA	gamma-aminobutyric acid
GABAR	GABA receptor
GCL	ganglion cell layer
GlyR	Glycine receptor
GYKI	(1-(4-aminophenyl)-3-methylcarbamyl-4-methyl-3,4-dihydro-7,8-methylenedioxy-5H-2,3-benzodiazepine hydrochloride
HEPES	4-(2-hydroxyethyl)-1-piperazineethanesulfonic acid
I-V	current-voltage
IPL	inner plexiform layer
IPSC	inhibitory postsynaptic current
L-AP4	L-2-amino-4-phosphonobutyric acid
MFA	meclofenamic acid
Na_V	voltage-gated sodium channel
NHS	normal horse serum
NMDA	N-Methyl-D-aspartic acid
OMS	object motion sensitive
OS	orientation selective
OSGC	orientation selective ganglion cell
PAC	polyaxonal amacrine cell
PBS	phosphate buffered saline
PSTH	peristimulus time histogram
RF	receptive field
RGC	retinal ganglion cell
SR-95531	(6-imino-3-(4-methoxyphenyl)-1(6H)-pyridazinebutanoic acid hydrobromide
SSI	spatial selectivity index
t-OFF α	transient OFF alpha
T/S/T	TPMPA/SR/TTX
TPMPA	(1,2,5,6-tetrahydrophyridin-4-yl)methylphosphonic acid
TTX	tetrodotoxin citrate
WFAC	wide-field amacrine cell

LIST OF FIGURES

ACKNOWLEDGEMENTS

I would like to acknowledge and thank the past and present members of the Taylor and Puthussery labs for their constant support, advice, and friendship. In particular, I thank Ilya Buldyrev and Somya Venkataramani, who gladly donated their time, experimental space, and advice towards my initial development as a vision scientist. Collectively, the lab has created an environment where I really look forward to coming to work on Monday morning. This stems directly from the easy going and supportive attitudes of my mentor, Dr. W. Rowland Taylor, as well as Dr. Teresa Puthussery; they've accepted my very frequent weekend rock climbing trips with open arms and only mild skepticism of its impact on my productivity.

Rowland possesses many qualities that I hope to emulate as a scientist. He has given me the freedom to cultivate projects from my own ideas and interests, but has always provided a helping hand and constructive criticism when I needed it. Over the last few years, I've come to know that he (and the rest of the lab) has a very collaborative attitude towards science. I'm grateful that I was exposed to such a progressive lab environment during graduate school, which has only made me more excited about doing research in the future and developing relationships with other labs.

I also thank my dissertation committee, Dr. Craig Jahr, Dr. Henrique von Gersdorff, Dr. Stephen David, Dr. Larry Trussell, and Dr. Eric Schnell for their guidance and advice during the course of my research. I also thank the neuroscience program administrator, Liz Lawson-Weber, and program director, Gary Westbrook, for their constant support. Finally I thank our funding from the NIH: EY014888, T32 EY023211, P30 EY010572, P30 NS061800, and the unrestricted departmental funding from Research to Prevent Blindness (New York, NY).

ABSTRACT

The retina is tasked with detecting light from the environment, and transmitting that visual information as an electrical signal to the brain. Visual signals are highly variable, making it difficult or impossible for retinal neurons of a single type to fully represent all of the salient visual features. Instead, the retina splits the visual input into many parallel channels, represented by the 30 or more ganglion cell types that signal to the brain. Each ganglion cell type, or channel, encodes a slightly different feature of the visual scene, such as high or low spatiotemporal frequencies, positive or negative contrast, direction of motion, and edge orientation, among others. Many of these feature selectivities are driven by the activity of complex inhibitory networks. Understanding the computations being made by different ganglion cells requires understanding how these inhibitory circuits are arranged, how light activates them, and how they influence the electrical signals being transmitted to ganglion cells. This dissertation presents experiments designed to address these questions in an inhibitory neuron that reports edge orientation, and in a ganglion cell that preferentially responds to fast image motion. The results are an important demonstration of how seemingly small details about a neuron's presynaptic circuit are critical for shaping its emergent function and feature selectivity.

CHAPTER 1

INTRODUCTION

Why the retina?

One of the goals for neuroscientists is to understand how individual neurons interact to generate an emergent property of a larger circuit. Given an input, what is the computation being made to produce the output that we observe? This is a difficult question to address in the brain; its vast interconnectivity precludes a clear definition of a circuit's input and output. The retina provides relief from this ambiguity because it is isolated from the rest of the brain, and thus the inputs and outputs are clearly defined.

On the input end, photons from the environment are detected by photoreceptors and transduced into an electrical signal that can be measured by an experimenter. The use of light to drive circuit activity affords several experimental advantages. First, light is the retina's natural stimulus. As such, the conclusions that can be drawn from physiological experiments in the retina closely reflect the circuit's function *in vivo*. This comes in contrast to experiments using stimulating electrodes or optogenetics to activate specific circuits in the brain, because there is uncertainty as to whether the circuit experiences a similar stimulus under natural conditions. Second is the researcher’s ability to manipulate the light used to stimulate retinal circuits. As will be discussed later, different cell types in the retina have differing sensitivities to specific visual features, such as spatiotemporal frequency, color, contrast, luminance, orientation, and motion. These sensitivity differences can be taken advantage of by designing the visual stimulus to have certain attributes, so as to suppress or activate specific classes of neurons within the circuit in

question. There is no other mammalian neural system where this level of control is currently possible. Thus, the retina lends itself to addressing very specific questions about the function of both individual neurons and their larger circuits.

The output of the retina is formed by trains of action potentials fired by retinal ganglion cells, which are sent to higher brain regions. Because all of the information about the visual input is contained in the action potentials fired by ganglion cells, researchers can garner a lot of information about how visual processing is carried out in the retina.

The retina can also be maintained as a whole piece of neural tissue. This is not the case for most preparations of brain tissue, which must be cut into slices to gain comparable experimental access. Slicing the tissue destroys a huge amount of circuitry that is likely important for the functionality of the neuron in question. This can be avoided in the retina, which can be isolated intact, allowing researchers to discuss results in the context of a circuit's function *in vivo*.

Finally, unlike brain tissue, the retina is transparent, as it must be for light to reach the photoreceptor layer. A transparent preparation is ideal for imaging neurons and their activity, because optical slices can be taken throughout the retinal volume. The use of 2-photon imaging in live retinal tissue has become a critical tool for vision researchers, as 2-photon activation of fluorescent dyes largely avoids photoreceptor activation. Thus, calcium or voltage indicators can be imaged in neurons simultaneously with their stimulation by visible light. These attributes make the retina an ideal preparation for studying the function of neural circuits.

Using rabbits for retina research

A host of model organisms have been used for retina research over the last century. Some of the first recordings were carried out in eel and horseshoe crab, followed by cat, rabbit, and more

recently primate and mouse, among others. Today, most labs use mice, since so many more genetic tools are available in mice compared to other species. However, much vision research is driven by its relevance to humans, which have a different retinal and cortical organization compared to mice. For example, the dense area of cone photoreceptors—the fovea, which allows for high spatial acuity vision in primates—is absent in mice. Other species, such as rabbits, are more similar to primates because they have a visual streak: a horizontally extended area of high photoreceptor and ganglion cell density that resembles the primate fovea.

Despite the experimental advantages afforded by genetic engineering in mice, the rabbit offers a superior preparation if genetic tools are not strictly necessary. Many of the reasons for this are technical and anecdotal, such as the ease of dissection given the larger size of a rabbit's retina, the fact that the vitreous humor isn't as resistant to a clean removal compared to the mouse, the retina recovers better from physical or hypoxic trauma, and the preparation usually lasts at least 8-9 hours before its health starts to deteriorate. Moreover, unlike the mouse, rabbit retinas are largely avascular, resulting in less light scattering, greater transparency, and thus superior optics. In a good rabbit retina preparation, the dendrites of individual ganglion cells can be traced through the retina's deeper layers. In Chapter 4, for example, I use this technique to help identify a specific type of ganglion cell by tracing its thick dendrites, which stratify in a particular layer of the retina, back to its cell body (soma). Finally, and perhaps most importantly, specific functional types of ganglion cells in the rabbit retina are more easily distinguishable than in the mouse, since there is a greater variety of soma sizes and shapes in the rabbit. For example, ON-OFF direction selective ganglion cells can be readily identified in the rabbit as having a medium-sized soma (15-20 μm diameter) that is not quite round, and a nucleus that is offset to one side

and crescent-shaped. In Chapter 3, the amacrine cell I study was reliably identified by having a small soma (10-15 μm diameter, major axis) that is elongated parallel to the visual streak without a visible nucleus. The relative ease in identifying different cell types in the rabbit is an important advantage, since any given ganglion or amacrine cell type will only make up 3-5% of the total population. Mouse ganglion cell somas are more homogenous and thus can't be identified nearly as easily without the expression of fluorescent proteins in specific cell types.

Fundamentals of Retinal Circuits

Although there is a lot that we don't know about how specific retinal circuits are arranged, the common organizing principles are well-established. Light is first detected by the outer segments of rod and cone photoreceptors. Photoreceptor outer segments express high levels of opsin proteins, each of which contains a single molecule of retinal bound within its structure. Incident photons trigger the photoisomerization of 11-cis-retinal to all-trans retinal, which causes a conformational change in the opsin protein. Since opsins are G protein-coupled receptors, this conformational change triggers the release of the G_α subunit from the G protein, leading to the closure of cation channels and a hyperpolarization of the photoreceptor neuron. Similarly, if the number of incident photons decreases, the photoreceptor will become relatively depolarized. This process underlies the transduction of a visual signal into an electrical signal in photoreceptors.

Photoreceptors increase or decrease the amount of glutamate being released in response to depolarizations or hyperpolarizations in their membrane potential, respectively. These changes in glutamate release are detected by two classes of postsynaptic neurons: horizontal cells and bipolar cells. Horizontal cells are inhibitory neurons that provide negative feedback to the photoreceptor. Bipolar cells, on the other hand, are excitatory neurons, and continue propagating

signals from photoreceptors through the retina. They are called bipolar cells because they comprise two major classes: ON and OFF. ON bipolar cells depolarize in response to decreases in glutamate release from photoreceptors, while OFF bipolar cells depolarize in response to increases in glutamate release. Thus, ON bipolar cells depolarize when light intensity increases (becomes brighter), whereas OFF bipolar cells depolarize when light intensity decreases (becomes darker). This split in the visual signal is the first step in establishing the retina's numerous parallel signaling pathways.

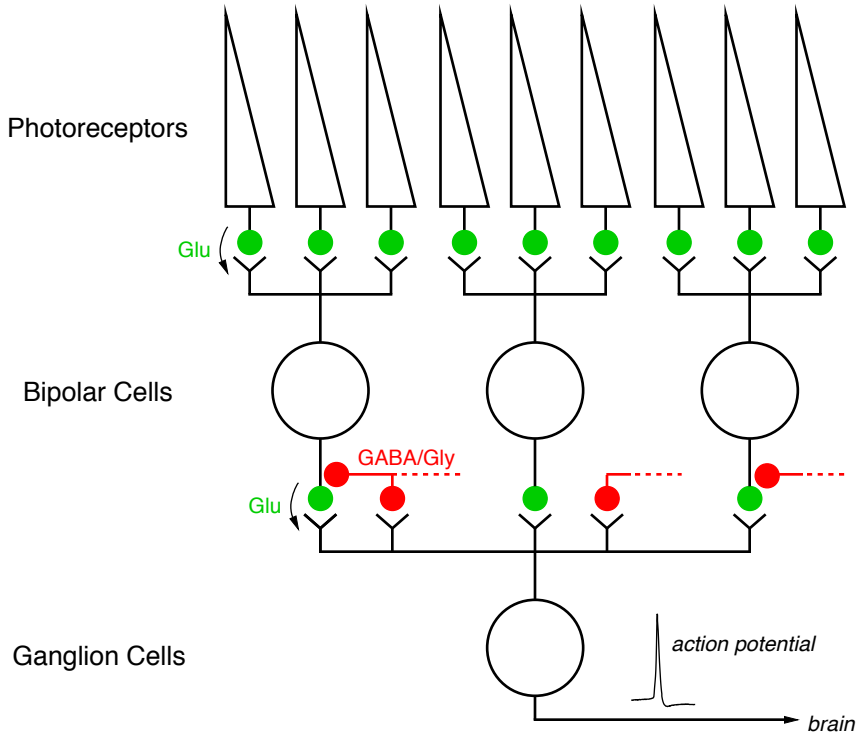

FIGURE 1.1. GENERAL LAYOUT OF RETINAL CIRCUITS

Light is transduced into an electrical signal in photoreceptors, which relay that signal to bipolar cells, and finally to ganglion cells via changes in glutamate (Glu) release. In the rabbit retina, ganglion cells pool inputs from many bipolar cells, which pool inputs from many photoreceptors. Using the neurotransmitters GABA or glycine (Gly), amacrine cells can inhibit the retinal circuit at various synaptic locations (bipolar cell axon terminals and ganglion cell dendrites). Amacrine cells can also inhibit other amacrine cells (not shown). Amacrine cell somas and presynaptic circuits are not shown. For clarity, horizontal cell circuits are not shown.

As in photoreceptors, changes in bipolar cell membrane potential are coupled to changes in glutamate release that are detected by two major classes of neurons: ganglion cells and amacrine cells. Ganglion cells are the output neurons of the retina, and send excitatory signals to different areas of the brain, such as the lateral geniculate nucleus and superior colliculus. Amacrine cells are inhibitory neurons that only signal within the retina, and release either GABA or glycine (known exceptions include dopaminergic amacrine cells, which release dopamine, starburst amacrine cells, which release GABA and acetylcholine, and vGlut3 amacrine cells, which release glutamate and glycine). Ganglion cells, bipolar cells, and other amacrine cells can all be subject to this inhibition, which modulates their activity (Figure 1.1). However, not all bipolar cells and ganglion cells receive the same pattern of inhibitory input from amacrine cells, and thus they respond to light in different ways. Indeed, differential inhibition is critical for establishing parallel signaling pathways in the retina, and is one of the main research topics addressed in this dissertation.

The general theme of my work is to determine how inhibitory circuits shape the light response of retinal neurons. The two major projects presented here identify the inhibitory circuits that shape the light response of a particular type of amacrine cell (Chapter 3) and ganglion cell (Chapter 4), and allow them to detect specific features of the visual input. The feature specificity of a given cell type is defined by the cell's receptive field properties.

Receptive fields in sensory systems

In humans, our nervous systems' interaction with the physical world is defined by our five major senses. Although each sense requires a different mechanism for detection, the underlying neural circuits that handle the incoming sensory information have common organizing principles. First,

each must transduce a physical signal (sound, light, pressure, odorants, or chemicals) into an electrical signal. Second, each system can be reduced down to small fundamental units that encode that signal. These units are typically localized to individual groups of neurons or even single neurons that relay sensory input to the brain or spinal cord, such as the hair cells of the cochlea, ganglion cells of the retina, corpuscles of the skin, glomeruli of the olfactory bulb, and taste buds of the tongue.

Using our sense of touch as an example, an individual corpuscle detects deformations in the skin in its immediate vicinity. This area of sensitivity is referred to as the neuron's receptive field. However, the receptive fields of mechanosensitive neurons are defined by more than just their spatial extent. For instance, some corpuscles only signal to the brain in response to vibrations in the skin, as would occur when rubbing your hand across a textured surface. Meissner's corpuscles are particularly sensitive to vibrations with temporal frequencies up to 40 Hz, whereas Pacinian corpuscles are tuned to respond to much higher frequency vibrations (Roudaut et al., 2012). Thus, in addition to having a spatial receptive field, these mechanosensitive neurons also have a temporal receptive field in the frequency domain. Other mechanosensitive neurons can be subdivided by their sensitivity to temperature or the intensity of skin deformations, providing further dimensionality to each neuron's 'receptive field'. Hair cells in the auditory system also have temporal receptive fields, which are defined by the range of vibrational frequencies that a given cell can detect. Neurons mediating taste and smell, on the other hand, have receptive fields defined by different chemical and odorant compositions (Tomchik et al., 2007; Galizia et al., 2010).

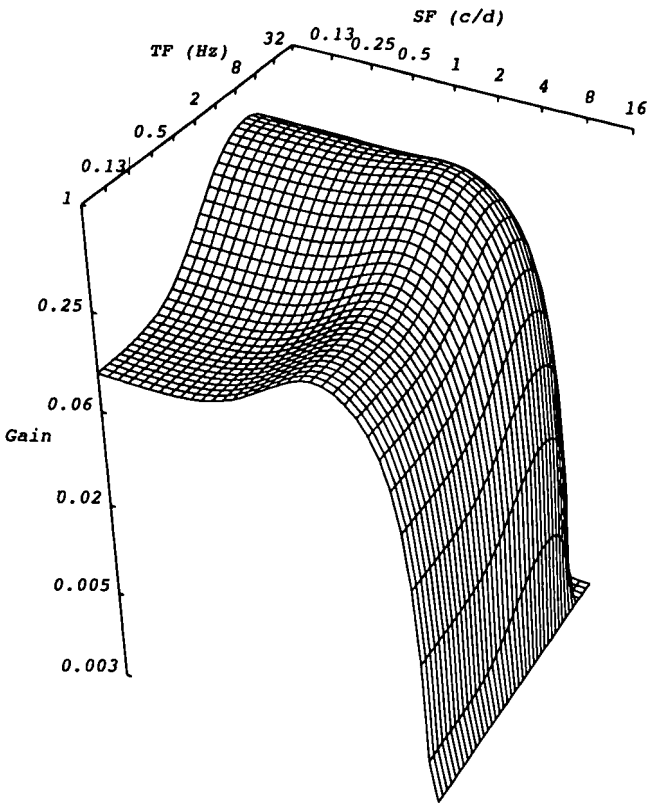

FIGURE 1.2. ADAPTED FROM FIGURE 13 OF BENARDETE AND KAPLAN (1997). THE SPATIOTEMPORAL RECEPTIVE FIELD OF A MIDGET GANGLION CELL IN THE PRIMATE RETINA.

Gain of the ganglion cell's response as a function of the temporal frequency (TF) and spatial frequency (SF) of the visual stimulus; c/d (cycles/degree).

As in these other systems, the visual system contains neurons that are functionally defined by the characteristics of their receptive fields. Analogous to our sense of touch, spatial receptive fields in the retina represent the area of visual space that can influence a given retinal neuron's activity. Similarly, the temporal receptive field is the range of temporal frequencies that can influence a retinal neuron's activity. For example, if a textured surface is moving across the visual field slowly, it has a lower temporal frequency, whereas if the same texture moves quickly, it has a higher temporal frequency. Since most retinal neurons respond to motion, a neuron's temporal receptive field is a large determinant of its response. The work in Chapter 4 is dedicated

towards understanding how temporal receptive fields are formed in retinal ganglion cells. Chapter 3 focuses on the spatial receptive field of specific type of amacrine cell.

Receptive fields can be defined as much by their spatial and temporal sensitivity as by their preferred color, contrast, orientation, and direction of motion. A retinal neuron's net response is thus a convolution of the visual stimulus by each receptive field. Figure 1.2, adapted from Benardete and Kaplan (1997), is a graphical representation of a ganglion cell's temporal and spatial receptive fields. From this plot, one general observation is immediately apparent: this neuron ignores visual inputs with low temporal frequencies (TF) and low spatial frequencies (SF), but responds vigorously at intermediate SF and TF. What circuitry is responsible for generating this stimulus selectivity? Identifying the circuits that form the receptive fields of retinal neurons is an important step in understanding visual processing in the retina. These types of questions have driven the research that I've undertaken for the last several years.

Circuits that shape receptive field properties

The bipolar cell is the first neuron to divide visual signals into parallel pathways: ON type bipolar cells depolarize in response to positive contrast (increments in light intensity), whereas OFF bipolar cells depolarize in response to negative contrast (decrements in light intensity). These opposing responses are due to the expression of different types of glutamate receptors on bipolar cell dendrites. In OFF bipolar cells, the specific glutamate receptor subtypes that are expressed can also influence the kinetics of the voltage response (Nirenberg and Meister, 1997; Dong and Werblin, 1998; Lukasiewicz and Shields, 1998; Flores-Herr et al., 2001; Eggers et al., 2007). In the ground squirrel, the expression of AMPA or kainate receptors on bipolar cell dendrites causes bipolar cells to have a more transient or sustained voltage response, respectively

(de Vries, 2000). In primate, kainate receptors dominate in all OFF bipolar cell types. However, the expression of different kainate receptor subtypes and auxiliary proteins diversifies their temporal properties (Puthussery et al., 2014). These studies hypothesized that dendritic glutamate receptors could affect the response kinetics of downstream ganglion cells, and thus shape their temporal receptive fields.

Recent work has shown that some bipolar cells express voltage-gated sodium channels (Pan and Hu, 2000; Zenisek et al., 2001; Ichinose et al., 2005; Ma et al., 2005; Saszik and DeVries, 2012; Puthussery et al., 2013). Sodium channels have been found primarily in bipolar cells with transient light responses, suggesting that they play a role in shaping bipolar cell kinetics. In the primate retina, the sodium channel expressing bipolar cells make synapses with parasol ganglion cells (Puthussery et al., 2013). Parasol cells are thought to be critical for detecting motion in the visual scene (for review, see Dacey, 2004); selective sodium channel expression in their presynaptic bipolar cells may support this role. The work presented in Chapter 4 provides evidence that a ganglion cell type with similar receptive field properties and central projections to parasol cells—the transient OFF alpha ganglion cells—also have sodium channels expressed in their presynaptic bipolar cells, which encourages faster response kinetics (Crook et al., 2004).

Bipolar cells also receive inhibitory inputs from amacrine cells. Previous studies have confirmed that these inhibitory inputs can play myriad roles in shaping receptive field properties (Nirenberg and Meister, 1997; Dong and Werblin, 1998; Lukasiewicz and Shields, 1998; Flores-Herr et al., 2001; Eggers et al., 2007). One classic example is center-surround organization in the retina. In some of the earliest recordings from ganglion cells, researchers recognized that a ganglion cell's spatial receptive field comprises a central excitatory region and a surrounding

inhibitory region (Kuffler, 1953). As a result, many ganglion cells are more sensitive to visual inputs that are restricted to their center receptive field, since they avoid activating inhibitory inputs from the surrounding region. Visual inputs that are broader—encompassing more of the inhibitory surround region—result in a lesser response from the ganglion cell due to increased inhibition (Flores-Herr et al., 2001). This system increases the spatial resolution of ganglion cells, and makes them more effective at detecting fine detail and edges. Different ganglion cell types receive varying degrees of surround inhibition, which diversifies the type of spatial information that they encode.

Surround inhibition can also change the temporal properties of bipolar cells, which may influence the temporal properties of their downstream ganglion cells. In particular, GABAergic feedback inhibition can truncate the time course of the excitatory input to ganglion cells (Nirenberg and Meister, 1997; Dong and Werblin, 1998). Moreover, others have shown that stimulating the surround receptive field can speed up ganglion cell spiking responses, and shift their temporal tuning to higher frequencies in the visual input (Shapley and Victor, 1979a). In Chapter 4, I explore how this mechanism controls the temporal receptive field properties of a specific type of ganglion cell.

In addition to changing the spatial and temporal receptive field properties of ganglion cells, amacrine-mediated inhibition can shape complex receptive field properties such as direction and orientation selectivity. Direction selective ganglion cells (DSGCs) respond to light moving in one of the four cardinal directions, but evoke no response to motion in the opposite direction. Direction selectivity is due in part to direct GABAergic inhibition from starburst amacrine cells (for review, see Demb, 2007). Starburst cells are not strictly direction selective themselves;

instead, they only respond to centrifugal (soma to distal dendrites), rather than centripetal, motion (Euler et al., 2002). Among several other mechanisms, asymmetric dendritic wiring—where a DSGC receives inhibition from starburst dendrites that are all pointed in roughly the same direction—causes the DSGCs to receive strong inhibition for object motion in one direction but not the other (Brigmann et al., 2011).

Orientation selective ganglion cells (OSGCs) only respond to edges in a particular orientation, either vertically or horizontally. In the OFF pathway, both horizontal and vertical orientation selectivity is due to GABAergic inhibition of the presynaptic bipolar cells (Venkataramani and Taylor, 2010). In the ON pathway, both presynaptic and direct inhibitory inputs contribute. The dendritic arbors of ON OSGCs are also elongated, resulting in stronger excitation to the ganglion cell for stimuli in the preferred orientation (Venkataramani and Taylor, 2016). Similar mechanisms have been described for OSGCs in the mouse retina (Nath and Schwartz, 2016). One of the outstanding questions in these studies has been the identity of the orientation selective amacrine cell that drives orientation tuning in ganglion cells. In Chapter 3, I address this by identifying and mapping the presynaptic circuitry of an orientation selective amacrine cell that could possibly mediate this receptive field property in ganglion cells.

Although ganglion and amacrine cell types have different receptive field properties, many of them have common circuit elements that help regulate responses. One such input is from the AII amacrine cell, an ON-type glycinergic amacrine cell that is known to inhibit OFF bipolar cell terminals and OFF ganglion cell dendrites (Grünert and Wässle, 1996; Maple and Wu, 1998; Molnar and Werblin, 2007; Marc et al., 2014). Thus, the AII amacrine cell communicates between the ON and OFF visual pathways. This type of crossover inhibition can perform

multiple functions, such as linearizing voltage responses in OFF bipolar cells, linearizing how neurons integrate signals of opposite contrast, reversing the sign of other inhibitory signals, or driving spiking through disinhibition, among others (Manookin et al., 2008; Molnar et al., 2009; Werblin, 2010). In Chapter 3, we identify a novel role for glycinergic crossover inhibition—reducing responses to randomly oriented fine textures in an orientation selective amacrine cell. In Chapter 4, the glycinergic crossover inhibition observed in transient OFF alpha ganglion cells helps to maintain sensitivity to higher temporal frequencies in the visual input.

COURSE OF DISSERTATION

The retina comprises a large number of circuits that handle visual information in different ways, but use the same basic circuit elements at their heart. Much, but certainly not all, of the variety in circuit function arises from divergent inhibitory connectivity. Thus, the retina offers a unique opportunity to study how slightly different inhibitory arrangements and properties can modulate the output from the same basic circuit design. In this dissertation, I examine how inhibition shapes the receptive field properties of two different cell types in the retina. The first is a newly identified orientation selective amacrine cell; the second is the well-studied transient OFF alpha ganglion cell.

In Chapter 3, I map the presynaptic circuitry of the new amacrine cell, and show that its orientation selective receptive field is formed by asymmetric excitatory inputs that are defined by its elongated morphology. In this circuit, inhibition plays two roles. First, it prevents spiking in response to negative contrast, allowing the amacrine cell to only report positive contrast signals. Second, it acts to prevent spiking in response to randomly oriented fine textures, allowing the cell to reliably deliver information about stimulus orientation across a range of intermediate spatial frequencies.

In Chapter 4, I examine how inhibition contributes to temporal tuning in transient OFF alpha ganglion cells. One major finding is that GABAergic inhibition of the presynaptic bipolar cells shifts the temporal tuning of the excitatory input to higher frequencies and faster kinetics. This study builds upon decades of work in alpha ganglion cells, and makes a strong step towards linking older models of temporal tuning with an experimentally-verified biophysical mechanism. This work also shows that multiple instances of feedback inhibition are present, but they act over

different spatial extents, frequency bands, and contrast ranges. Thus, the ganglion cell's temporal tuning is maintained over a wide range of visual conditions.

Finally, in Chapter 5 I discuss my work in the context of both past and present studies in the field, and discuss how it contributes to our current knowledge of retinal circuit function.

CHAPTER 2

MATERIALS AND METHODS

Tissue preparation

All procedures involving animals were done in accordance with the National Institutes of Health guidelines, and were approved by the Oregon Health and Science University Institutional Animal Care and Use Committee. Male or female pigmented rabbits, aged 5 weeks and older, were dark-adapted for at least one hour. Under dim red or infrared illumination, rabbits received an intramuscular injection of ketamine (50 mg/kg) and xylazine (10 mg/kg). After inducing anesthesia, sodium pentobarbital (40 mg/kg) was delivered intravenously, followed by 2.5 mL potassium chloride (3 M). Both eyes were enucleated, hemisected, and had the vitreous humor removed before being placed in a bath of Ames' medium (Ames and Nesbett, 1981; U.S. Biologicals) that was equilibrated with carbogen (95% O_2/5% CO_2) at pH 7.4. Retinas were isolated by gently separating the retina and pigment epithelium from the sclera using forceps and precision scissors. The retina could then be separated from the pigment after separation from the sclera. A piece of inferior retina (~1 cm^2) was placed in a recording chamber photoreceptor side down and continuously perfused at 4-5 mL/min with Ames' medium at 34°C. The retina was always placed in the same orientation in the recording chamber.

Cell Identification

Retinal neurons were visualized using a video camera mounted on an upright Olympus BX-51 microscope with infrared (900 nm) differential interference contrast optics. For most experiments, a 20x (0.95 NA) water immersion objective was used for visualizing somas and

delivering a visual stimulus. The 20x objective permitted visual stimuli of over 1.1 mm diameter. For wider field stimulation, a 40x objective (0.8 NA) was used to identify somas, before being switched to a 10x (0.3 NA) or 5x objective for visual stimulation up over 2.2 mm and 4.5 mm, respectively.

In Chapter 3, $PA_{1/3}$ cells were identified as having somas that were elongated parallel to the visual streak, ~10-15 μm along the major axis. Cells were much smaller than a typical ganglion cell, and the nucleus could not be visualized. Cells also had 2-3 thick primary dendrites emanating from the soma. During extracellular recordings, light-evoked spikes were usually monophasic. Spike amplitudes adapted strongly, consistent with sodium channel inactivation, and recovered over the course of a light step (Figure 3.2A). Upon establishing a whole-cell recording, the input resistance was typically 400-500 MΩ. By including 0.4% AlexaFluor-488/594 hydrazide in the recording pipette, the morphology of many cells could be recovered (Figure 3.1).

In Chapter 4, transient OFF alpha ganglion cells were identified by having the largest somas in the ganglion cell layer. In most preparations, their thick dendrites could be located in the inner plexiform layer (IPL), and traced back to the soma. Other types of alpha ganglion cells have dendrites that stratified in different layers of the IPL, and have noticeably smaller somas. Light responses were stereotyped by a transient burst of spikes during a negative contrast step. The spike rate decayed gradually over the course of the light step. Very little background spiking was observed, which served as a good indicator of whether the cell was a transient or sustained OFF alpha cell (van Wyk et al., 2009). After establishing a whole-cell recording, the input resistance

was 20.6 ± 1.11 MΩ (n = 13). By including 0.4% AlexaFluor-488/594 hydrazide in the recording pipette, the characteristic morphology of some cells was confirmed (Figure 4.1A).

Electrophysiology and Pharmacology

Patch electrodes were pulled to a resistance of 5-6 MΩ for $PA_{1/3}$ cells, and 3-4 MΩ for alpha ganglion cells. For extracellular recordings, pipettes were filled with Ames' medium. For voltage clamp recordings, electrodes were filled with an intracellular solution containing the following (in mM): 128 Cs-Methanesulphonate, 6 CsCl, 10 Na-HEPES, 5 Phosphocreatine-Na2, 1 EGTA, 2 Mg-ATP, 1 Na-GTP, 3 QX-314 chloride. The pH of internal solution was adjusted to pH 7.3 using CsOH. Cesium was included in place of potassium to block voltage-gated potassium currents, thereby improving voltage clamp at positive potentials. QX-314 was included to block voltage-gated sodium channels. For current clamp recordings, all solutions were the same except potassium was used in place of cesium, and QX-314 was not included. Currents were sampled at 10kHz, and filtered through a 4 pole Bessel filter in an EPC-10 patch clamp amplifier (HEKA). Further filtering was performed offline. Voltages were corrected for a liquid junction potential of -13 mV. In $PA_{1/3}$ cells, the average series resistance was 16.7 ± 0.46 MΩ (n = 103), and was compensated up to 70%; in alpha ganglion cells, it was ~10 MΩ and compensated up to 80%.

The following pharmacological agents were added directly to the superfusion solution: SR-95531 (6-imino-3-(4-methoxyphenyl)-1(6H)-pyridazinebutanoic acid hydrobromide, 10 μm, Tocris Bioscience #1262), TPMPA (1,2,5,6-tetrahydropyridin-4-yl)methylphosphinic acid, 100 μM, Tocris Bioscience #1040), strychnine (0.5 μM or 1 μM, Sigma # S-8753), L-AP4 (L-(+)-2-amino-4-phophonobutyric acid, 25 μM or 50 μM, Tocris Bioscience # 0103), AP5 (D-(-)-2-amino-5-phophonopentanoic acid, 50 μM, Abcam Biochemicas # 120003), GYKI-53655 (1-(4-

aminophenyl)-3-methylcarbamyl-4-methyl-3,4-dihydro-7,8-methylenedioxy-5H-2,3-benzodiazepine hydrochloride, 50 μM, Tocris Bioscience #2555), tetrodotoxin citrate (TTX; 200 nM, Abcam Biochemicals # 120055), and 2-[(2,6-dichloro-3-methylphenyl)amino] benzoic acid sodium salt (meclofenamic acid; 100 μM; Sigma, catalog #M-4531).

Visual Stimulation

Visual stimuli were generated using Igor Pro, and presented on a CRT computer monitor with a refresh rate of 85 Hz. Visual stimuli were presented through the microscope objective and focused onto the photoreceptors. Stimuli that were temporally modulated as a sine wave were designed such that the monitor's refresh rate was divisible by the modulation frequency. Contrast was defined as $100 \cdot (L_{max} - L_{min})/(L_{max} + L_{min})$, where L_{max} and L_{min} are the maximum and minimum intensities of the stimulus, respectively. The background light intensity was ~10^5 photons/μm^2/s, well above the scotopic range. For oriented bar stimuli, a 150 x 1000 μm bar was presented at 6 different angles separated by 30 degrees. In Chapter 3, receptive fields were mapped in voltage clamp at a holding potential of -73 mV, by flashing 60 x 60 μm squares of light (80% contrast) at different positions across the receptive field.

Intracellular Labeling

In Chapter 3, as described in Murphy-Baum and Taylor (2015):

"$PA_{1/3}$ cells were dye-filled by including 0.4% AlexaFluor-488/594 hydrazide in the recording pipette. Retinas were fixed in 4% paraformaldehyde for 45 minutes, followed by two 5 minute washes in 0.1M phosphate buffer saline (PBS) pH 7.4. Confocal micrographs were obtained on an Olympus FV1000 confocal microscope with a 40x oil-immersion objective (1.3 NA). Images

displaying cellular morphology are maximum intensity Z-projections of an image stack. Figures 1D-F are single frames from an image stack. Primary antibodies against choline acetyltransferase (goat-anti-ChAT, Millipore AB144P) were detected with anti-goat AlexaFluor-594 conjugated secondary antibodies to measure the stratification depth of $PA_{1/3}$ cells. For immunostaining, fixed retinas were blocked for 3 hours in 3% Normal Horse Serum (NHS), 0.5% Triton X-100, 0.025% NaN_3 in PBS, pH 7.4. Primary antibodies were diluted in the same solution and applied for 4 days at ~25ºC. After two 15 minute washes in PBS, secondary antibodies were applied in 3% NHS, 0.025% NaN_3 in PBS pH 7.4 overnight at room temperature.

In some cells, 0.3% Neurobiotin was included in the recording pipette to test for coupling via gap junctions. A whole-cell patch-clamp recording was maintained for 10-20 minutes to allow the dye to fill the neuron, before gently pulling the pipette off the cell. In order to allow additional time for the dye to spread throughout the cell, the retina was held in the recording chamber with constant perfusion for a further 2-3 hours before fixing. A few representative cells that had been filled with AlexaFluor dye or Neurobiotin were morphologically reconstructed using the Neuromantic neuronal reconstruction tool (Myatt et al., 2012). Analysis of confocal image stacks was done using Fiji (ImageJ; Schindelin et al., 2012)."

Data analysis and Statistics

All data analysis was done using custom routines in Igor Pro (WaveMetrics). The work in Chapter 3 involves calculating light-evoked synaptic conductances from currents recorded at a range of holding potentials. As written in Murphy-Baum and Taylor (2015):

"Light-evoked synaptic conductances were calculated as described previously (Taylor and Vaney, 2002), with a few modifications. Briefly, current-voltage (I-V) relations were measured at 10 ms

intervals over a range of voltage steps from -103 mV to +17 mV in 20 mV increments. The total light-evoked conductance was calculated as the difference between the I-V relation at each time point and the "leak" I-V relation measured just prior to the onset of the light stimulus. To avoid errors in calculating the net light-evoked currents due to a sloping baseline during positive voltage steps, a single exponential trend was subtracted from the current traces for each voltage step prior to the leak subtraction. The excitatory and inhibitory conductances could then be calculated at each time point using the observed I-V reversal potential along with the cation and chloride reversal potentials (Taylor and Vaney, 2002).

Accurate calculation of the inhibitory and excitatory conductance components is dependent on the values assigned to the cation and chloride reversal potentials. $PA_{1/3}$ cells have extensive dendritic processes, and the estimation of inputs located distally to the voltage-clamped soma is particularly susceptible to space clamp errors. Space clamp errors cause the membrane potential at points remote from the recording electrode to lie between the command potential and the zero-current or resting potential, with the result that there is a positive shift in the measured cation reversal potential. We measured the magnitude of such positive shifts by blocking all inhibitory inputs with strychnine, SR-95531, and TPMPA, and recording the isolated excitatory currents in response to flashed annuli and spots. For annuli, the measured excitatory reversal potential was progressively more positive as the annulus activated more distal inputs. In the same experiments, at the largest diameters ($\geq$ 600 μm), the maximum positive shift in the reversal potentials measured for the spot stimuli (average ~8 mV, 600 μm diameter, n = 3) was considerably less than for the annuli (average ~26 mV, 600 μm diameter, n = 3). This is to be expected since the bulk of the synaptic conductance is activated at diameters less than ~600 μm (see area-response

measurements below) where the voltage clamp errors are smaller. In order to partially mitigate the effects of space clamp errors we used the cation reversal potential appropriate for each stimulus spot diameter, as this was the primary stimulus used in this study. This procedure obviated the erroneous calculation of negative inhibitory conductances that arises when the measured synaptic reversal potential is more positive than the reversal potential assigned to excitation. The chloride reversal potential (E_{Cl}) was calculated to be -70 mV. Because E_{Cl} lies close to the resting membrane potential of the cell, where the total membrane current is generally small, space clamp errors will not be as large and the actual membrane potential will be closer to the command potential. Therefore we did not attempt to correct the values of E_{Cl} during the conductance analysis.

As shown in Figure 3.4, $PA_{1/3}$ cells receive synaptic inputs mediated by NMDA receptors. In order to account for the I-V relations, the excitation was modeled as the sum of a linear AMPA I-V relation and a nonlinear NMDA I-V relation. The nonlinear NMDA conductance utilized the same reversal potentials as the linear excitatory conductance, and was calculated as described previously (Venkataramani and Taylor, 2010).

Conductances were normalized according to the equation:

$$G_{norm} = (G_{avg} / G_{cell}) \cdot G_{diam}$$

where G_{norm} is the normalized conductance for a particular stimulus diameter, G_{cell} is the average peak conductance across all stimulus diameters for a single cell under control conditions, G_{avg} is the mean G_{cell} across all cells, and G_{diam} is the peak conductance for a particular stimulus diameter. Excitatory conductances were normalized using the peak excitatory conductance during a bright flash, while inhibitory conductances were normalized using the peak inhibitory

conductance during a dark flash. The normalization factor G_{avg}/G_{cell}, obtained under control conditions, was also used to normalize the conductances during drug applications.

Receptive field sizes were estimated from area-response data and fit to a difference of Gaussians function:

$$R(s) = K_{exc}\int_0^{s/2} e^{-(s/\sigma_{exc})^2}\,ds - K_{inh}\int_0^{s/2} e^{-(s/\sigma_{inh})^2}\,ds$$

where R is the spike rate (or peak conductance) evoked by a stimulus of diameter s, K_{exc} and K_{inh} are the amplitudes of the excitatory and inhibitory Gaussians, respectively, and σ_{exc} and σ_{inh} are their space constants. For conductance area response curves, points were taken at either the peak conductance for either the dark or bright flash, or at the time point most relevant for the particular drug application. All area response curves were generated using normalized conductance data.

The contribution of the tonic excitatory input in producing quasi-linear responses was estimated from the ratio of the magnitude of the integrated excitatory conductance during the negative (OFF) and positive (ON) phases of the visual stimuli (Figure 3.9C). For spiking responses, the change in frequency-doubling with increasing spatial frequency was calculated by dividing the integral of the peri-stimulus spike time histogram (PSTH) during the second half of the contrast reversing cycle by the integral over the full cycle (Figure 3.9F). An integral ratio of 1 indicates no frequency-doubling, while a ratio of 0.5 indicates complete frequency-doubling, with no response at the fundamental frequency."

In Chapter 4, the above conductance analysis was not used because the visual stimulus being presented was time consuming, and it wasn't practical to repeat the stimulus for multiple holding potentials and drug applications. Instead, we estimated the excitatory input to the cell as the

current recorded at the chloride reversal potential, -70 mV by our calculation. Although this treatment may be less accurate than a multi-point conductance analysis, especially in discriminating NMDA and AMPA-mediated inputs, it provides a reasonable estimation of the excitatory input to the cell.

The spatial selectivity index (SSI; Chapter 4) was calculated from area response measurements as $(R_{max} - R_{big})/(R_{max} + R_{big})$, where R_{max} and R_{big} are the spike counts for the spot that produced the maximal response and the largest spot tested, respectively. Area response data was fit as described above, except the EPSC data was not normalized. The discrete Fourier transform was calculated at the stimulus frequency to obtain the magnitude and phase of the fundamental component (F1). The "best frequency" was estimated from the F1 amplitude versus temporal frequency plots by fitting a 5^{th} order polynomial and finding the frequency of the maximum F1 amplitude.

Error bars in figures represent ± standard error of the mean, as do the shaded areas on the current traces. In Chapter 3, data sets were compared using two-tailed Student's t tests. In Chapter 4, data sets were tested for normality using the Shapiro-Wilk test. Normally distributed data sets were compared using two-tailed Student's t tests. Data sets that were not normally distributed were compared using two-tailed Wilcoxon signed-rank tests. For experiments involving the serial application of multiple drugs (i.e. control, TTX, and TTX/SR/TPMPA), comparisons were made between each condition and the one directly prior to it. In the above example, TTX is compared with control, and TTX/SR/TPMPA is compared with TTX. Results were considered significant for $P < 0.05$.

Computational Modeling

In Chapter 4, we modeled the change in F1 phase and F1 amplitude following GABAR blockade. The F1 component of the EPSC was modeled as the sum of excitatory and inhibitory signals, represented by sine functions:

$$S_{exc} = A_{exc} \sin(2\pi ft) \tag{1}$$

$$S_{inh} = A_{inh} \sin(2\pi f(t - \Delta t)) \tag{2}$$

$$S_{EPSC} = S_{exc} + S_{inh} \tag{3}$$

where A_{exc} and A_{inh} are the the amplitudes of the excitatory and inhibitory signals, Δt is the time delay between them, and f is the temporal frequency. The phase of S_{EPSC} is given by:

$$\varphi = -\tan^{-1}\left(\frac{(A_{exc}\sin(\theta_{exc}) + A_{inh}\sin(\theta_{inh})}{A_{exc}\cos(\theta_{exc}) + A_{inh}\cos(\theta_{inh})}\right) \tag{4}$$

where $\theta = 2\pi f \cdot \Delta t$

Since we are interested in the phase and amplitude of inhibition relative to excitation, θ_{exc} is set to 0, and dividing through by A_{exc} produces:

$$\varphi = -\tan^{-1}\left(\frac{A\sin(2\pi f\Delta t)}{1 + A\cos(2\pi f\Delta t)}\right) \tag{5}$$

where $A = A_{inh}/A_{exc}$. The amplitude ratio of S_{EPSC} (EPSC in control) to S_{exc} (EPSC during GABAR blockade) is calculated as:

$$r = \sqrt{1 + 2A\cos(2\pi f\Delta t) + A^2} \tag{6}$$

The change in S_{exc} produced by GABAergic inhibition is shown in Figure 4.4A and was fit with Equation (5). The amplitude ratio, S_{ESPC}/S_{exc} (Figure 4.4B), was fit with Equation (6). We considered the possibility that excitation and inhibition could have different temporal tuning functions, and thus different amplitude ratios as a function of temporal frequency (Frishman et al., 1987). We approximated the temporal tuning functions of excitation and inhibition using two

Gaussian functions with different best frequencies, which allowed us to calculate their ratio, A, as a function of temporal frequency (Figure 4.4B, inset). The ratio of two Gaussian functions that are offset by some arbitrary x value (i.e. shifted temporal tuning curves) is given by the equation:

$$A = B \cdot e^{f/\tau} \tag{7}$$

where τ and B are constants and f is the temporal frequency. If the widths, w, of the Gaussian functions are equal, then the constant, B, is:

$$B = e^{\frac{-\Delta f(\Delta f + 2 f_0)}{w^2}} \tag{8}$$

where Δf is the difference in best frequency between the two Gaussians, and f_0 is the best frequency of the first (excitatory) Gaussian. The constant τ is given by:

$$\tau = \frac{w^2}{2\Delta f} \tag{9}$$

f_0 was fixed as the best frequency following GABAR blockade, as determined in Figure 4.2B-C. Thus, this modified model has three free parameters—w, Δf, and Δt—that are optimized during fitting. S_{exc} and S_{inh} were calculated using the best-fit values of Δt and A, and are illustrated in Figure 4.4D at two temporal frequencies for comparison against the real data.

CHAPTER 3

The Synaptic and Morphological Basis of Orientation Selectivity in a Polyaxonal Amacrine Cell of the Rabbit Retina

Benjamin L. Murphy-Baum[1] and W. Rowland Taylor[1]

[1]Casey Eye Institute
Department of Ophthalmology
Oregon Health and Science University
Portland, OR 97239

[This manuscript is presented as published in Murphy-Baum and Taylor (2015) *J Neurosci* 35:13336-50)]

PREFACE

In the cat, Hubel and Weisel (1962) first described columns of neurons in the primary visual cortex that only fire in response to visual inputs with particular orientations. They proposed that each cortical neuron receives input from spatially aligned thalamic neurons. Subsequent work involving paired recordings from neurons in the LGN and cortex, and cortical inactivation studies have supported their original hypothesis (for review, see Priebe, 2016). However, orientation selectivity has been identified earlier in the visual pathway, in the LGN of rodents (Scholl et al., 2013), as well as in the retina of both rabbits and mice (Venkataramani and Taylor, 2010, 2016; Nath and Schwartz, 2016). Thus, there may be different mechanisms driving cortical orientation selectivity depending on the species.

In rabbits, the earliest sign of orientation selectivity is in retinal ganglion cells, which rely on GABAergic inhibition from amacrine cells for their orientation tuning. Although orientation selective (OS) amacrine cells have been described in the past (Bloomfield, 1994), there has been no systematic study of the circuitry associated with these neurons or how they form their OS receptive fields. The amacrine cells that we identified are distinct from those described by Bloomfield, but have many morphological similarities to some of the polyaxonal amacrine cells described by Famiglietti (1992b). The functional characterization of these orientation selective amacrine cells is critical towards understanding how this fundamental feature selectivity first arises in the visual pathway. I conducted this study under the mentorship and guidance of Dr. W. Rowland Taylor. I designed and performed the experiments, analyzed the data, and wrote the manuscript. Dr. Taylor provided guidance with experimental design, and assisted in the data analysis and the preparation of the manuscript.

INTRODUCTION

Synaptic inhibition plays a critical role in shaping the spatiotemporal properties of neurons. In cortex, both local feedback and longer range feedforward afferents modulate excitatory signals by altering synaptic gain, exerting temporal control, and sharpening stimulus selectivities. In particular, cortical feedback inhibition has been shown to function locally, as in the temporal control of principal neuron excitation, and globally, as in the pacing of gamma oscillations across populations of interneurons and pyramidal cells (for review, see Isaacson and Scanziani, 2011). The array of different functions seen in cortical inhibitory circuits is dependent on the diverse morphology, stratification, and specific connectivity of inhibitory interneurons.

As in the cortex, the retina utilizes a variety of inhibitory interneurons to regulate the spatiotemporal properties of excitatory signals both locally and globally. This diverse group of interneurons, the amacrine cells, comprise upwards of 30 different morphological subtypes (MacNeil et al., 1998; MacNeil and Masland, 1999) and are thought to perform inhibitory tasks over a wide range of spatial scales. GABAergic amacrine cells shape many of the feature selectivities found in retinal ganglion cells (RGCs), such as direction of motion (Caldwell et al., 1978; Ariel and Daw, 1982; Kittila and Massey, 1997), orientation (Venkataramani and Taylor, 2010), spatiotemporal frequency (Russell and Werblin, 2010; Venkataramani et al., 2014), and local object motion (Ölveczky et al., 2003, 2007; Baccus et al., 2008). Many of these inhibitory roles require spatial integration over large areas, which is thought to be the province of wide-field amacrine cells (WFACs). However, WFACs can also be specialized for local dendritic processing, as in the reciprocal feedback circuitry between A17 amacrine cells and rod bipolar cells (Hartveit, 1999; Chavez et al., 2006; Grimes et al., 2010). Moreover, retinal inhibitory

circuits often utilize serial GABAergic synapses between amacrine cells (Dowling and Boycott, 1966, 1968; Pourcho and Owczarzak, 1989; Chun and Wässle, 1989; Koontz and Hendrickson, 1990; Marc and Liu, 2000), which are important for the spatial and temporal regulation of bipolar cell outputs (Zhang et al., 1997; Eggers and Lukasiewicz, 2010, 2011).

Of the ~30 morphologically described amacrine cells in the rabbit retina, the majority of functional recordings have come from only three cell types: a narrow-field glycinergic cell (AII amacrine cell), and two wide-field GABAergic cells (starburst and A17 amacrine cells). Here, we have identified a morphologically distinct type of WFAC in the rabbit retina that can be further classified as a polyaxonal amacrine cell (PAC). PACs were originally identified in the rabbit by Famiglietti (1992a-c), and are characterized by their multiple, thin axon-like processes that have been shown in the primate to transmit signals for millimeters across the retina (Greschner et al., 2014). However, unlike these previous examples, the PAC described here displays strong orientation selectivity due to its dendritic structure and the arrangement of its synaptic inputs, and may represent a major source of orientation selective signaling in the retina. We used voltage clamp recordings and pharmacological manipulations to elucidate the synaptic mechanisms that produce the spatiotemporal receptive field properties of these neurons.

RESULTS

Anatomical properties of a displaced polyaxonal amacrine cell

The PAC that we have targeted has a soma displaced to the ganglion cell layer, and was initially identified by extracellular spike recordings. The cells typically had small, oblong somas (10-15 μm diameter, major axis) that were oriented roughly parallel to the visual streak. The size and

shape of the soma, the distinct spiking pattern, the physiological receptive field size, the dendritic morphology, and the characteristics of the synaptic inputs defined the cell type. We visualized the dendritic morphology by filling the cells with a fluorescent dye, AlexaFluor-488, during the recordings. Two types of processes could be distinguished: thicker, spiny dendrites that arose from the soma, and thinner, aspiny, putative axons. The axons always branched off a dendrite and extended for millimeters across the retina, far beyond the reach of the larger caliber dendritic arbor (Figure 3.1A, B). Overall, the dendritic arbors tended to be elongated parallel to the visual streak, with a maximum extension of 729 ± 24 μm (n = 10). We measured the vertical stratification depth of the dendrites to determine whether the cells are likely to receive inputs from ON or OFF bipolar cells. The stratification depth was determined relative to the dendrites of ON and OFF starburst amacrine cells, which were revealed by staining retinas with antibodies against choline acetyltransferase (ChAT). The ON and OFF ChAT bands narrowly stratify in layers S2 and S4 of the inner plexiform layer (IPL; Figure 3.1C). Typically, the PACs had two or three primary dendrites, which extended along the ganglion cell layer for 115 ± 9 μm (n = 9) before rising to stratify in S3, just above the ON-ChAT band, and in S1, just above the OFF-ChAT band (Figure 3.1C-F). In all cases (n = 9) the dendrites first branched to S3 before transitioning to S1, with the result that the S1 dendritic segments tended to be more distal than those in S3. Occasionally, a dendrite would return to S3 after branching in S1 (Figure 3.1C). The transitions between S3 and S1 were typically abrupt, leaving little dendritic length for potential synaptic contacts in intervening layers. This stratification pattern implies convergent input from the two major signaling pathways in the retina, as layers S3 and S1 contain ON and OFF bipolar

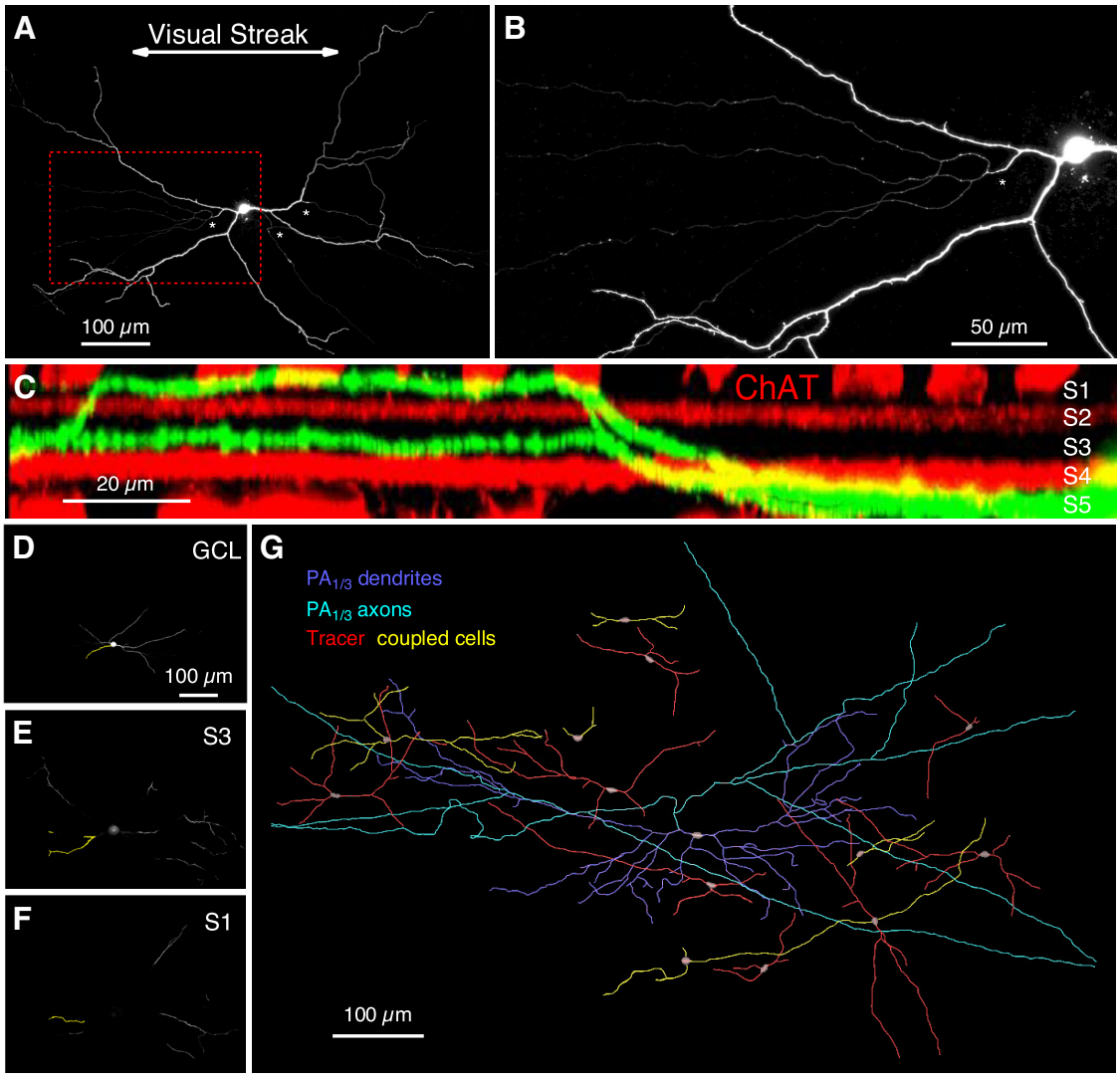

FIGURE 3.1. A POLYAXONAL AMACRINE CELL IN THE RABBIT RETINA

A, A polyaxonal amacrine cell ($PA_{1/3}$) filled with AlexaFluor-488 fluorescent dye, with asterisks marking axonal branches. **B**, Enlarged view of the demarcated area in **A**, showing multiple axons branching from thicker proximal dendrites. **C**, XZ image stack of a $PA_{1/3}$ cell (green) with staining for choline acetyltransferase (ChAT, red), showing dendritic stratifications in layers S1 and S3 of the IPL. **D-F**, Same cell as in **C**, images of the main dendritic stratification levels in the GCL, S3, and S1. Yellow dendrites correspond to those seen in **C**. **G**, A reconstruction of a $PA_{1/3}$ cell filled with 0.3% Neurobiotin, revealing a network of electrically coupled cells.

cell axon terminals, respectively. Furthermore, the putative axons narrowly stratified to the S3/S4 border, suggesting that their postsynaptic targets are likely ON-type cells.

PACs with elongated dendritic arbors have been described in previous morphological surveys in the rabbit retina, namely PA3 and Type V cells (Famiglietti, 1992c; Völgyi, 2001). These cells

share many features with the PAC described here, but later we will discuss some key differences. Because of our uncertainty as to its novelty, we will refer to this cell type as $PA_{1/3}$ after its dendritic bistratification and axonal processes.

Tracer coupling

Electrical or tracer coupling via gap junctions has been observed in many cell types in the retina (Raviola, 1973; Lamb and Simon, 1976; Smith and Vardi, 1995; Vardi and Smith, 1996; DeVries et al., 2002), including PACs (Völgyi, 2001; Wright and Vaney, 2004; Greschner et al., 2014), and has been shown to produce correlated firing between coupled cells (Vardi and Smith, 1996; for review, see Bloomfield and Völgyi, 2009). The addition of 0.3% Neurobiotin to the recording electrode revealed that $PA_{1/3}$ cells are tracer coupled to a number of other cells in close proximity (Figure 3.1G). Many of the coupled cells appear to be morphologically uniform, with two or three primary dendrites that extend for several hundred microns. Although the tracer fills were limited, the cells appear to be morphologically similar to $PA_{1/3}$ cells. However, it was not possible to clearly identify them.

An orientation biased receptive field

The stratification of the dendrites to S3 and S1 indicate that $PA_{1/3}$ cells are positioned to receive inputs from both ON and OFF bipolar and amacrine cells. To test this, we first recorded extracellular action potentials in $PA_{1/3}$ cells in response to a spot, centered on the soma and square-wave flickered at 0.5 Hz with 80% contrast. Under photopic background illumination of 10^3 photons/μm^2/s, $PA_{1/3}$ cells fired tonically at 4.6 ± 1.7 Hz (n = 154). During the positive contrast phase of the flicker stimulus, the cells fired a transient burst of spikes (74.7 ± 3.2 Hz,

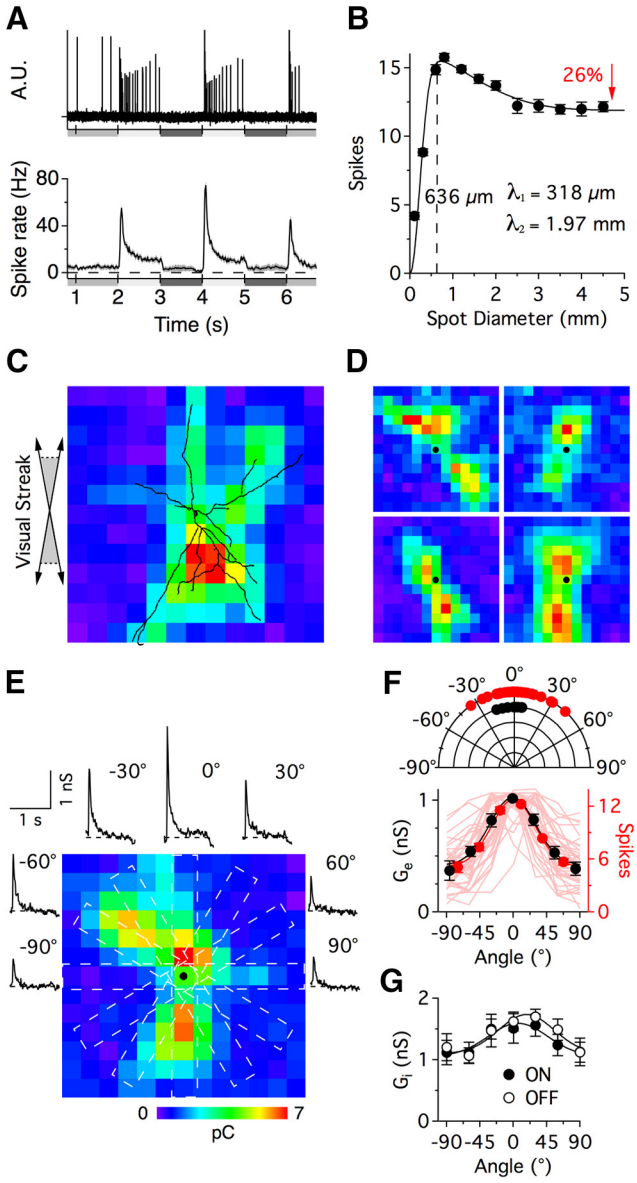

FIGURE 3.2. RECEPTIVE FIELD PROPERTIES OF $PA_{1/3}$ CELLS.

A, Example extracellular recording (top) and average peri-stimulus spike time histogram (bottom, n = 128) showing action potentials in response to a 600 µm diameter flashing spot stimulus. Luminance is indicated by the shaded bars underneath the traces. **B**, Spike count in response to a flashing spot ranging from 100 - 4500µm diameter (n = 128) is fit with a difference of Gaussians function; the two Gaussians have space constants of 318 µm and 1.97 mm. Surround suppression was limited to a 26% reduction in the spike output. **C**-**E**, Receptive field mapping of the excitatory inputs using a 60x60 µm flashing square stimulus, with black dots indicating the soma position. In **C**, the dendrites of the recorded cell were reconstructed and overlaid on the receptive field map. Angled arrows (left) portray uncertainties in the exact orientation of the retina between recording and imaging. **E**, Excitatory conductance measurements in response to an angled flashing bar stimulus (portrayed by white dotted bars) encircle the RF map, and correspond to the indicated stimulus angle. LEGEND CONTINUED ON NEXT PAGE →

600 µm diameter spot) that rapidly declined (~80 ms time constant) to a maintained level of 11.0 ± 2.1 Hz (Figure 3.2A). The cells did not respond to the negative contrast phase of the stimulus. Therefore, despite the consistent dendritic stratification in the OFF sublamina, $PA_{1/3}$ cells can be classified as ON-type cells. The extent of the physiological receptive field (RF) was estimated by plotting the number of spikes elicited over a range of stimulus spot diameters (area response curve, Figure 3.2B). Fitting the data to a difference of Gaussians function indicated that the physiological RF had a spatial extent of ~636 µm (2λ), which closely matches the average maximal extent of $PA_{1/3}$ dendritic arbors (~730 µm), indicating that the excitatory input is delineated by the dendritic arbor.

The sparse branching and elongated dendritic arbor suggested that the structure of the excitatory receptive field might show marked asymmetries. Thus, we mapped the excitatory receptive field at higher spatial resolution under voltage clamp (V_h= -73 mV) using an array of 60 µm squares arranged in a checkerboard (60 µm x and y offsets). We presented the stimulus at each location in isolation, and estimated the response as the integral of the light-evoked EPSCs. The spatial structure of the resulting response maps correlated closely with the dendritic arbors of the cells (Figure 3.2C), and were elongated parallel to the visual streak (Figure 3.2C-E). It is noteworthy that the maps did not show excitatory input beyond the limits of the dendritic arbor, suggesting that potential inputs onto axonal processes do not contribute to the excitatory drive.

FIGURE 3.2 CONTINUED → **F**, Bottom, Average peak excitatory conductances (black, n = 9) and spike counts (red, n = 37) versus stimulus angle, with 0° corresponding to the maximal response. The individual spike tuning curves shown in the background are not normalized to 0°. Top, Preferred stimulus angle for individual spike tuning curves (red), obtained by taking the peak of a Gaussian fit to the data. The dominant orientations of the dendritic arbors in a separate population of cells is shown in black, and were obtained using the 'Directionality' algorithm in ImageJ. **G**, Inhibitory conductances recorded during both the bright and dark flashes were tuned similarly to the excitatory inputs. Scale, each pixel on the RF maps is 60x60 µm.

Typically the response maps showed two “hot spots” located in the dendrites on either side of the soma (Figure 3.2D). The generally weaker input over the soma is consistent with the finding noted above, that the primary dendrites extended for ~115 μm in the GCL before rising to stratify in S3, where they can first receive inputs from bipolar cells.

The asymmetry of the excitatory receptive field could confer orientation sensitivity on $PA_{1/3}$ cells, and thus provide a substrate for orientation selectivity (OS) in rabbit RGCs, which has been shown to arise presynaptically from the activity of unspecified GABAergic amacrine cells (Venkataramani & Taylor, 2010). To test this, we centered a flashing bar (150 x 1000 μm) over the soma and varied its orientation. We found that the spike output was maximal for stimuli that were parallel to the major axis of the cell (n = 37, Figure 3.2F, red). The preferred orientation was calculated as the angle at the peak of a Gaussian fit to the data. Measurements of the dominant orientation of the dendritic arbors, obtained using the 'Directionality' algorithm (developed by Jean Yves Tinevez; Liu, 1991) provided in ImageJ (Schindelin et al., 2012), indicated that the morphological orientation was similar to the preferred orientation obtained from the spiking data (Figure 3.2F, top). The excitatory conductances in a subset of cells exhibited similar orientation tuning (n = 9, Figure 3.2E-F, black). The inhibitory conductances showed weak orientation tuning along the same axis as the excitatory conductances (Figure 3.2G), an arrangement that would be expected to countermand rather than enhance orientation tuning. Thus, OS responses are likely not due to inhibition, but to the asymmetry of the dendritic arbor and the arrangement of the excitatory inputs.

$PA_{1/3}$ cells receive ON excitation and ON-OFF inhibition

The spiking responses suggest that $PA_{1/3}$ cells receive a net excitatory drive through their dendrites in the ON sublamina. However, since these cells are bistratified, it is possible that they receive synaptic input from both the ON and OFF pathways. To determine which visual pathways drive the synaptic conductances, $PA_{1/3}$ cells were voltage clamped to a series of holding potentials between -103 mV and +17 mV. At each voltage, light-evoked currents were recorded in response to a flashing spot of different sizes. Current traces from a single cell and population averages are shown in Figure 3. Current-voltage (I-V) relations were calculated at 10 ms intervals during the voltage steps, and at each time point the excitatory and inhibitory conductances were calculated from best-fit I-V curves (see Methods). We incorporated a NMDA-mediated conductance to account for a nonlinearity in the I-V relations (Venkataramani and Taylor, 2010; see Methods). This analysis revealed an excitatory conductance that was activated during steps of positive contrast and suppressed with negative contrast (Figure 3.3C, F, green), whereas inhibitory conductances occurred during both positive and negative contrast steps (Figure 3.3C, F, red). These results agree with the spiking observed during the ON phase of the stimulus (positive contrast), and its sharp cessation during the OFF phase (negative contrast). Together, these data suggest that excitation arises from the ON pathway, while both ON and OFF pathways contribute inhibition. This hypothesis is consistent with the effects of applying the mGluR6 receptor agonist *L*-AP4, which selectively blocks signal transmission through ON bipolar cells (Slaughter and Miller, 1981). Blocking ON bipolar cells completely suppressed the excitatory conductance for all tested stimulus diameters (Figure 3.4A, C). Inhibition was suppressed during the ON phase, while the OFF phase inhibition was unaffected (Figure 3.4B,

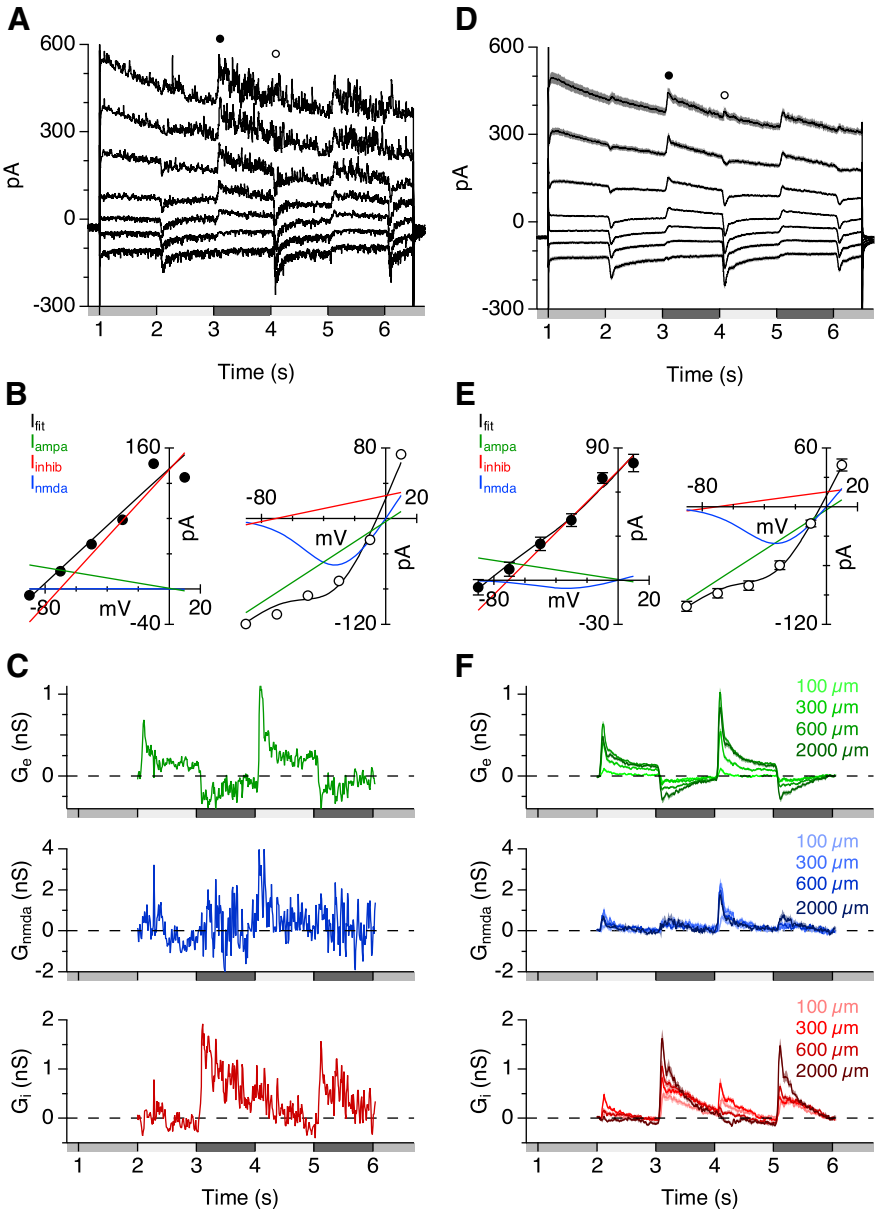

FIGURE 3.3. CONDUCTANCE MEASUREMENTS ALLOW FOR THE SEPARATION OF INHIBITORY, AMPA/KAINATE-MEDIATED, AND NMDA-MEDIATED INPUTS.

A–**C**, Data from a single cell for a 600 µm diameter flashing spot stimulus. **D**–**F**, Average data (n = 49-91). **A**, **D**, Light-evoked currents in $PA_{1/3}$ cells during a series of voltage steps from -103 to +17 mV. **B**, **E**, The resulting I–V relations at the indicated time points in **A** and **D** during dark (left) and bright (right) light flashes. The solid lines indicate component fits to linear excitatory (AMPA/kainate, green), linear inhibitory (red), and NMDA-mediated (blue) currents. The black line is the total fit, which is a summation of the three components. **C**, **F**, Conductance calculations from the I–V curves measured every 10 ms during the light stimulus for AMPA/kainate receptor-mediated excitation (top), NMDA receptor-mediated excitation (middle), and inhibition (bottom). A range of stimulus diameters is shown for the average traces in **F**.

D).

As noted above, the nonlinearity in the I-V relations was accounted for by including a NMDA component in the conductance analysis (Figure 3B, E). We reasoned that if ON bipolar cells activate NMDA receptors on $PA_{1/3}$ cells, then bath applying GYKI-53655 (GYKI), an AMPA receptor antagonist, should limit the excitatory inputs to those mediated by NMDA receptors. In the presence of GYKI, the nonlinearity of the I-V relations was enhanced (Figure 3.4E), as the inward current was strongly reduced at more negative potentials, consistent with the suppression of a linear AMPA receptor mediated input. Addition of the NMDA receptor antagonist *D*-AP5 abolished the excitatory conductance seen in the presence of GYKI (Figure 3.4E). These results establish a minimal model for the synaptic inputs to $PA_{1/3}$ cells, which is illustrated in Figure 3.4F.

Presynaptic inhibition modulates the excitatory inputs

The spiking responses to a flashing spot of increasing diameter revealed that $PA_{1/3}$ cells receive surround inhibition, which suppressed spiking by ~26% for wide-field stimulation (Figure 3.2B). Surround inhibition has been shown to originate from WFACs, which can produce strong, presynaptic suppression of both excitatory and inhibitory inputs to RGCs (Taylor, 1999; Flores-Herr et al., 2001; Buldyrev and Taylor, 2013; Venkataramani et al., 2014). Such presynaptic inhibition contributes to generating the center-surround organization of receptive fields in the retina, which enhances sensitivity to local contrast (Cook and McReynolds, 1998; Taylor, 1999; Flores-Herr et al., 2001; Völgyi et al, 2002). However, horizontal cells in the outer plexiform layer (OPL) can also produce presynaptic suppression in response to wide-field stimuli (Mangel, 1991; Dacey et al., 2000; Kamermans et al., 2001; McMahon et al., 2004; Ichinose and

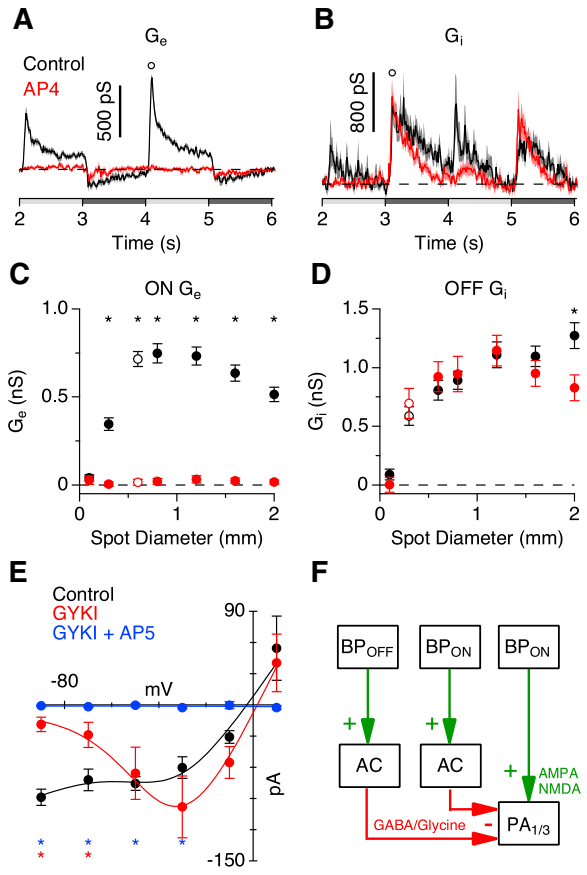

FIGURE 3.4. EXCITATORY INPUTS ARE ON PATHWAY DRIVEN, WHEREAS INHIBITORY INPUTS USE BOTH THE ON AND OFF PATHWAYS.

A–D, Conductance traces (**A**, **B**) correspond to the stimulus diameters indicated by the open symbols in the area response curves (**C**, **D**). Data points were taken at the indicated time points in the conductance traces. Excitatory (**A**, **C**) and inhibitory (**B**, **D**) conductances in the presence of the mGluR6 agonist L-AP4 in response to a flashing spot stimulus (n = 19). **E**, I–V curve of the excitatory currents in response to a 600 µm diameter bright spot in the presence of the AMPA/kainate receptor antagonist GYKI-53655 and the NMDA receptor antagonist D-AP5 (n = 5). **F**, Proposed circuitry outlining the inhibitory and excitatory inputs to $PA_{13/}$ cells. *$p < 0.05$, Student's t test.

Lukasiewicz, 2005; Davenport et al., 2008; Babai and Thoreson, 2009). We sought to determine whether the observed surround inhibition in $PA_{1/3}$ cells could be attributed to amacrine cells in the IPL or horizontal cells in the OPL. In order to distinguish between these two possibilities, we tested the effect of TTX, a voltage-gated sodium channel blocker, on light-evoked currents, as several studies have shown that IPL-mediated surround inhibition in bipolar cells and RGCs is

sensitive to TTX (Taylor, 1999; Demb et al., 2001; Flores-Herr et al., 2001; Shields and Lukasiewicz, 2002; Vigh et al., 2011; Buldyrev and Taylor, 2013; Venkataramani et al., 2014). TTX should have no effect on the excitatory conductance if the surround is mediated by the OPL, as horizontal cells do not fire action potentials, and hyperpolarize in response to positive contrast. Bath application of TTX increased the peak ON excitatory conductance for spot diameters ≥ 600 μm (Figure 3.5A). This result suggests that feedback inhibition from spiking amacrine cells onto bipolar cell axon terminals contributes to the inhibitory surround of the receptive field.

Bipolar cell axon terminals are known to express $GABA_C$ receptors (Feigenspan et al., 1993; Lukasiewicz and Werblin, 1994; Zhang and Slaughter, 1995; Zhang et al., 1997; Lukasiewicz and Wong, 1997; Lukasiewicz and Shields, 1998; Euler and Wassle, 1998; Dong and Werblin, 1998; Wässle et al., 1998; Shields et al., 2000; Vigh and von Gersdorff, 2005; Vigh et al., 2011), and in some cases $GABA_A$ receptors (Völgyi et al, 2002; Russell and Werblin, 2010; Lukasiewicz and Shields, 1998; Vigh and von Gersdorff, 2005; Eggers and Lukasiewicz, 2006; Eggers et al., 2007). We selectively blocked different GABA receptor subtypes to determine which receptor types were mediating feedback inhibition of bipolar cell terminals. Application of the $GABA_C$ receptor antagonist TPMPA potentiated the excitatory conductance and tended to increase its duration for spot diameters > 300 μm (Figure 3.5B, E, orange). In contrast, the excitatory conductance was attenuated in the presence of the $GABA_A$ receptor antagonist SR-95531 (SR), and displayed a rapidly damped oscillation that substantially reduced the duration ($p=0.0006$, $n = 16$) of the excitatory response (Figure 3.5C, E, red). During extracellular recordings, SR had the same effect on the spike rate as it did on the excitatory conductance

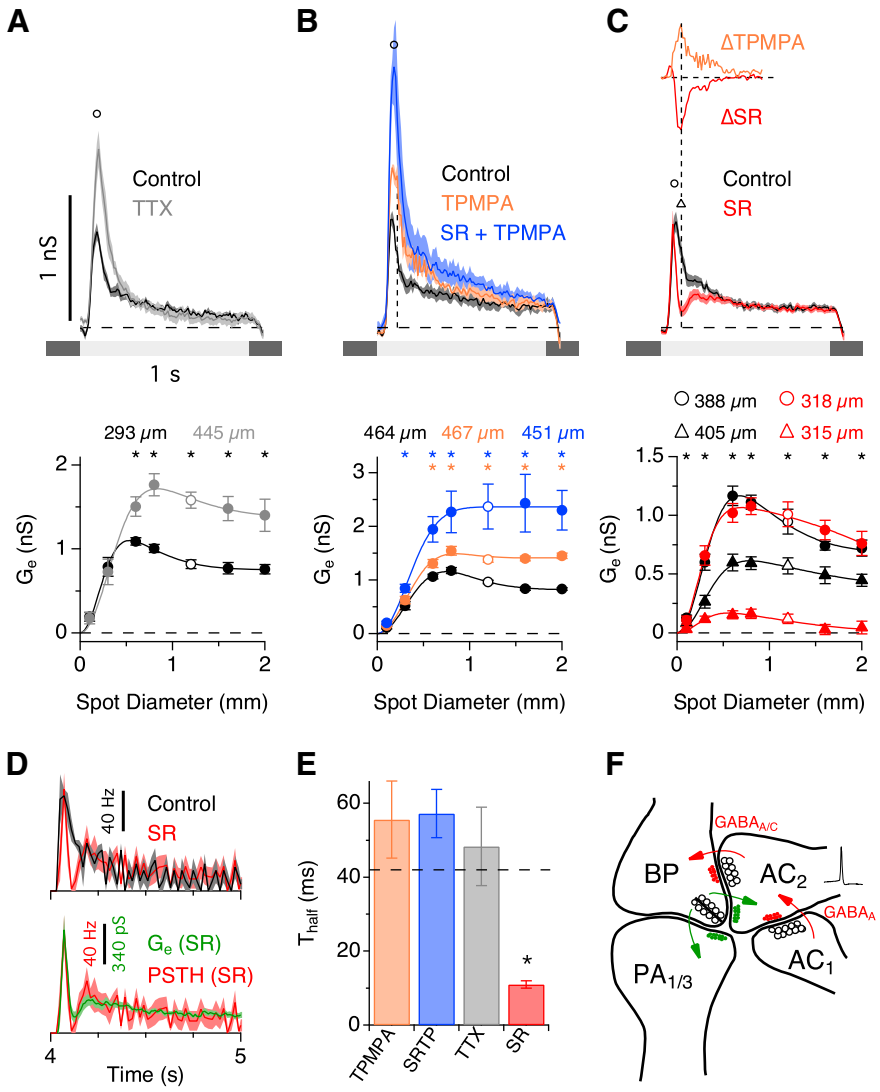

FIGURE 3.5. SERIAL GABAERGIC FEEDBACK INHIBITION MODULATES THE TEMPORAL AND SPATIAL RECEPTIVE FIELD PROPERTIES OF $PA_{1/3}$ CELLS.

A-C, Conductance traces (top) correspond to the stimulus diameters indicated by the open symbols in the area response curves (bottom). Data points were taken at the indicated time points in the conductance traces. The excitatory conductance in the presence of the voltage-gated sodium channel antagonist TTX (**A**; n = 5-7), the $GABA_C$ receptor antagonist TPMPA (**B**, orange; n = 7), the $GABA_A$ receptor antagonist SR-95531 (**C**, red; n = 16), and both $GABA_A$ and $GABA_C$ receptor antagonists together (**B**, blue; n = 6). Space constants for difference of Gaussian fits (solid lines) are shown above the area response curves. In **C**, the significance markers * refer to the area response measurement taken at the delayed time point, 120 ms after light onset (triangles). **C**, inset, Comparison of the time course of the change in conductance for both SR and TPMPA applications. **D**, Spike rate in the presence of SR versus control (top; n = 5), and spike rate versus the excitatory conductance, both in the presence of SR (bottom). **E**, Measurements of time to 50% decay (T_{half}) for the different drug applications. **F**, Minimal circuit that could account for proposed serial feedback inhibition onto bipolar cell terminals. Note that AC_2 is a wide-field spiking amacrine cell. *$p<0.05$, Student's t test.

(Figure 3.5D), indicating that changes in the kinetics of the excitatory conductance have equivalent effects on the spike output.

The attenuated excitatory response during $GABA_A$ receptor blockade and the potentiated response during $GABA_C$ receptor blockade are suggestive of a feedback loop involving serial inhibition between two amacrine cells. A simple model that would account for our data is illustrated in Figure 3.5F. Here, blocking $GABA_A$ receptors disinhibits $GABA_C$ receptor mediated feedback inhibition, causing the observed oscillatory and attenuated excitatory response (Figure 3.5C, red). Conversely, blocking $GABA_C$ receptors disinhibits bipolar cell terminals, causing a potentiation of the excitatory response (Figure 3.5B, orange). In support of this model, the change in conductance produced by $GABA_A$ or $GABA_C$ receptor blockade had the same delayed time course (Figure 3.5C, inset), suggesting that serial feedback inhibition modulates the amount of GABA released onto bipolar cell terminals. Serial synapses such as this have been described in both electron microscopy (Dowling and Boycott, 1966, 1968; Pourcho and Owczarzak, 1989; Chun and Wässle, 1989; Koontz and Hendrickson, 1990; Marc and Liu, 2000) and functional studies (Zhang et al., 1997; Eggers and Lukasiewicz, 2010, 2011; Chen et al., 2011).

If $GABA_C$ receptors are solely responsible for presynaptic suppression of bipolar cell terminals, then co-application of SR and TPMPA should produce effects similar to the application of TPMPA alone. However, we found that blocking both $GABA_A$ and $GABA_C$ receptors caused a much larger increase in the excitatory conductance than that achieved with $GABA_C$ receptor blockade alone (Figure 3.5B, blue). Together, these results support the hypothesis that a spiking WFAC (AC_2 in Figure 3.5F) produces surround inhibition by activating

both $GABA_A$ and $GABA_C$ receptors on bipolar cell terminals. Our data suggest that the relative strength of the two inhibitory serial synapses controls both the time course and the magnitude of the excitatory conductance, which in turn modifies the spiking output of $PA_{1/3}$ cells.

Excitation is modulated by local microcircuits

The data in Figure 3.5 indicates that GABAergic feedback inhibition is highly active during wide-field visual stimulation (area-response curves). Upon close examination, however, the effects produced by the GABA receptor antagonists (SR+TPMPA) appear to be active on a smaller spatial scale than those produced by TTX. This seems reasonable, given that TTX only blocks action potential generation but not the active postsynaptic receptors. Subthreshold depolarizations may still be able to trigger feedback inhibition onto cone bipolar cell terminals, as is the case with reciprocal feedback inhibition from A17 amacrine cells onto rod bipolar cells (Hartveit, 1999; Chavez et al., 2006; Grimes et al., 2010). Consistently, TTX didn't potentiate the excitatory conductance nearly as much as SR + TPMPA (Figure 3.5A-B), suggesting that a portion of the feedback inhibition remained unblocked even though action potentials had been silenced. Thus, we hypothesized that feedback inhibition onto bipolar cell terminals can be activated on both local and wide-field spatial scales using spike-independent and spike-dependent mechanisms, respectively (Bieda and Copenhagen, 1999). We tested this by comparing the effects of TTX and GABA receptor blockade (SR + TPMPA) on the excitatory conductance over a range of spatial scales. Blocking GABA receptors enhanced the excitatory conductance for both very small and large stimulus diameters (Figure 3.6A), whereas TTX had no effect on the excitatory conductance unless the stimulus was ≥ 600 μm in diameter (Figure 3.6B). These findings are consistent with the idea that the TTX-sensitive feedback inhibition is

mediated by spiking in WFACs that require a relatively large stimulus to reach spike threshold. In contrast, the effects of blocking GABA receptors raise the possibility that inhibitory feedback can also operate on small spatial scales similar in size to the receptive field of a single bipolar

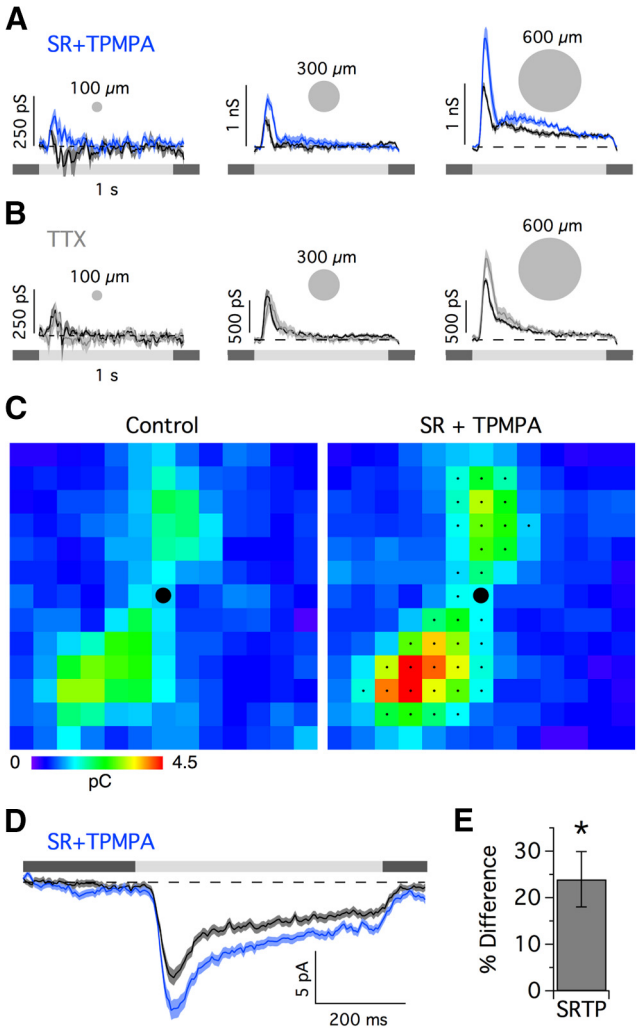

FIGURE 3.6. GABAERGIC FEEDBACK INHIBITION CAN OPERATE LOCALLY WITHOUT USING ACTION POTENTIALS. Excitatory conductance for the 100, 300, and 600 µm diameter stimulus spots in the presence of SR + TPMPA (**A**) and TTX (**B**). **C**, Receptive field map of the excitatory charge transfer (V_{hold} = -73 mV) under control conditions (left) and with GABAergic blockade (right). **D**, For each cell, EPSCs from stimulus positions which passed greater charge than the average charge transfer across all stimulus positions were selected and averaged. The selected positions for the cell in **C** are indicated by the small black dots (n = 203 stimulus positions across 9 cells). **E**, % Difference in charge transfer for control versus SR+TPMPA for the selected stimulus positions (n = 9). *p < 0.05, Student's t test.

cell in the rabbit retina (Mills and Massey, 1992; MacNeil et al., 2004), where it could be activated by graded potentials rather than spiking activity.

We tested whether single bipolar cells can activate feedback inhibition by mapping the excitatory inputs to $PA_{1/3}$ cells as described earlier, before and after GABAergic blockade (Figure 3.6C-E). Since bipolar cell receptive fields in mammalian retinas are typically around 20-60 µm in diameter (Berntson and Taylor, 2000; Famiglietti, 1981; Mills and Massey, 1992; MacNeil et al., 2004; Schwartz et al., 2012), each 60 µm stimulus square is large enough to activate only one or two bipolar cells of a given type at each location. The narrow stratification of the dendrites, and the finding that excitation is driven exclusively through the ON pathway, make it likely that only one or two of the 5 types of ON bipolar cells make input to $PA_{1/3}$ cells. At each stimulus location, the average excitatory charge transfer ($\int I_{EPSC}\, dt$) measured from EPSCs was 24.0 ± 5.9% larger in the presence of SR + TPMPA when compared to control (Figure 3.6E). Thus, the total stimulus area required to evoke TTX-sensitive feedback (283,000 μm^2; 600 µm diameter spot) is ~80x larger than that needed to evoke SR/TPMPA-sensitive feedback (3600 μm^2; 60 µm square). These data suggest that each bipolar cell activates local reciprocal GABAergic feedback inhibition that limits the strength of feedforward excitation. Serial GABAergic inhibition from other WFACs can further modulate the feedback strength (Figure 3.5B-C).

Feedforward glycinergic and GABAergic inhibition operate on different spatial scales

In addition to modulating the excitatory inputs, inhibition also acts directly on $PA_{1/3}$ cells through both the OFF and ON pathways. In order to determine the neurotransmitters involved and examine the spatial scale of the inhibition, we recorded light-evoked inhibitory currents in the presence of different receptor antagonists.

OFF inhibition was mediated by both $GABA_A$ and glycine receptors, since their respective antagonists (SR and strychnine) reduced the OFF inhibitory conductance (Figure 3.7A-B), while applying both antagonists together fully eliminated it (Figure 3.7A, inset). A difference of Gaussians function was fit to the area response plots to estimate the spatial extent of the inhibition. The glycinergic and $GABA_A$ inhibitory components had different spatial dimensions. The glycinergic component, recorded in the presence of SR, had a spatial extent of ~534 μm (2λ, Figure 3.7A), which is similar in size to the $PA_{1/3}$ receptive field (2λ = 636 μm, Figure 3.2B). Assuming the glycinergic inputs arise from numerous overlying amacrine cells, and not a single concentric cell, this result suggests that the receptive fields of the glycinergic amacrine cells are narrow relative to the dendritic arbor of $PA_{1/3}$ cells. Thus, similar to the excitatory inputs from presynaptic bipolar cells, the extent of the glycinergic input is delineated by the $PA_{1/3}$ dendritic arbor. If the receptive fields of the glycinergic neurons were comparable to or larger than the RF center of $PA_{1/3}$ cells, then the glycinergic input would be activated over a correspondingly more extensive area, as is observed for the GABAergic inhibitory inputs. GABAergic inhibition was recorded in the presence of the glycine receptor antagonist strychnine and had a spatial extent of ~1.5 mm (2λ, Figure 3.7B), suggesting that it originates from overlapping WFACs that also cover large surrounding regions. These data are consistent with expectations from previous studies that have shown WFACs in mammalian retinas to be mostly GABAergic (Pourcho and Goebel, 1983), and narrow-field amacrine cells to be mostly glycinergic (Menger, 1998; Pourcho and Goebel, 1985).

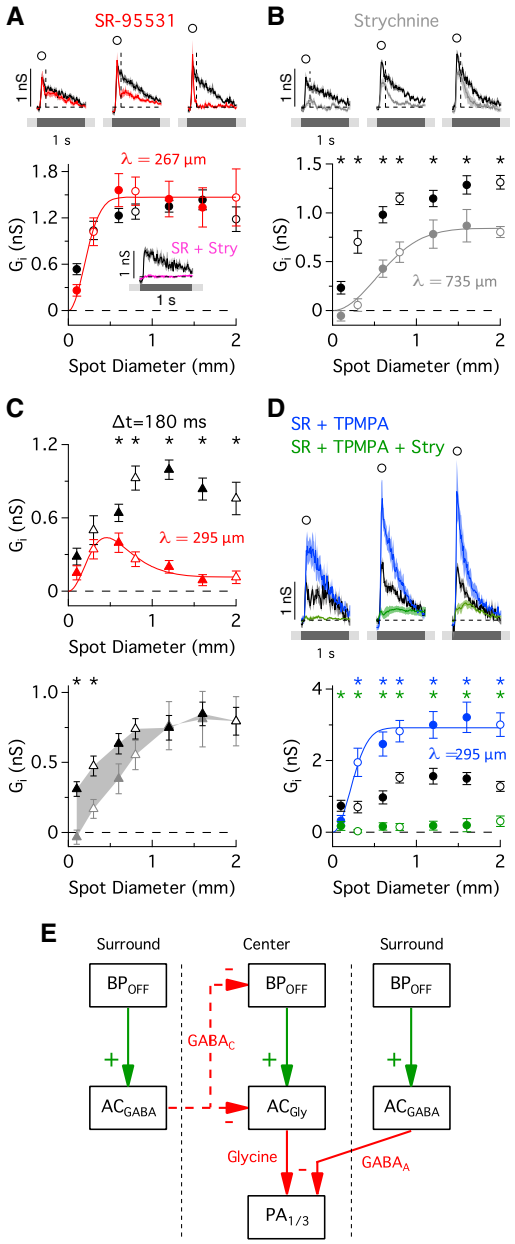

FIGURE 3.7. GABAERGIC AND GLYCINERGIC OFF INHIBITORY INPUTS.

A–**D**, Inhibitory conductances (top) are shown for stimulus diameters indicated by the open symbols in the area response curves (bottom) during application of SR (**A**, **C**, red; n = 16), strychnine (**B**, **C**, gray; n = 12), SR and TPMPA (**D**, blue; n = 5–7), and SR, TPMPA, and strychnine (**D**, green; n = 5–7). Data points were taken at the indicated time points in the conductance traces. **A**, Inset, Excitatory conductance in the presence of SR and strychnine (pink; n = 6) in response to a 600 µm diameter stimulus spot. Difference of Gaussians fits to the area response curves were used to estimate the spatial extent (space constant, λ) of the inhibitory inputs. **C**, Area response curves for SR (top) and strychnine (bottom) applications at a delayed time point, 180 ms after onset of a dark spot when SR had its greatest effect (the time point is indicated by the vertical dashed lines on the conductance traces in **A** and **B**). LEGEND CONTINUED ON NEXT PAGE →

$GABA_C$ mediated surround inhibition regulates the ON and OFF glycinergic inputs

The OFF glycinergic conductance, recorded during $GABA_A$ receptor blockade, became more transient as the size of the stimulus increased (Figure 3.7A, red traces). This behavior is illustrated by plotting the amplitude of the inhibitory conductance at a fixed time point 180 ms after light offset, when SR had its greatest effect (Figure 3.7C, top, red). The resulting area-response plot demonstrates that the glycinergic conductance is reduced to nearly zero in response to wide-field stimulation, and thus is subject to strong, but delayed surround suppression. In support of this finding, strychnine only blocked inhibition for small spot diameters at the delayed time point, indicating that the glycinergic conductance was not present during wide-field stimulation (Figure 3.7C, bottom). This putative surround inhibition of the glycinergic input was abolished by blocking $GABA_C$ receptors, which enhanced the OFF inhibition (Figure 3.7D, blue). Subsequent application of strychnine strongly suppressed this conductance, indicating that it was largely glycinergic. It is noteworthy that the estimate of the spatial extent of the glycinergic conductance was similar (λ = 250 - 300 μm) under several experimental conditions ($GABA_A$ receptor blockade in Figures 7A, 7C, red; $GABA_{A/C}$ receptor blockade in 7D, blue). Together, these data demonstrate that surround suppression of the OFF glycinergic inhibition is mediated by $GABA_C$ receptors, similar to the presynaptic suppression of excitation described above. A circuit model summarizing the data is shown in Figure 3.7E.

FIGURE 3.7 CONTINUED → **E**, Proposed minimal circuit diagram that can account for the effects that the GABAergic and glycinergic antagonists have on the OFF inhibitory conductance. Dashed red lines indicate alternative possibilities for mediating surround inhibition of the glycinergic inputs. BP, bipolar; AC, amacrine cell. *$p < 0.05$, Student's t test.

The inhibition observed during the ON phase of the stimulus was smaller and more variable across cells. The ON inhibition was completely suppressed by blocking glycine receptors (Figure 3.8A), and displayed a strong receptive field surround that was blocked by applying GABA receptor antagonists (Figure 3.8B). Although TPMPA alone did increase the inhibitory conductance for large stimulus diameters (not shown), blocking both $GABA_A$ and $GABA_C$ receptors produced a larger and more reliable effect. A circuit model summarizing the ON glycinergic inputs is shown in Figure 3.8C. We should emphasize that the circuit diagrams proposed in Figures 5, 7 and 8 are preliminary, and were constructed to contain the smallest number of connections that are consistent with the data.

Together, these data demonstrate that $PA_{1/3}$ cells receive feedforward glycinergic inhibition via both the ON and OFF pathways. Similar to the ON excitatory inputs, the OFF glycinergic

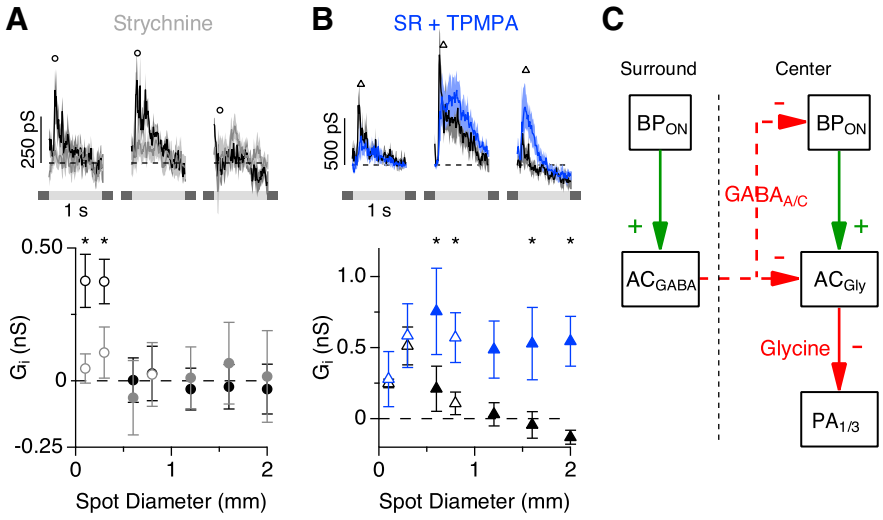

FIGURE 3.8. GABAERGIC INHIBITION CONTROLS THE SPATIAL EXTENT OF THE ON GLYCINERGIC INPUTS. ON Inhibitory conductances in the presence of strychnine (**A**, n = 12) and SR + TPMPA (**B**, n = 6). The time point when the drug had the greatest effect was used for the area response curves. In **A** it corresponds to the peak conductance (100 ms after light onset), while in B it corresponds to a slightly delayed time point (160 ms after light onset). **C**, Proposed minimal circuit diagram. Dashed red lines indicate alternative possibilities for mediating surround inhibition of the glycinergic inputs. *p < 0.05, Student's t test.

inhibition was suppressed by a $GABA_C$ mediated surround. In the case of the ON glycinergic inhibition, its surround receptive field is likely mediated by both $GABA_A$ and $GABA_C$ receptors. The extent of the presynaptic surround for the glycinergic inhibitory inputs was similar to that seen for the excitation.

Receptive field organization

Transmission from photoreceptors through bipolar cells is inherently nonlinear since bipolar cells typically display low levels of maintained glutamate release during steady background illumination. Therefore, increases in release during preferred contrast stimuli tend to be larger than decreases in release during non-preferred contrasts. Such rectification of bipolar cell output has been shown to produce nonlinear, "frequency-doubled" responses in Y-type ganglion cells during stimulation with a contrast reversing grating (Enroth-Cugell and Robson, 1966; Hochstein and Shapley, 1976; Troy et al., 1989; Demb et al, 2001). These nonlinear response properties allow Y-cells to respond to movement of fine textures with spatial dimensions smaller than the RF center, which enhances their sensitivity to motion. If $PA_{1/3}$ cells are like Y-cells, they will respond to randomly oriented fine textures in the visual scene indiscriminately, as null and preferred oriented gratings of high spatial frequency would provide approximately the same amount of positive contrast to drive the cell. In general, this would reduce the signal:noise for orientation signals. A potential solution to this problem is to sum contrast within the RF center linearly, so that positive and negative contrast signals cancel, producing little or no response to high spatial frequency stimulation.

To test the linearity of the contrast summation in $PA_{1/3}$ cells, we used a sinusoidal contrast reversing grating stimulus where the phase of the grating was systematically adjusted from one

trial to the next (Figure 3.9A). For a purely linear system there should be a null point, at which positive and negative contrast regions are equal and thus sum to zero. For each stimulus phase, spiking responses in $PA_{1/3}$ cells were measured as the integral of the peri-stimulus spike time histogram (PSTH) during a single contrast reversing cycle. PSTHs were accumulated for multiple cycles over several trials. As expected for linear summation, the response amplitude passed through a minimum when the bright and dark areas over the RF were approximately equal (phase = 0°; Figure 3.9A-B). However, a residual response at the null position was frequency-doubled, with the response at each half-cycle being approximately equal, as expected for nonlinear summation of contrast (Figure 3.9A). Spiking at the null point was reduced by 59.1 ± 5.8% (n = 6) relative to the phase that gave the maximal response (90° out of phase; Figure 3.9B), indicating a quasi-linear summation of contrast.

Mechanisms for generating a quasi-linear summation of contrast

The reduction in spiking at the null point in Figure 3.9B could be due to a spike threshold in $PA_{1/3}$ cells, partial linear summation of the synaptic inputs, or a combination of these and other mechanisms. A spike threshold could reduce responses at the null point, because a null-phase grating drives half of the receptive field with positive contrast at a given time, and therefore will produce smaller excitatory postsynaptic potentials (EPSPs) than a grating at the optimal phase, which delivers positive contrast across the entire receptive field, and thus is more likely to generate EPSPs that reach spike threshold. The quasi-linear summation of contrast may also result from postsynaptic summation of excitatory inputs, since the data in Figure 3.3F (green) shows that the excitatory conductance is modulated above and below a baseline level during positive and negative contrast phases of the stimulus, respectively. The reduction in the

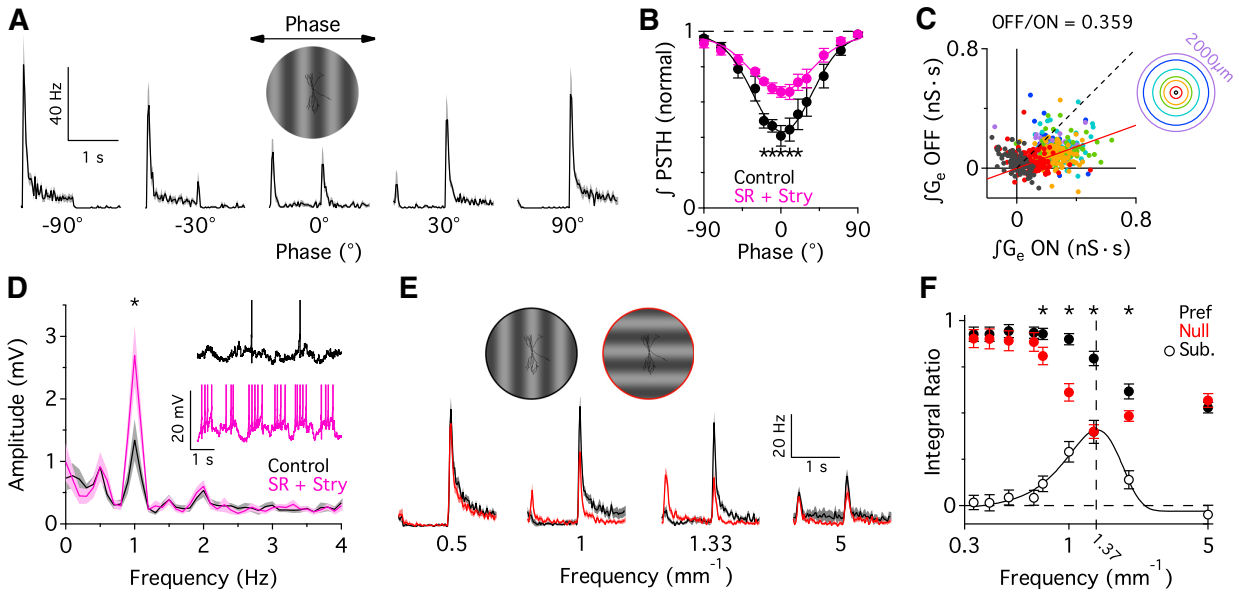

FIGURE 3.9. OFF INHIBITION AND TONIC ON EXCITATION CONTRIBUTE TO A QUASI-LINEAR SUMMATION OF CONTRAST.

A contrast reversing grating was used to probe the linearity of the input summation. **A**, PSTHs for a single contrast reversing cycle at different phases (grating positions relative to the soma; n = 8). Gratings were oriented in the 'preferred' orientation, parallel to the visual streak. **B**, Normalized integral of PSTH versus phase angle under control conditions and with inhibitory blockade (10 µM SR + 1 µM strychnine, pink, n = 6). **C**, Integrated excitatory conductance during positive vs. negative contrast stimuli (includes 7 stimulus diameters out to 2mm; n = 58-72). The reduction of the excitatory conductance in response to negative contrast is 35.9% of its increase in response to positive contrast (red fitted line). Colored rings indicate the stimulus spot size (100 µm – 2000 µm). **D**, Fourier analysis of voltage responses produced by a sine-wave, contrast reversing grating, with phase set to the null point (0°). The contrast reversal was sine-wave modulated at 0.5 Hz. Blocking inhibition (pink) produced a significant increase in the amplitude at 1 Hz ($p = 0.02$, n = 8). Inset, sample voltage responses from a single cell. **E**, PSTHs in response to contrast reversing gratings with antinodes centered over the soma (phase = 90º) for both preferred (parallel to the visual streak, black) and null (perpendicular to the visual streak, red) orientations over a range of spatial frequencies (n = 9). **F**, Integral ratio ($\int PSTH_{half\text{-}cycle}/\int PSTH_{whole\text{-}cycle}$) versus spatial frequency for both null and preferred oriented gratings (n = 25). Open circles are a subtraction between preferred and null oriented gratings, and is fit with a Gaussian function. *$p < 0.05$, Student's t test.

excitatory conductance during the negative phase was 35.9% as large as the increase during the positive phase (Figure 3.9C), indicating that the net excitatory input will be partially rectified, obviating perfect cancellation.

The inhibitory inputs show similar, but opposite rectification, since the amount of inhibition activated by negative contrast is larger than that activated by positive contrast (Figure 4.3F, red). Previous studies have shown that cross-over inhibition between the ON and OFF pathways is capable of producing more linear summation of contrast by effectively canceling concurrent excitatory currents (Molnar et al., 2009; Werblin, 2010). To examine the potential role of cross-over inhibition from the OFF pathway in generating quasi-linear summation of contrast in these ON-type $PA_{1/3}$ cells, we applied SR + strychnine to block $GABA_A$ and glycine receptors. Blocking inhibition caused an increase in the baseline spike rate from 1.0 ± 0.27 Hz to 6.4 ± 0.67 Hz (n = 6, p = 0.0001), but it also reduced the attenuation of the normalized spike rate at the null point (34.3 ± 3.0% attenuation versus 59.1 ± 5.8% under control conditions, p = 0.0004, n = 6; Figure 3.9B), suggesting that inhibition contributes to generating a more linear summation of contrast. Consistently, the addition of SR + strychnine during current clamp recordings increased the strength of frequency-doubling at the null point, as evident from a significant increase in the response amplitude measured at the second harmonic of the stimulus frequency (p = 0.02, n = 8; Figure 3.9D). Overall, our data suggests that modulation of tonic excitatory input from the ON pathway and cross-over inhibitory inputs from the OFF pathway enable $PA_{1/3}$ cells to integrate positive and negative contrast signals more linearly.

Orientation selective responses depend on stimulus structure

The elongation of the dendritic arbor, and the quasi-linear summation of contrast just described, underlie the orientation selectivity of $PA_{1/3}$ cells. It is obvious that $PA_{1/3}$ cells will be insensitive to the orientation of objects that are large relative to their dendritic extent (low spatial frequency limit). Similarly, high spatial frequency stimuli that are much finer than the dimensions of the

receptive field center will produce similar activation regardless of the orientation; however, the quasi-linear summation of contrast will reduce the overall responsiveness, resulting in a low-pass characteristic as a function of spatial frequency. The low-pass corner frequency will differ as a function of orientation due to the elongation of the receptive field, and therefore OS responses will be strongest over an intermediate range of frequencies, and are expected to display a bandpass characteristic as a function of spatial frequency.

To determine the range of spatial frequencies that produce OS responses, we tested the spatial frequency tuning along the major and minor axes of $PA_{1/3}$ cells. Spiking responses to sine wave contrast reversing gratings, with antinodes centered over the soma (phase = 90°), were recorded from $PA_{1/3}$ cells for spatial frequencies ranging from 0.33 to 5 cycles/mm. PSTH's at four spatial frequencies are shown in Figure 3.9E. As expected, the spike rate was insensitive to orientation for the lowest and highest spatial frequencies. However, the responses were OS over intermediate frequencies, where spike rates were larger and less frequency-doubled for preferred versus null oriented gratings. We estimated the range of spatial frequencies that produced OS responses by comparing the relative strength of frequency-doubled responses. For both preferred and null oriented gratings, we calculated the integral of the PSTH over the second half of the contrast reversing cycle as a fraction of the integral over the whole cycle. An integral ratio of 0.5 indicates a fully frequency-doubled response, whereas a value of 1 indicates responses in phase with the fundamental stimulus frequency. As expected, the transition from fundamental to frequency-doubled responses occurred at lower spatial frequencies for null oriented gratings (Figure 3.9F). The difference between the preferred and null tuning curves indicates a bandpass characteristic for orientation selectivity, with an optimal frequency of about 1.37 mm^{-1}. This

corresponds to a bar width of ~365 μm, which is close to the typical width along the minor axis of the dendritic arbor.

DISCUSSION

The results demonstrate that orientation selective responses in $PA_{1/3}$ cells arise from the elongation of the dendritic arbor, the arrangement of the excitatory inputs, and a quasi-linear summation of contrast in the RF center. We found that both local and wide-field serial feedback inhibition regulate the kinetics, gain, and spatial extent of the excitatory inputs. Direct inhibitory inputs from the OFF pathway contributed to the suppression of responses to high spatial frequencies, which optimized the generation of OS signals. The data demonstrate how synaptic inputs from the ON and OFF visual pathways can combine to tune neural responses to specific information in the visual input.

Anatomical comparison with other studies

PACs represent a well-conserved amacrine cell type that have been identified in primate, mouse, salamander, and rabbit retinas (Dacey, 1989; Famiglietti, 1992a-c; Stafford and Dacey, 1997; Völgyi et al., 2001; Ölveczky et al., 2003, 2007; Lin and Masland, 2006). In the rabbit retina, Famiglietti morphologically identified four different types of PACs (PA1-4), which differed in dendritic and axonal arbor size, branching, orientation, stratification depth, and soma position. Subsequently, Völgyi et al. (2001) surveyed the morphology and provided the first recordings of six different types of PACs (Types I-VI). $PA_{1/3}$ cells show the closest resemblance to Famiglietti's PA3 and Völgyi's Type V cells, although each has features not found in $PA_{1/3}$ cells. The main differences lie in the stratification of $PA_{1/3}$ dendrites in S3 (not found in Type V cells), the narrow

axonal stratification to the S3/4 border (PA3 cell axons stratify to multiple layers of the IPL), and the lack of spiking in response to negative contrast (exhibited by Type V cells). Thus, PA3 cells show the closest resemblance to $PA_{1/3}$ cells, however the differences in axonal stratification suggest that $PA_{1/3}$ cells likely represent a novel population.

Functional roles for $PA_{1/3}$ cells

Previous studies have shown that OS signals in ganglion cells are generated by the activity of presynaptic GABAergic amacrine cells (Venkataramani & Taylor, 2010). OS amacrine cells have been reported in the mammalian retina (Bloomfield, 1994), but here we describe the first example of an OS polyaxonal amacrine cell, which could be the source of the inhibition that drives OS responses in some ON-type ganglion cells (Levick, 1967). We show that orientation selectivity relies on two key properties of $PA_{1/3}$ cells. First is the morphology of the dendritic arbors, which are elongated parallel to the preferred orientation. Second is the quasi-linear summation of the synaptic inputs, which depends on the tonic excitatory drive from the ON pathway as well as inhibitory signals that cross over from the OFF pathway (Molnar et al., 2009; Werblin, 2010). The quasi-linear summation of contrast suppresses responses to high spatial frequencies, thereby preventing randomly oriented fine textures in the visual environment from inappropriately driving $PA_{1/3}$ cells.

An alternative functional role for $PA_{1/3}$ cells is suggested by the area-response measurements, which demonstrate that these cells have relatively weak surround receptive fields (Figure 3.2B). Consequently, they respond strongly to low spatial frequencies (Figure 3.9), where the responses are independent of orientation. Together, these receptive field properties would allow $PA_{1/3}$ cells to contribute to surround suppression in ganglion cells that have concentric center-surround

receptive fields. This idea is in line with studies showing that surround suppression depends on spiking activity in WFACs (Cook and McReynolds, 1998; Flores-Herr et al., 2001; Taylor and Wässle, 1999).

Previous analyses have concluded that PACs are involved in suppressing responses to global background motion in so-called objection motion sensitive (OMS) ganglion cells, namely the ON brisk transient and ON-OFF direction-selective ganglion cells in the rabbit, and the fast OFF ganglion cells in the salamander (Ölveczky et al., 2003, 2007; Baccus et al., 2008). To subserve this function, PACs should have sparse and transient signaling, nonlinear input summation, large receptive fields that are likely electrically coupled to other PACs, and receive little surround inhibition. $PA_{1/3}$ cells fulfill several of these requirements, except that they summate inputs quasi-linearly, and thus respond weakly to the high spatial frequency stimuli that have been shown to trigger OMS inhibition in the rabbit (Figure 3.9E; Ölveczky et al., 2003). Overall, it seems unlikely that generating OMS signals is the primary role of these cells.

Our discussion of the possible functional roles for $PA_{1/3}$ cells is based on data obtained under photopic background illumination. Recent work has shown that background illumination is a strong determinant of neural response properties in the retina (Tikidji-Hamburyan et al., 2015). For instance, the strength of surround inhibition (Hoggarth et al., 2015) and the linearity of a cell's response to contrast (Grimes et al, 2014) can vary dramatically depending on whether the light levels are in the scotopic or photopic range. Since morphological features largely determine OS sensitivity in $PA_{1/3}$ cells, it seems likely that this receptive field property would be robust against changes in background illumination; however, we cannot rule out the possibility that the characteristics of contrast summation in the RF center may change.

Inhibitory circuits in the ON and OFF pathways

The results show that inhibitory inputs to $PA_{1/3}$ cells arise from the ON and OFF pathways and consist of glycinergic and GABAergic components. The ON and OFF glycinergic inputs are restricted to the receptive field center, and receive $GABA_C$ receptor mediated surround inhibition (Figures 7-8). $GABA_C$ receptors are found primarily on bipolar cell axon terminals, and are rarely observed on postsynaptic dendrites (Wässle et al., 1998). Therefore it is likely that the $GABA_C$ mediated surround inhibition of the ON and OFF glycinergic inputs is formed via feedback onto presynaptic bipolar cell terminals, rather than by serial inhibitory connections.

We propose that the OFF inhibition contributes to a quasi-linear summation of contrast within the RF center such that negative contrast activates inhibition that reduces the cell's excitability and cancels excitatory input activated by positive contrast. For such a mechanism to work effectively at the highest spatial frequencies, the excitatory bipolar cells and inhibitory amacrine cells should have approximately equal spatial resolution. In this context, a possible role for the inhibitory surround observed for the OFF glycinergic amacrine cells is to adjust their spatial tuning to higher frequencies to better match the spatial frequency tuning of the excitatory bipolar cell inputs.

Mechanisms of GABAergic feedback inhibition

The opposing effects of $GABA_A$ and $GABA_C$ receptor antagonists on the excitatory conductance provided strong evidence for serial inhibition, which is commonly observed in the retina (Dowling and Boycott, 1966, 1968; Pourcho and Owczarzak, 1989; Chun and Wässle, 1989; Koontz and Hendrickson, 1990; Zhang et al., 1997; Marc and Liu, 2000; Eggers and Lukasiewicz, 2010, 2011; Chen et al., 2011). Blocking $GABA_A$ receptors reduced the duration of

the excitatory inputs, while blocking both $GABA_A$ and $GABA_C$ receptors increased the amplitude of the excitatory inputs and tended to extend their duration. We propose that these effects occur through serial inhibitory connections, such that disinhibition of a second amacrine cell enhances GABAergic feedback onto bipolar cell terminals (Figure 3.5F). Under GABAergic blockade, changes in the amplitude and duration of the excitatory inputs were reflected in altered spike rates, demonstrating considerable scope for serial GABAergic feedback to modulate physiological function. Since bipolar cell signals diverge onto multiple types of postsynaptic cells (Asari and Meister, 2014), the effects of feedback inhibition identified here likely influence the functional properties of many other amacrine and ganglion cells.

The effects of TTX revealed an additional spatial dimension to the control of excitatory inputs to $PA_{1/3}$ cells. Blocking action potentials only enhanced the excitatory conductance for large stimuli ($\geq$ 600 μm), whereas blocking GABAergic transmission enhanced excitatory inputs for stimuli similar in size to single bipolar cells (Figure 3.6). These results indicate that feedback inhibition onto cone bipolar cells presynaptic to $PA_{1/3}$ cells is active on two spatial scales. Short range inhibition is contributed by local microcircuits that use graded potentials, and long-range inhibition is driven by spiking WFACs in the surround. These characteristics are reminiscent of GABAergic inhibition onto rod bipolar cell terminals, which receive reciprocal feedback via graded potentials in A17 amacrine cells (Hartveit, 1999; Chavez et al., 2006; Grimes et al., 2010), as well as longer range lateral feedback inhibition from amacrine cells in the surround (Chavez et al, 2010). Having both local and wide-field inhibition regulate glutamate release from bipolar cells may allow for dynamic regulation of the gain and kinetics of bipolar cell output over a wide range of spatial scales.

ADDITIONAL EXPERIMENTS

In Chapter 3, we found that GABAergic feedback was operating on two different spatial scales using different mechanisms. Wide-field GABAergic feedback was driven by action potentials (i.e. it was TTX sensitive), whereas local GABAergic feedback was not. This result mirrors the two modes of GABAergic feedback that are found in rod bipolar cells, which receive local spike-independent feedback from A17 amacrine cells and spike-dependent feedback from unspecified wide-field amacrine cells (Chávez et al., 2010). This raised the question of whether spatially distinct feedback mechanisms were a common feature of most ganglion cell circuits. To address this question, I began recording EPSCs from a variety of known ganglion cell types in response to an expanding spot stimulus. By applying TTX first, I blocked spike-dependent feedback. Subsequent application of GABAR antagonists revealed the remaining GABAergic feedback that was spike-independent. Some ganglion cell types did have both mechanisms in place, whereas in other cell types it was less apparent. A general survey of the experimental results are presented in Figure 3.10.

To help limit my project goals, I decided to focus on the ON and OFF alpha ganglion cell types, and then eventually focused entirely on the OFF alpha ganglion cells. One of the obvious features of transient OFF alpha cells was that local, spike-independent GABAergic feedback was slow to rise and more sustained, whereas wide-field, spike-dependent GABAergic feedback was fast to rise and very transient. The spatial and kinetic differences between these two mechanisms were more apparent and reproducible in transient OFF alpha ganglion cells than in any other ganglion cell type I recorded from. The differing temporal properties led to our hypothesis that GABAergic feedback might play a role in temporal tuning. Indeed, we found that the role of

GABAergic feedback in temporal tuning is much more complex and dynamic than originally expected.

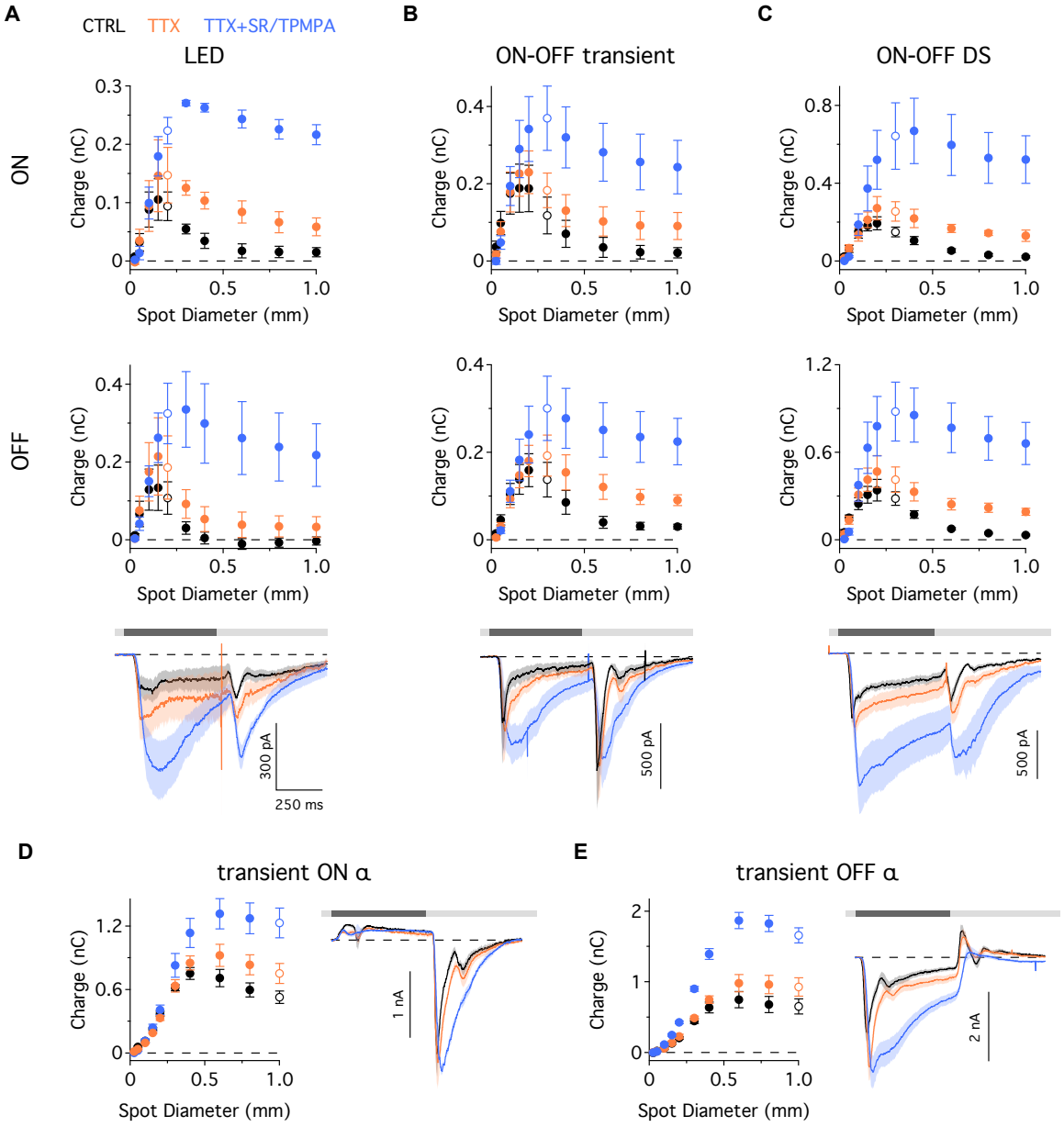

FIGURE 3.10. SPIKE-DEPENDENT AND SPIKE-INDEPENDENT FEEDBACK IN RETINAL GANGLION CELLS.

A-C, Charge transfer versus spot diameter for three ON-OFF type ganglion cells: local edge detector cells (**A**; n = 4), ON-OFF transient cells (**B**; n = 6), and ON-OFF direction selective cells (**C**; n = 4). ON response (top) and OFF responses (middle) are shown, as well as the underlying EPSCs (bottom) for the spot diameter indicated by the open circles in the area response plot. **D-E**, Same as in **A-C**, but for transient ON alpha (**D**; n = 5) and transient OFF alpha (**E**; n = 5) ganglion cells. Charge transfer versus spot diameter (left) and underlying EPSCs (right are shown. Stimulus timing and contrast (40%) is shown above the EPSCs.

CHAPTER 4

Mechanisms generating temporal tuning in transient OFF alpha ganglion cells have distinct frequency and contrast selectivities

Benjamin L. Murphy-Baum[1] and W. Rowland Taylor[1,2]

[1]Casey Eye Institute
Department of Ophthalmology
Oregon Health and Science University
Portland, OR 97239

[2]UC Berkeley School of Optometry
Minor Hall
University of California
Berkeley, CA 94720

[This manuscript is presented as prepared for submission to *Neuron* (2017)]

PREFACE

This chapter describes how presynaptic circuits generate the temporal receptive field properties of a specific ganglion cell type in the rabbit retina. I conducted this study under the mentorship and guidance of Dr. W. Rowland Taylor. I designed and performed the experiments, analyzed the data, and wrote the manuscript. Dr. Taylor provided guidance with experimental design, and assisted in the data analysis and the preparation of the manuscript.

This study builds upon the large body of work on alpha, or Y-type, ganglion cells that began in the 1960s. Early work focused on the nonlinear spatial summation that these cells possess, which then gave rise to many studies investigating the process of contrast gain control. Contrast gain control describes how increasing contrast reduces a ganglion cell's response per unit contrast, speeds up response kinetics, and shifts the temporal tuning to higher frequencies. Most recent work has attempted to refine existing computational models of contrast gain control. Here, we test the temporal tuning functions of transient OFF alpha ganglion cells under different pharmacological conditions. We identify the biophysical mechanisms that produce temporal tuning to higher frequencies; namely, Na_V activity in the presynaptic bipolar cells, GABAergic feedback inhibition through the OFF pathway, and glycinergic feedback inhibition through the ON pathway. Furthermore, this study provides evidence that GABAergic feedback has opposing functionality at different frequency bands due to a phase shift relative to excitation. This study provides much needed biophysical evidence for how temporal tuning is established in retinal ganglion cells.

SUMMARY

Most of the 30 or more ganglion cell types in the mammalian retina are sensitive to motion. Alpha ganglion cells, which have cellular homologues in most mammalian species, are particularly sensitive to rapid motion. Their selectivity for higher temporal frequency visual inputs represents one of the earliest descriptions of parallel signaling in the retina, yet its synaptic basis remains unclear. Here, we show that a convergence of excitatory and inhibitory synaptic mechanisms shift the temporal tuning of transient OFF alpha ganglion cells (t-OFF α) to higher temporal frequencies. OFF GABAergic feedback suppresses the excitatory input at low frequencies, but potentiates it at high frequencies. Crossover glycinergic feedback and sodium channel activity in the presynaptic bipolar cells also potentiate high frequency excitatory inputs. We found that these mechanisms have different spatiotemporal receptive field properties and contrast sensitivities. Their different stimulus selectivities allow these mechanisms to shift the temporal tuning of t-OFF α cells to higher frequencies and faster response kinetics over a wide range of visual conditions.

INTRODUCTION

Sensory systems encode the salient features of the physical environment. Because neural signals have limited bandwidth, sensory systems have evolved parallel circuit pathways that are each devoted to signaling a narrow range of the total sensory input (Schreiner et al., 2000; Tomchik et al., 2007; Galizia and Rössler, 2010). This is a prominent feature of the visual system, where each of the 30 or more types of retinal ganglion cells operate in parallel to detect different visual features before relaying those signals to the brain (Baden et al., 2016).

In the mammalian retina, alpha ganglion cells are sensitive to rapid motion in the visual scene, since they are bandpass-tuned to higher temporal frequencies in the visual input (Shapley and Victor, 1978) and have faster response kinetics than many other ganglion cell types (Baden et al., 2016). Their receptive field properties resemble those of upsilon (Petrusca et al., 2007) and parasol (Crook et al., 2008) ganglion cells of the primate retina, the latter of which comprise the magnocellular pathway, where lesions are associated with deficits in motion perception (Merigan et al., 1991). Their large and minimally overlapping receptive fields (Wässle et al., 1983) may allow alpha cells to improve temporal resolution through spatial integration; however, the synaptic mechanisms involved in optimizing their temporal tuning are not well understood.

Numerous mechanisms could contribute to establishing the temporal tuning of ganglion cell responses. Many of these mechanisms are localized to the presynaptic bipolar cells, where they shape the temporal properties of glutamate release. Bipolar cell glutamate release can be shaped through synaptic mechanisms such as inhibition from amacrine cells (Nirenberg and Meister, 1997; Dong and Werblin, 1998; Lukasiewicz and Shields, 1998; Flores-Herr et al., 2001; Eggers et al., 2007), or through intrinsic mechanisms such as the expression of different types of dendritic glutamate receptors (DeVries, 2000; Puller et al., 2013; Puthussery et al., 2014) and voltage-gated channels (Pan and Hu, 2000; Zenisek et al., 2001; Ichinose et al., 2005; Ma et al., 2005; Saszik and DeVries, 2012; Puthussery et al., 2013). The characteristics of exocytosis could also play a role (Awatramani and Slaughter, 2000; Baden et al., 2014). Although these mechanisms have been documented, little is known about how they interact to shape temporal tuning within specific neural circuits. This study demonstrates how multiple instances of inhibitory feedback, along with presynaptic sodium channel activity that likely originates in

bipolar cells, can operate synergistically to tune ganglion cell excitatory responses to higher temporal frequencies in the visual input.

RESULTS

Identifying transient OFF alpha ganglion cells in the rabbit retina

In the rabbit retina, four types of alpha ganglion cells can be distinguished: ON and OFF types come in both sustained and transient varieties (Caldwell and Daw, 1978). By contrast, only three types are found in the mouse retina, which seems to lack the transient ON type (Pang et al., 2003; van Wyk et al., 2009). Alpha cells can be selectively targeted for electrical recordings since they have the largest somas in the ganglion cell layer. The t-OFF α cells studied here can be differentiated from the sustained type by their lower background firing rates, higher maximum firing rates (van Wyk et al., 2009), and more transient light-evoked spiking responses (Pang et al., 2003; Murphy and Rieke, 2006). Their large receptive fields (λ_{exc} = 299 ± 25.6 μm, *n* = 12; difference of Gaussian fit, see Methods), weak surround suppression [spatial selectivity index (SSI) = 0.134 ± 0.022, *n* = 12; see Methods], and low input resistance (R_i = 20.6 ± 1.11 MΩ, *n* = 13; Figure 4.9) provide additional criteria to distinguish t-OFF α cells from other OFF-type ganglion cells. These attributes allow for the rapid and consistent identification of a single type of alpha ganglion cell (Figure 4.1A).

Excitatory inputs contribute to temporal tuning in t-OFF α ganglion cells

To measure the temporal receptive field properties of t-OFF α cells, we recorded light-evoked excitatory postsynaptic currents (EPSCs) at the chloride reversal potential (V_h = -70 mV; Figure 4.1B). t-OFF α cells were stimulated with a spot of light (1 mm diameter, 40% contrast),

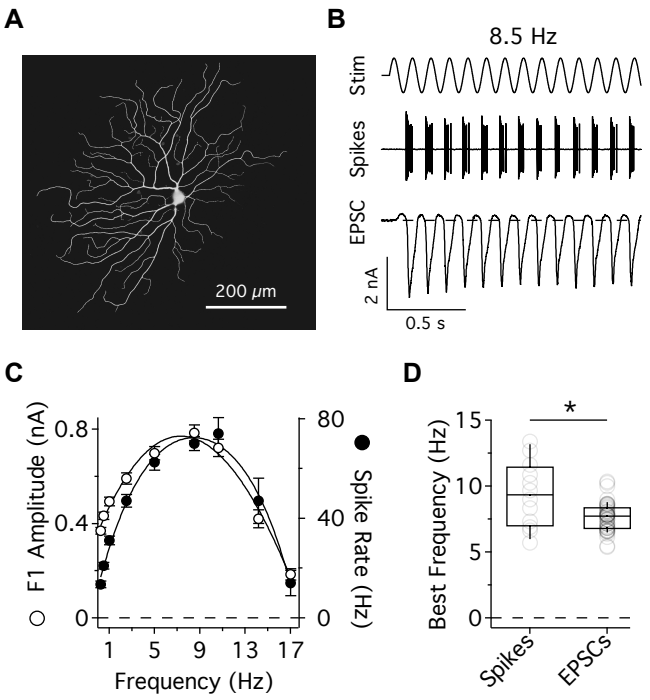

FIGURE 4.1. TEMPORAL TUNING OF t-OFF α GANGLION CELLS.

A, Confocal image of a t-OFF α cell filled with Neurobiotin. The cell was fixed soon after filling, so little gap junction coupling is seen. **B**, Spikes and excitatory postsynaptic currents (EPSCs) from a single cell in response to an 8.5 Hz sine wave modulated spot (1mm diameter, 40% contrast). **C**, Temporal tuning curve of spike rate (closed circles; $n = 12$) and the fundamental response (F1) amplitude of the EPSCs (open circles; $n = 45$). **D**, Stimulus frequency that evoked the largest response, calculated from the peak of a polynomial fit to the data in (**C**). Boxes include 25-75 percentiles, whiskers include 10-90 percentiles, and the horizontal line is the median. *$P < 0.05$, Student's t test.

centered over the receptive field, that was modulated as a sine wave at different temporal frequencies (0.25 – 17 Hz). EPSC amplitudes were estimated from their Fourier transform at the stimulus frequency (F1 amplitude; see Methods). The stimulus frequency that evoked that largest F1 amplitude—the best frequency—was estimated as the peak of a polynomial fit to the F1 amplitude versus frequency plots (see Methods; Figure 4.1C-D). For a 1 mm spot at 40% contrast, the best frequency was 7.67 ± 0.16 Hz ($n = 45$). The action potential output, recorded extracellularly, had a slightly higher best frequency (9.37 ± 0.72 Hz; $P = 0.03$, $n = 12$). Although

the best frequencies are significantly different, the data suggest that the excitatory input is tuned to relatively high frequencies, and is a major determinant of the ganglion cell's spike output (Schwartz et al., 2012). The following experiments examine the mechanisms that produce the temporal tuning of the EPSCs, which are driven by the presynaptic bipolar cells.

Na_V-dependent and Na_V-independent GABAergic feedback suppress the excitatory input at low temporal frequencies

The GABAergic inhibition that bipolar cells receive (Lukasiewicz and Shields, 1998; Eggers et al., 2007) can lead to more transient excitatory responses in downstream ganglion cells (Nirenberg and Meister, 1997; Dong and Werblin, 1998). However, the extent to which inhibitory feedback can produce higher temporal sensitivity in specific ganglion cell types remains unclear. To address this, we measured the temporal tuning of light-evoked EPSCs after blocking the $GABA_A$ (10 μM SR-95531) and $GABA_C$ (100 μM TPMPA) receptor types that are expressed on cone bipolar cell terminals (Euler and Wässle, 1998; Lukasiewicz and Shields, 1998). Bath application of the GABA receptor (GABAR) antagonists potentiated the F1 amplitude at low, but not high, temporal frequencies (Figure 4.2A-B). As a result, the neuron's best frequency was significantly lower compared to control (Control: 7.07 ± 0.23 Hz; SR/TPMPA: 3.43 ± 0.17 Hz; $P < 0.001$, $n = 13$; Figure 2C), suggesting that GABAergic inhibition is critical for tuning the excitatory input to higher temporal frequencies.

GABAergic amacrine cells typically have large receptive fields (Pourcho and Goebel, 1983). Consequently, many of these neurons depend on action potentials—and therefore voltage-gated sodium channel (Na_V) activity—to propagate inhibitory signals over long distances (Cook and McReynolds, 1998; Taylor, 1999; Flores-Herr et al., 2001; Shields and Lukasiewicz, 2003; Vigh

et al., 2011). We used the sodium channel blocker, TTX (200 nM), to test whether GABAergic feedback relies on sodium channel activity. To ensure that any effects of TTX were not due to blocking sodium channels on the postsynaptic ganglion cell, we included 3 mM QX-314 (intracellular Na_V blocker) in the electrode solution. Before presenting visual stimuli, we waited several minutes for QX-314 to diffuse throughout the cell. TTX potentiated the F1 amplitude at

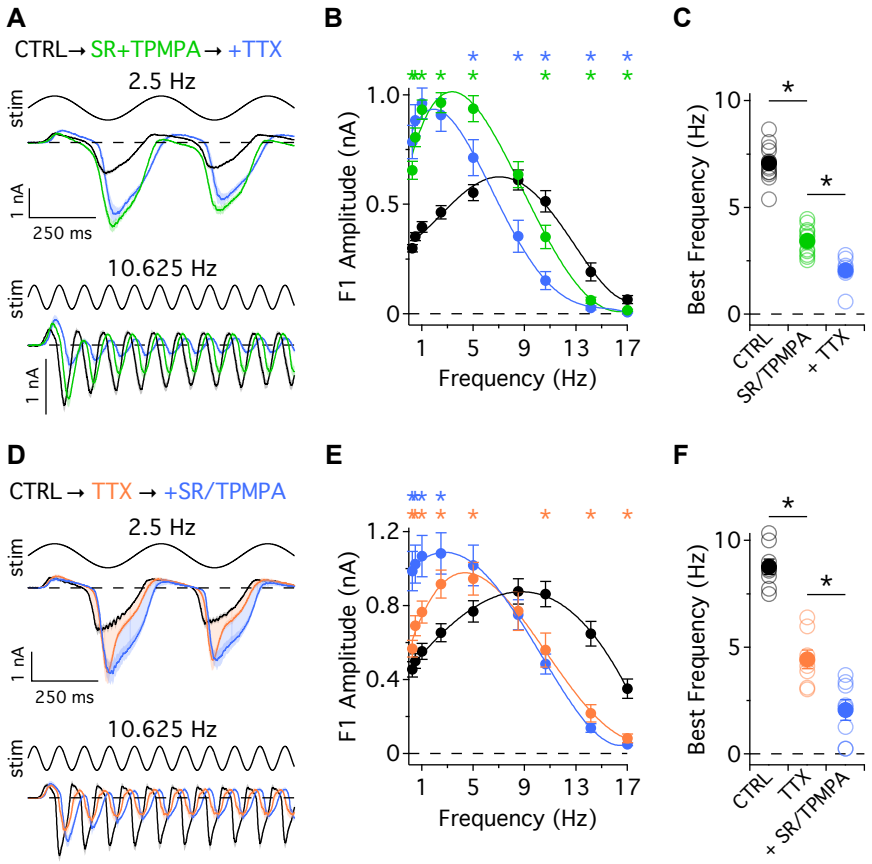

FIGURE 4.2. Na_V ACTIVITY DRIVES GABAERGIC FEEDBACK AT LOW TEMPORAL FREQUENCIES.
A, EPSCs in response to low and high frequency stimuli after $GABA_A$ and $GABA_C$ receptor blockade (10 µM SR-95531 and 100 µM TPMPA; green; $n = 13$) followed by subsequent sodium channel blockade (200 nM TTX, 10 µM SR-95531, and 100 µM TPMPA; blue; $n = 6$). **B**, F1 amplitude versus temporal frequency of the stimulus for the drug applications in (**A**). **C,** Best frequency for the drug applications in (**A**), calculated from the peak of polynomial fits to the data. **D**-**E**, Same as in (**A**) and (**B**), but the antagonists were applied in reverse order ($n = 8$). Shaded regions in (**D**) indicate Na_V-dependent (orange) and Na_V-independent (blue) effects. **F**, Best frequency for the drug applications in (**D**). *$P < 0.05$, Student's t test. Unpaired comparisons were made for the data in (**B**).

low frequencies, but suppressed it at high frequencies (Figure 4.2D-E). Similar to the GABAR antagonists, blocking sodium channels significantly reduced the neuron's best frequency (Control: 8.77 ± 0.35 Hz; TTX: 4.43 ± 0.43 Hz; $P < 0.001$, $n = 8$; Figure 4.2F).

If sodium channel activity is driving GABAergic feedback, then the effect of TTX should be occluded by blocking GABARs. At low frequencies, blocking GABARs fully occluded the effect of TTX on the EPSC amplitude (Figure 4.2A-B). However, blocking sodium channels only partially occluded the effect of GABAR blockade, indicating the presence of both Na_V-dependent (orange shading; Figure 4.2D, top) and Na_V-independent (blue shading; Figure 4.2D, top) GABAergic feedback. Both components of GABAergic feedback act to suppress the excitatory input during low frequency visual stimulation and shift the temporal tuning to higher frequencies (Figure 4.2C, F).

Na_V-dependent and Na_V-independent GABAergic feedback have different spatial properties

If the Na_V-dependent GABAergic feedback arises from wide-field spiking amacrine cells (Cook and McReynolds, 1998; Taylor, 1999; Flores-Herr et al., 2001; Shields and Lukasiewicz, 2003; Vigh et al., 2011), then it should be more spatially extensive than the Na_V-independent component, which presumably reflects local, and possibly reciprocal, feedback inhibition (Bieda and Copenhagen, 1999; Hartveit, 1999; Grimes et al., 2010). To test this prediction, we measured the area-response function of t-OFF α cells by recording EPSCs evoked by spots of different sizes (Figure 4.3). The two components of GABAergic feedback were isolated by first applying TTX to measure the Na_V-dependent component, and subsequently adding the GABAR antagonists to measure the remaining GABAergic feedback that was Na_V-independent. The

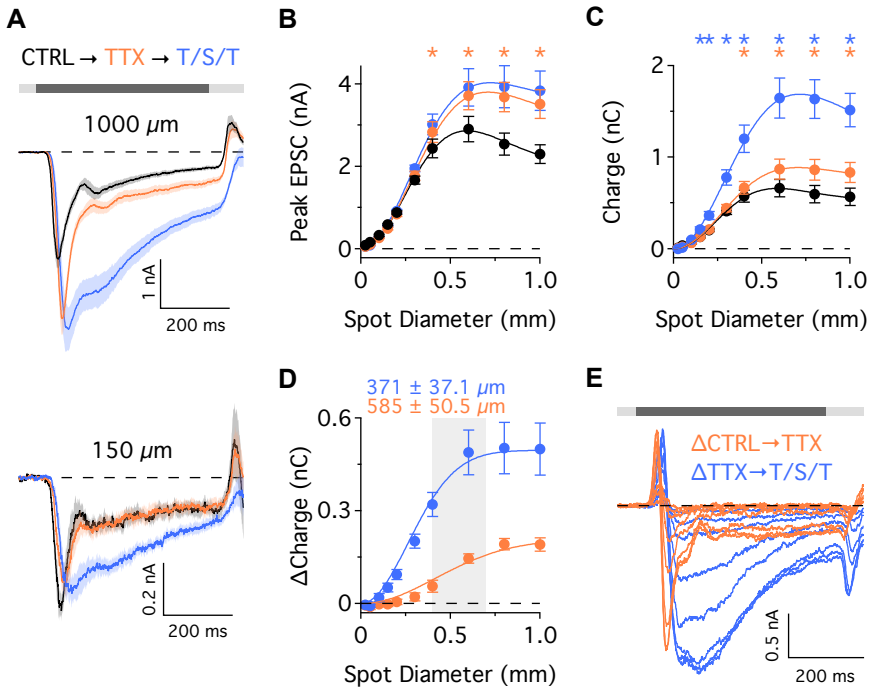

FIGURE 4.3. NAV-INDEPENDENT AND NAV-DEPENDENT GABAERGIC FEEDBACK OPERATE OVER DIFFERENT SPATIAL SCALES.

A, EPSCs in response to a negative contrast step for a 1000 µm (top) and 150 µm (bottom) diameter spot ($n = 7$) after sodium channel blockade (orange, TTX) followed by subsequent GABAR blockade (blue, T/S/T). Stimulus timing is indicated by the shaded bar above the graph. **B-C**, Peak EPSC amplitude (**B**) and total charge transfer (**C**) in response to spots of different sizes for the pharmacology in (**A**). **D**, Change in charge transfer during each subsequent drug application. Solid lines are difference of Gaussian fits to the data. Average space constants of the positive Gaussian used in the fits are quoted. The shaded region indicates the expected dendritic arbor size of OFF alpha cells at the eccentricity of the recordings (within 2-3 mm of the visual streak; Peichl, 1987). **E**, Difference EPSCs for each subsequent drug condition. *$P < 0.05$, Student's t test.

effects of TTX were only significant for spot diameters comparable to, or larger than, the receptive field center, while the Nav-independent component was active for stimulus diameters as small as 150 µm, well within the center receptive field (Figure 4.3A-D). It was also slower to activate and more sustained than the Nav-dependent component (Figure 4.3E). These data indicate that at low temporal frequencies, GABAergic feedback can be driven both by sodium

channel activity in wide-field amacrine cells, and by local, graded depolarizations that are independent of sodium channel activity.

GABAergic feedback potentiates the excitatory input at high temporal frequencies

Contrary to its effect at low temporal frequencies, blocking GABARs reduced the excitatory input at high frequencies (Figure 4.2A-B). This reduction in F1 amplitude was coupled with a shift in the F1 phase such that the EPSCs arrived later in the stimulus cycle (Figure 4.4A-C). These two frequency-dependent effects can occur if inhibition from amacrine cells arrives at bipolar cell terminals with some time delay relative to excitation from photoreceptors (Ratliff et al., 1969; Winters and Hamasaki, 1976; Gouras and Zrenner, 1979; Enroth-Cugell et al., 1983; Benardete and Kaplan, 1997; Kaplan and Benardete, 2001; Molnar and Werblin, 2007). For example, if inhibition is delayed by 20 ms, then it will be 180° out of phase with excitation if the modulation frequency is 25 Hz. In this scenario, inhibition will turn off as excitation turns on, causing it to potentiate (i.e. disinhibit) the ganglion cell's excitatory response rather than inhibit it.

We made a simple model to infer the properties of feedback inhibition that could account for the frequency-dependent changes in the F1 phase and F1 amplitude that occurred following GABAR blockade. The model assumes that the F1 component of the EPSC is the sum of two sine waves. The first sinusoid represents the isolated excitatory drive to bipolar cells from photoreceptors. The second sinusoid represents GABAergic feedback inhibition that arrives at the same bipolar cell terminals with some time delay. These signals are summed before being relayed as an excitatory input to the postsynaptic ganglion cell. The two input sinusoids can be directly compared to the experimental data. The excitatory sine wave is analogous to the EPSCs

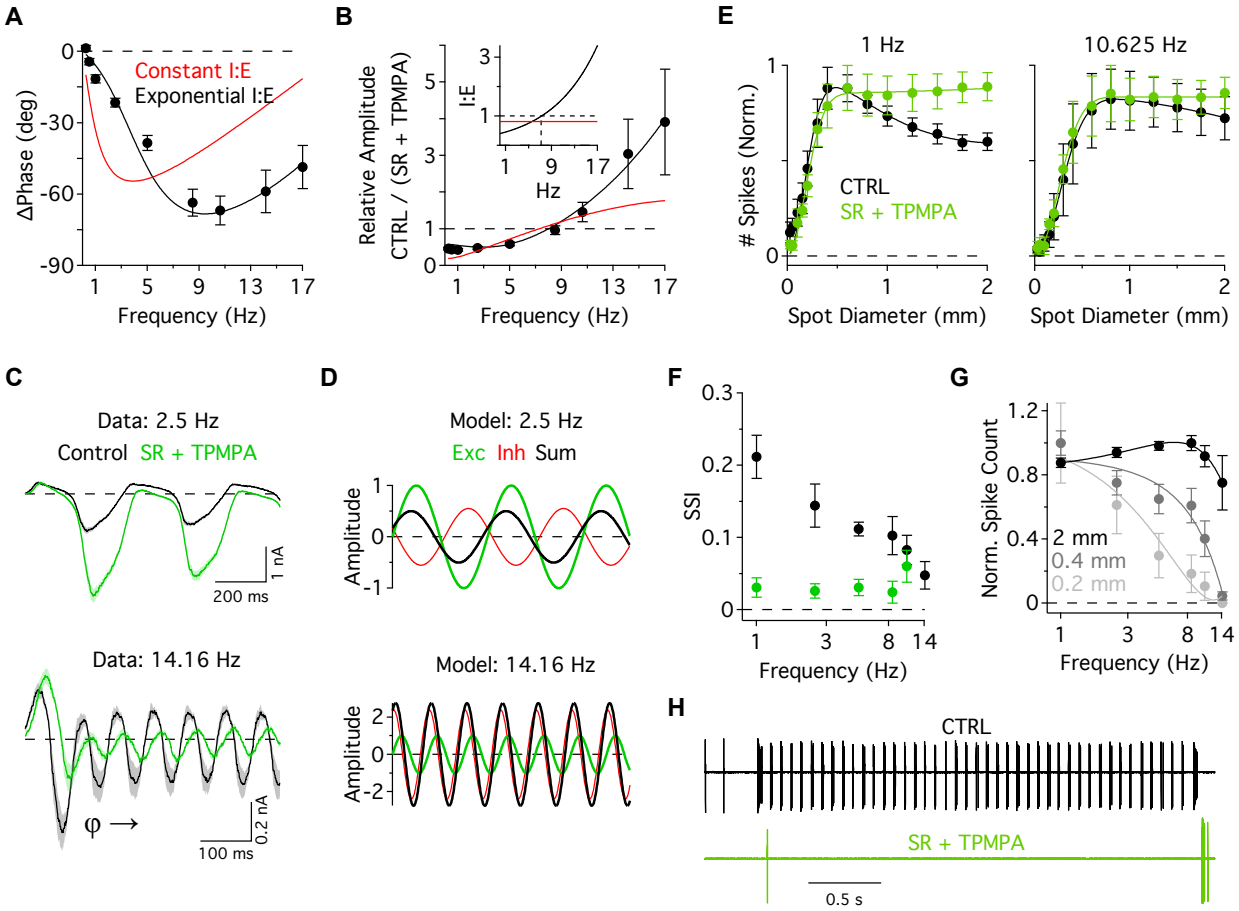

FIGURE 4.4. TEMPORAL DELAY BETWEEN EXCITATION AND INHIBITION CONTRIBUTES TO SPATIOTEMPORAL COUPLING.

A, Change in phase of the F1 component of the EPSCs following GABAR blockade. **B**, Ratio of F1 amplitudes under control conditions and following GABAR blockade. Red lines in (**A**) and (**B**) are the model fit to the data, using a constant I:E ratio across temporal frequency. Black lines are the same fit, but using an I:E ratio that varies as an exponential function with temporal frequency (See Supplemental Experimental Procedures). The resulting I:E ratios are shown in the inset of (**B**). **C**, EPSCs in response to a low (2.5 Hz) and high (14.16 Hz) frequency stimulus following GABAR blockade. **D**, The calculated excitatory (green), inhibitory (red), and summed (black) sine waves using the parameters from the model fit to the experimental data. **E**, Normalized spike count versus spot diameter for a 1 Hz or 10.625 Hz flickering spot at 40% contrast following GABAR blockade (n = 5). Solid lines are difference of Gaussian fits to the data. **F**, Spatial selectivity index (SSI) for the data in versus temporal frequency for the data in (**E**). **G**, Normalized spike count versus stimulus frequency for three different spot sizes (n = 10). **H**, Spiking response to a 1 mm diameter, 14.16 Hz stimulus after GABAR blockade.

recorded after GABAR blockade (Figure 4.4C-D, green), whereas the summed sine wave (excitation + inhibition) is analogous to the EPSCs recorded under control conditions (Figure

4.4C-D, black).

Initially we assumed that the excitatory and inhibitory signals had identical temporal tuning properties. We fit the data by allowing the time delay and the relative amplitude of the inhibitory and excitatory sine waves (I:E ratio) to vary. The two parameters were fit simultaneously to the phase and amplitude data shown in Figures 4A and 4B. This model was unable to accurately capture the changes in phase and amplitude that occurred following GABAR blockade (Figure 4.4A-B, red line). Therefore, we considered the possibility that the excitatory and inhibitory signals had different temporal tuning properties (Frishman et al., 1987). This would result in an I:E ratio that varied as a function of temporal frequency. Since the temporal tuning curves are well-approximated by Gaussian functions, we allowed the I:E ratio to vary as the ratio of two Gaussian functions with different best frequencies. This resulted in an exponential relationship between I:E ratio and temporal frequency (Figure 4.4B, inset). In order to constrain the model, we assumed that the temporal tuning curve of the excitatory sine wave was the same as the tuning curve measured following GABAR blockade (Figure 4.2B, green). The width (10.6 Hz) and best frequency (3.8 Hz) of the fitted Gaussian were used as fixed parameters in the model. We allowed the width and best frequency of the unknown inhibitory temporal tuning curve to vary along with the time delay between inhibition and excitation. This model produced a good empirical fit (Figure 4.4A-B, black lines), and indicated that the data could be accounted for if the best frequency for inhibition was ~6.8 Hz higher than excitation, with a time delay of 19.7 ms. The latter value is similar to previous estimates (Winters and Hamasaki, 1976; Gouras and Zrenner, 1979; Enroth-Cugell et al., 1983; Benardete and Kaplan, 1997; Molnar and Werblin, 2007; Cui et al., 2016).

Using the converged fit parameters, we generated the underlying sine waves for excitation, inhibition, and their summation (Figure 4.4D). These compared well with the EPSCs recorded under control conditions (analogous to the 'sum' sine wave) and following GABAR blockade (analogous to the excitatory sine wave). Overall, the model suggests possible dynamic properties for presynaptic inhibition; inhibition is weaker than excitation at low temporal frequencies and is suppressive, but is stronger than excitation at higher frequencies and becomes disinhibitory.

GABAergic signaling contributes to spatiotemporal coupling

The phase delay between excitation and inhibition has been implicated in weakening both color-opponent (Gouras and Zrenner, 1979) and spatial (Ratliff et al., 1969; Derrington and Lennie, 1982; Enroth-Cugell et al., 1983; Dawis et al., 1984; Frishman et al., 1987) surround receptive fields in ganglion cells at high temporal frequencies. We observed the latter phenomenon by recording spiking activity while presenting t-OFF α cells with spots of different sizes (Figure 4.4E). The spots were sine-wave modulated over a range of temporal frequencies. The strength of the surround receptive field, as measured by the spatial selectivity index (SSI; see Methods), became weaker with increasing temporal frequency (Figure 4.4F). Moreover, the spiking response to high temporal frequency stimuli was attenuated when the stimulus spot was confined to the center receptive field. Larger spots that stimulated both the center and surround evoked spikes at much higher temporal frequencies (Figure 4.4G). These data demonstrate the familiar trade-off between spatial and temporal resolution in ganglion cells (Derrington and Lennie, 1982; Enroth-Cugell et al., 1983; Dawis et al., 1984; Frishman et al., 1987; Benardete and Kaplan, 1997; Kaplan and Benardete, 2001).

Notably, blocking GABARs decreased the SSI for low and intermediate temporal frequencies, effectively eliminating the relationship between spot size and temporal frequency. In other words, under GABAR blockade, the area response curves retained more or less the same shape across temporal frequency (Figure 4.4E). Moreover, cells were unable to fire action potentials in response to the 14.16 Hz stimulus in the presence of the GABAR antagonists, suggesting that GABAergic disinhibition is critical for driving spiking at these higher temporal frequencies (Figure 4.4H).

Presynaptic Na_V activity boosts the excitatory input at high frequencies

Similar to the GABAR antagonists, TTX suppressed the F1 amplitude at high temporal frequencies (Figure 4.2A-B) and delayed the phase (Figure 4.10). It's possible that these effects reflect GABAergic mechanisms, since sodium channel activity can drive GABAergic inhibition (Figures 4.2 and 4.3). However, GABAR blockade did not fully occlude the effect of sodium channel blockade on either the F1 amplitude (Figure 4.2) or the F1 phase (Figure 4.10). These GABAR-independent effects of TTX might be explained by the presence of sodium channels in the presynaptic bipolar cells, which could boost depolarizations, leading to larger and faster postsynaptic EPSCs (Pan and Hu, 2000; Ichinose et al., 2005; Saszik and DeVries, 2012; Puthussery et al., 2013). Knowing that a component of GABAergic feedback is driven by sodium channel activity, we re-examined how TTX affects the EPSCs following GABAR blockade over a range of stimulus frequencies (1, 5, and 10.625 Hz). Although TTX reduced the EPSC amplitude during its rising phase at all frequencies (Figure 4.5A), it only reduced the F1 amplitude at high frequencies (Figure 4.5C). One possible explanation is that at low frequencies, the stimulus cycle is long relative to the time course of sodium channel activation, and thus

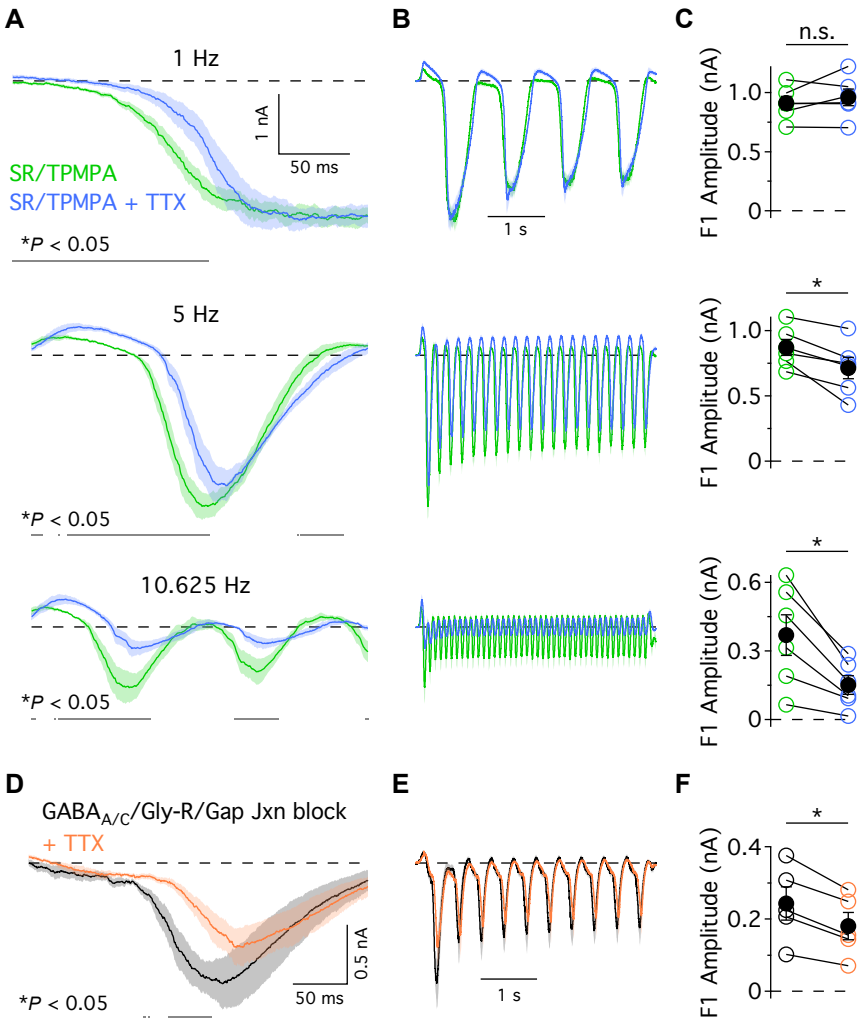

FIGURE 4.5. NAV ACTIVITY ONLY SUPPRESSES PEAK EPSC AMPLITUDES AT HIGH TEMPORAL FREQUENCIES.
A, Expanded timescale of the EPSCs in (**B**) after GABAR blockade (green), followed by subsequent sodium channel blockade (blue; $n = 6$). EPSCs for three temporal frequencies are shown, all at 40% contrast. In (**A**), time points where statistical comparisons between the two conditions reached $P < 0.05$ (Student's t test) are marked below the EPSCs. **C**, F1 amplitude of the EPSCs under each drug condition. **D**, EPSCs after GABA receptor, glycine receptor, and gap junction blockade (black), and with subsequent sodium channel blockade (orange). Stimulus was 2.5 Hz, 40% contrast. **E**, Expanded time scale of the EPSCs in (**D**). **F**, F1 amplitude for the EPSCs under each drug conditions in **D**-**E**. *$P < 0.05$, Student's t test.

blocking sodium channels delays the rise but has little effect on the peak EPSC amplitude (Figure 4.5B-C). At higher frequencies, sodium channels are presumably still active during peak

inward currents due to the shorter stimulus cycle, and TTX is able to reduce the peak EPSC amplitude.

However, TTX could affect the F1 amplitude by blocking sodium channels at other locations within the retinal circuitry. First, OFF cone bipolar cells receive inhibitory inputs from glycinergic AII amacrine cells (Marc et al., 2014), which are known to express sodium channels and exhibit spiking activity (Boos et al., 1993; Tamalu and Watanabe, 2007; Tian et al., 2010; Trenholm et al., 2012). Second, in principle, sodium channels in serially arranged glycinergic amacrine cells could produce a disinhibitory effect on bipolar cell terminals. Third, alpha ganglion cells are coupled to both ganglion and amacrine cells via gap junctions (Xin and Bloomfield, 1997; Schubert et al., 2005; Völgyi et al., 2005). Blocking sodium channel activity in these coupled neurons could conceivably reduce the excitatory input to t-OFF α cells at high frequencies.

To further test the hypothesis that sodium channels in bipolar cells are boosting the excitatory input, we attempted to isolate the excitatory input from bipolar cells. To this end, we recorded EPSCs while blocking $GABA_{A/C}$ receptors (10μM SR-95531, 100 μM TPMPA), glycine receptors (GlyRs; 0.5 μM strychnine), and gap junctions [100 μM meclofenamic acid (MFA)]. MFA was pre-applied to the retina for at least 20 minutes before establishing a whole-cell recording to ensure complete wash-in of the drug (Veruki and Hartveit, 2009). The GABAR and GlyR antagonists were washed in after the start of the recording. In the presence of these antagonists, the addition of TTX still reduced the EPSC amplitude during its rising phase (Control inhibitory cocktail: 890 ± 151 pA; +TTX: 333 ± 76.6 pA; $P = 0.011$, $n = 5$; Figure 4.5D), and reduced the F1 amplitude (Control inhibitory cocktail: 244 ± 46.5 pA; +TTX: 180 ±

37.9 pA; $P = 0.003$, $n = 5$; Figure 4.5F). Together, these data suggest that a significant portion of the sodium channel activity that boosts the excitatory input at high temporal frequencies is localized to the presynaptic bipolar cells.

Glycinergic crossover inhibition boosts excitatory signals

Most OFF cone bipolar cells receive glycinergic crossover inhibition from the ON pathway (Grünert and Wässle, 1996; Maple and Wu, 1998; Molnar and Werblin, 2007; Marc et al., 2014). Due to its sign inversion relative to excitation (ON versus OFF pathway), crossover feedback inhibition tends to reinforce light-evoked voltage changes in OFF bipolar cells (Molnar and Werblin, 2007; Molnar et al., 2009). However, it is unclear how crossover feedback influences temporal tuning in downstream ganglion cells.

We found that the application of either strychnine—a selective GlyR antagonist—or L-AP4—a mGluR6 receptor agonist and ON pathway blocker—reduced the light-evoked outward current in t-OFF alpha cells, consistent with a reduction in crossover feedback inhibition (Figure 4.6A-B). Inward currents were also reduced, albeit to a lesser extent. Both treatments reduced the F1 amplitude at all frequencies (Figure 4.6C-D), although the L-AP4 data indicates that higher frequency inputs are reduced to a greater extent (Figure 4.6E), consistent with the observed reduction in best frequency (Figure 4.6F). The effects of blocking the ON pathway had a moderate contrast dependence; F1 amplitudes were reduced more significantly at high contrast, regardless of the modulation frequency (Figure 4.11). The changes in phase that occurred with GlyR or ON pathway blockade were small, and largely due to reductions in the outward current during positive contrast transitions, making crossover inhibition unlikely to be responsible for the changes in phase induced by GABAR or Na_V blockade.

In summary, glycinergic signals from the ON pathway contribute to the excitatory input by disinhibiting OFF bipolar cells. They make a minor contribution to temporal tuning by boosting signals at higher temporal frequencies. By comparison, GABAR or sodium channel blockade produced much stronger reductions in the best frequency (Figure 4.2C, F).

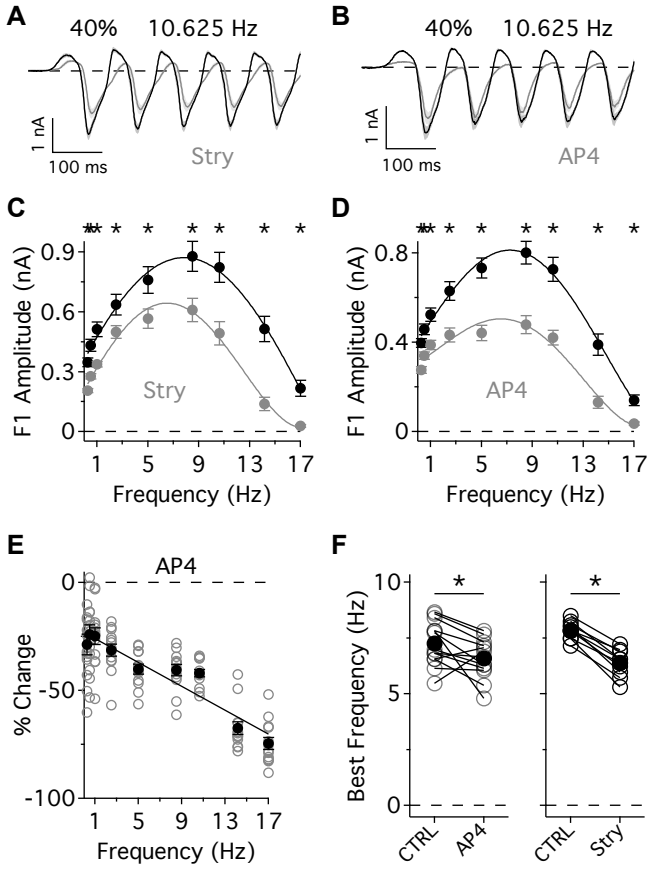

FIGURE 4.6. CROSSOVER GLYCINERGIC FEEDBACK FROM THE ON PATHWAY SHIFTS TEMPORAL TUNING TO HIGHER FREQUENCIES.

A-**B**, Average EPSCs after glycine receptor (0.5 µM strychnine; *n* = 10) or ON pathway (50 µM L-AP4; n = 13) blockade for an 8.5 Hz stimulus at 40% contrast. **C**-**D**, F1 amplitude versus frequency for strychnine and L-AP4 applications. **E**, Percent change in F1 amplitude versus frequency during ON pathway blockade with L-AP4. Solid line is a linear fit to the data. **F**, Best frequency for L-AP4 and strychnine applications.

Temporal tuning mechanisms have different contrast sensitivities

Y-type (alpha) ganglion cells have been used as a model cell type to study the mechanisms of contrast gain control, which is characterized by a reduction in the gain of ganglion cell responses after a sudden increase in contrast (Shapley and Victor, 1978, 1979b; Enroth-Cugell and Freeman, 1987; Benardete and Kaplan, 1999; Demb et al., 2001; Kim and Rieke, 2001; Zaghloul et al., 2005; Cui et al., 2016). However, these changes in gain vary across temporal frequency, since increases in contrast speed up responses and shift the temporal tuning of Y cells to higher frequencies (Shapley and Victor, 1978; Shapley and Victor, 1979b; Enroth-Cugell and Freeman, 1987; Benardete and Kaplan, 1999). Because contrast can influence the temporal tuning and kinetics of ganglion cell responses, we tested how contrast affects the GABAergic and Na_V-dependent mechanisms identified here.

Light-evoked EPSCs were measured over a wide range of contrasts (2-80%), each tested over our standard range of temporal frequencies (0.25-17 Hz). Average contrast response functions are shown for three different temporal frequencies in Figure 3.7A. The complete data from these experiments are displayed as contour plots, with the average F1 amplitudes (z/color axis; $n = 8$) plotted as a function of the contrast and temporal frequency of the visual stimulus (Figure 4.7B-D, left column). For orientation purposes, the F1 amplitude versus frequency data presented in Figure 2E represents a horizontal slice through the contour plots at 40% contrast.

We bath-applied TTX to measure the contribution of Na_V-dependent mechanisms to the excitatory input (Figure 4.7C). To visualize the absolute changes in the F1 amplitude across this stimulus space, we subtracted the TTX data from control (Figure 4.7E, difference contour). This illustrates how sodium channel activity contributes to the excitatory input: it boosts responses at

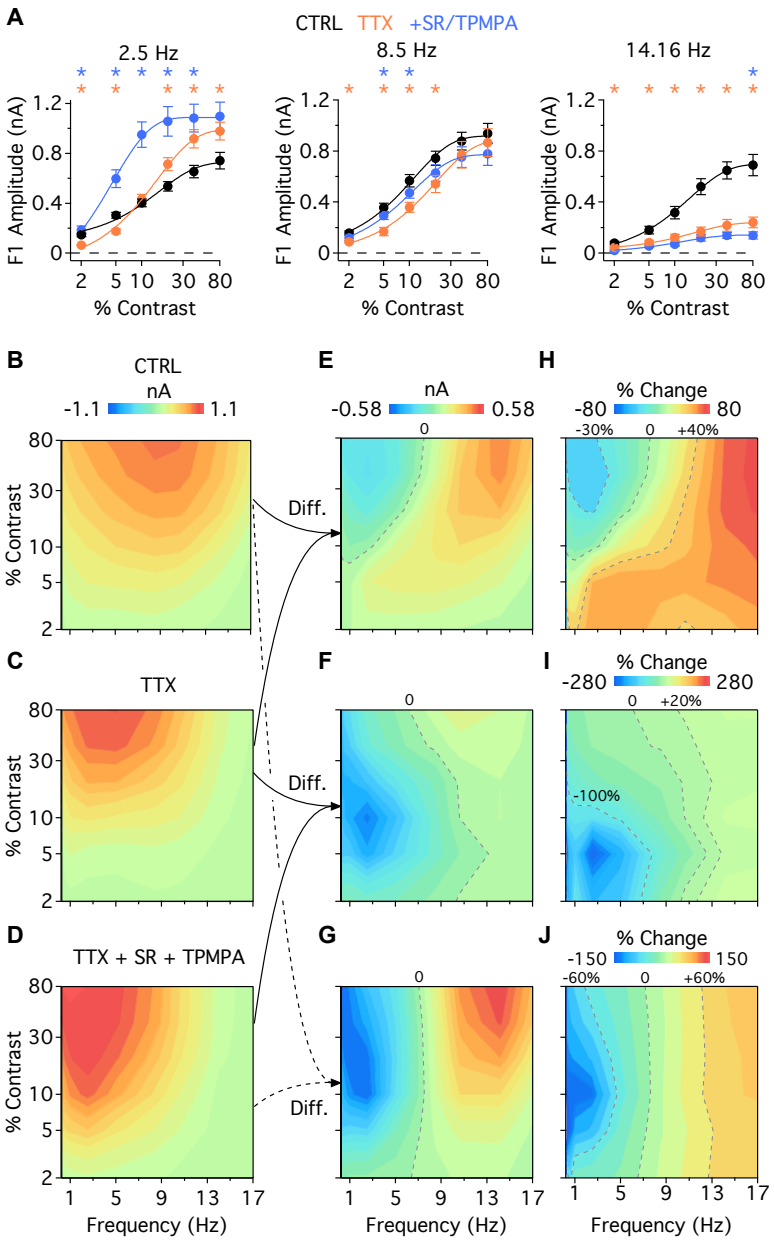

FIGURE 4.7. INFLUENCE OF Na_V ACTIVITY AND GABAERGIC FEEDBACK DEPENDS ON BOTH TEMPORAL FREQUENCY AND CONTRAST.

A, Average F1 amplitudes versus contrast for three different temporal frequencies in the presence of TTX (orange), followed by subsequent GABAR blockade (blue; $n = 8$). **B-D**, Average contour plots of F1 amplitude (color, z axis) versus the contrast (y axis) and temporal frequency (x axis) of the visual stimulus ($n = 8$). **E-G**, Difference contour plots of the F1 amplitude for the indicated drug condition. **E**, Control minus TTX. **F**, TTX minus TTX/SR/TPMPA. **G**, Control minus TTX/SR/TPMPA. Dotted lines are the zero contour on each plot. **H-J**, Percent change contour plots for the same drug conditions indicated in (**E-G**). Select contours are marked with dotted lines. *$P < 0.05$, Student's t test.

high frequencies across all contrasts (orange/red regions; Figure 4.7E), and suppresses responses at low frequencies and high contrast (green/blue regions; Figure 4.7E). The data in Figure 2 shows that sodium channels drive GABAergic feedback at low temporal frequencies, leading to a suppression of the excitatory input. The present data, however, shows a strong contrast dependence to this mechanism: it is only active at high contrast.

Subsequent GABAR blockade revealed any remaining GABAergic mechanisms that act independently of sodium channel activity (Figure 4.7D). The difference contour plot shows that Na_V-independent GABAergic inhibition acts to suppress the excitatory input primarily at low and intermediate contrasts (Figure 4.7F). These data indicate that the Na_V-dependent and Na_V-independent components of GABAergic feedback suppress the excitatory input not only over different spatial domains (Figure 4.3), but also over different contrast ranges.

At high frequencies, Na_V-dependent mechanisms were almost entirely responsible for potentiating the excitatory input at all contrasts. Notably, the combined effect of Na_V-dependent mechanisms and GABAergic mechanisms (subtracting Na_V + $GABA_{A/C}$ block from control) is to suppress the excitatory input at low frequencies and potentiate it at high frequencies relatively independently of contrast (Figure 4.7G). This is even more apparent in the corresponding percent change plots, which provide a clearer look at the contrast dependence of the various processes (Figure 4.7H-J). Importantly, blocking both sodium channels and GABARs reduced the neuron's best frequency at every contrast (Figure 4.12). Thus, the distinct stimulus selectivities of these mechanisms enable t-OFF α cells to have higher frequency temporal tuning over a wide range of contrasts.

The changes in phase exhibited similar contrast sensitivities to the changes in amplitude. Na_V-dependent phase advance was most prominent at high contrast (Figure 4.13A, CTRL - TTX), whereas Na_V-independent GABAergic phase advance was present primarily at low and intermediate contrasts (Figure 4.13B, TTX – T/S/T). The Na_V-dependent phase advance was at least partially due to GABAergic signaling, since blocking GABARs in isolation shifted the phase at both low and high contrast (Figure 4.13D). Thus, Na_V-dependent and Na_V-independent GABAergic mechanisms act synergistically to advance the phase of the excitatory input independently of contrast (Figure 4.13C, CTRL – T/S/T).

DISCUSSION

The spatiotemporal properties and contrast response functions of alpha ganglion cells have been studied for decades (Enroth-Cugell and Robson, 1966). It has long been known that alpha cells are bandpass tuned to higher frequencies (Shapley and Victor, 1978), have fast kinetics, and have a high axonal conduction velocity (Cleland et al., 1971), all of which implicate them as contributing to fast motion detection. Although many labs have modeled the responses of these cells (Shapley and Victor, 1981; Enroth-Cugell and Freeman, 1987; Frishman et al., 1987; Victor, 1988; Zaghloul et al., 2005; Cui et al., 2016), the present study is the first to provide a detailed description of the underlying circuitry and specific neurotransmitters that allow alpha cells to detect rapid changes in the visual input. To this end, we identified three inhibitory feedback mechanisms that are distinguishable based on their neurotransmitter (GABA versus glycine), visual pathway (OFF versus ON), TTX sensitivity, spatial extent, temporal tuning, and contrast sensitivity. Feedback inhibition shifts the temporal tuning of the excitatory input to higher

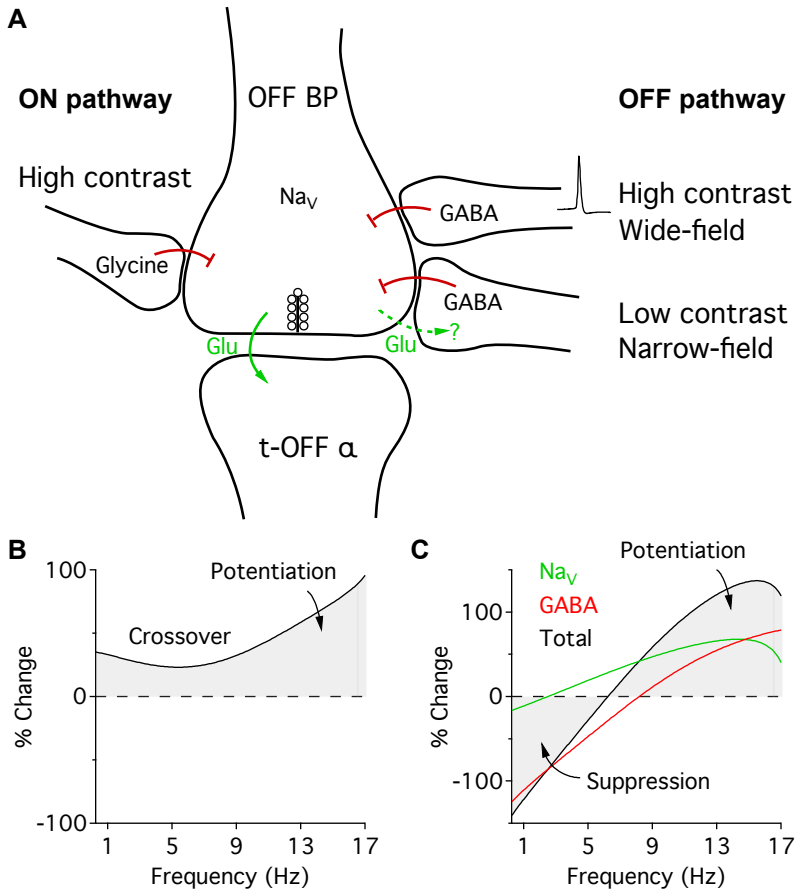

FIGURE 4.8. MECHANISMS OF TEMPORAL TUNING IN t-OFF α CELLS.

A, Potential synaptic arrangement of GABAergic and glycinergic feedback inhibition, and their stimulus selectivities. Dotted arrow indicates that Na_V-independent GABAergic feedback might operate using reciprocal synapses, but this remains unclear. **B-C**, Frequency dependence of temporal tuning mechanisms. **B**, Contribution of crossover inhibition to the excitatory input expressed as percent change from control. Solid lines were calculated as the percent change between polynomial fits to the F1 amplitude versus frequency data in Figure 6D. **C**, Contribution of GABAergic and bipolar-expressed Na_V activity to the excitatory input. Solid lines were calculated as in (**B**), but using the polynomial fits in Figure 2B. 'Na_V' is the contribution of Na_V activity in the presynaptic bipolar cells, 'GABA' is the contribution of GABAergic feedback as a whole, and 'Total' is the summed contribution of both mechanisms.

frequencies by suppressing low frequency inputs via the OFF pathway (GABA; Figure 4.2), and by boosting high frequency inputs via the ON pathway (glycine; Figure 4.6). A simplified model suggests that OFF GABAergic disinhibition potentiates high frequency inputs due to its temporal delay relative to excitation (Figure 4.4). In addition, we identified sodium channel activity that

potentiates the excitatory input at high frequencies independently of GABAergic, glycinergic, or gap junctional signaling (Figure 4.5). Thus, we localized this sodium channel activity to the presynaptic bipolar cells. Together, these mechanisms shift the temporal tuning of t-OFF α cells to higher frequencies and produce faster response kinetics over a wide range of visual conditions (Figure 4.8).

Two modes of GABAergic feedback inhibition have distinct stimulus selectivities

Action potentials in amacrine cells can drive inhibition that originates from the surround receptive field (Cook and McReynolds, 1998; Taylor, 1999; Flores-Herr et al., 2001; Shields and Lukasiewicz, 2003; Chávez et al., 2010; Vigh et al., 2011). Local inhibition, which originates from within the center receptive field, relies more on graded potentials (Bieda and Copenhagen, 1999; Hartveit, 1999; Murphy-Baum and Taylor, 2015). We observed this pattern of wide-field Na_V-dependent GABAergic inhibition and narrow-field Na_V-independent GABAergic inhibition in t-OFF α cells (Figure 4.3). Although the aforementioned studies have mostly considered these two feedback systems as separable by their spatial extent, we found that in t-OFF α cells they are also separable by their contrast sensitivity. The wide-field Na_V-dependent component operates at high contrast, whereas the narrow-field Na_V-independent component is more active at low and intermediate contrasts (Figure 4.7). The different contrast sensitivities might arise because weak, low contrast stimuli are sufficient to drive local inhibition through graded responses, but fail to drive spiking in wide-field amacrine cells. The neural substrate for such local inhibitory connections has been well-established in the form of dyad synapses, which are ubiquitous in vertebrate retinas (Dowling and Boycott, 1966; Dowling, 1968). In a natural environment, where the animal will experience visual inputs over a range of contrasts and spatial frequencies, these

two feedback systems may be critical for maintaining the ganglion cell's temporal tuning over a wide dynamic range.

GABAergic feedback contributes to spatiotemporal coupling

Even in the earliest ganglion cell recordings, it was recognized that the surround response is delayed relative to the center response (Kuffler, 1953; Barlow et al., 1964), possibly because inhibitory signals pass through at least one more neuron than the direct excitatory inputs. This idea became relevant to subsequent studies of contrast gain control, which in part describes the phenomenon where increasing the stimulus contrast shortens the latency, or advances the phase, of ganglion cell responses (Shapley and Victor, 1978; Enroth-Cugell and Freeman, 1987; Benardete and Kaplan, 1999; Zaghloul et al., 2005). Initial studies describing contrast gain control led to a thorough description of spatiotemporal receptive field interactions: altering one visual parameter changes the shape of the tuning functions of the others (Kaplan and Benardete, 2001).

Ratliff et al. (1967) first suggested that this spatiotemporal inseparability could be due to a time delay between center excitation and lateral inhibition. This idea was incorporated in later attempts to model the frequency-dependent changes in the response phase and amplitude (Gouras and Zrenner, 1979; Enroth-Cugell et al., 1983; Dawis et al., 1984; Frishman et al., 1987). Although the models put forth by these studies accurately describe the phase and amplitude changes that occur at different spatiotemporal frequencies and contrasts, the data is insufficient to localize where in the retinal circuitry this interaction is taking place.

Here, we used essentially the same model as Frishman et al. (1987), but we recorded excitatory currents instead of spiking responses, and modulated surround inhibition using

pharmacology rather than by stimulus design, so as to identify the specific receptors involved. Thus, our model furthers previous work by localizing the spatiotemporal interaction to GABAergic inhibition of the presynaptic bipolar cells. We offer this model as a qualitative description of how GABAergic feedback inhibition can advance the timing of the excitatory input and have opposing effects on its amplitude over different frequency bands. The model is especially useful in showing that the relationship between the phase advance and temporal frequency is sensitive to the relative strength of excitation and feedback inhibition. The particular shape and magnitude of the phase and relative amplitude versus frequency plots (Figure 4.4A-B) suggest that the temporal tuning curves of excitation and feedback inhibition are different. Namely, inhibition must be stronger than excitation at higher temporal frequencies to account for our data (Frishman et al., 1987; Benardete and Kaplan, 1997; but see Dawis et al., 1984). The relatively large difference in best frequency between excitation and inhibition is unsurprising, since the excitatory input to t-OFF α cells is low pass without GABAergic feedback (Figure 4.2B).

The two major parameters of our model, the time delay and the I:E ratio, control both the maximum phase shift and the frequency at which it occurs. In this context, it is notable that the change in phase following GABAR blockade was largest for frequencies close to the ganglion cell's best frequency. Thus, when the ganglion cell is operating in its optimal frequency range in terms of response amplitude, feedback inhibition is also producing maximal phase advancement.

Role of glycinergic feedback in temporal tuning

ON glycinergic inputs to alpha cell dendrites can drive spiking through disinhibition, particularly at low contrast (Manookin et al., 2008; van Wyk et al., 2009). However, less is known about the

utility of the ON glycinergic inhibition that the presynaptic OFF bipolar cells receive (Marc et al., 2014). Blocking either GlyRs (0.5 μM strychnine) or the ON pathway (50 μM L-AP4) had similar effects both on the EPSC waveform and the temporal tuning of t-OFF α cells. EPSCs were reduced, especially with regard to the outward current during positive contrast transitions, and the best frequency was significantly lower than in control (Figure 4.6). This shift in the best frequency was not as large as that evoked during GABAR or sodium channel blockade (Figure 4.2).

The amacrine cells that most likely deliver the glycinergic feedback, AII amacrine cells, are narrow-field and are known to have a strong surround receptive field (Bloomfield and Xin, 2000). Therefore, it is possible that AII amacrine cells are suppressed during the presentation of our relatively broad stimulus, causing us to underestimate its contribution to temporal tuning. More work involving both spatial and temporal manipulations is required to investigate this.

Role of presynaptic sodium channel activity in temporal tuning

In the vertebrate retina, the presence of TTX-sensitive sodium channels in select types of bipolar cells is well established (Pan and Hu, 2000; Zenisek et al., 2001; Ichinose et al., 2005; Ma et al., 2005; Saszik and DeVries, 2012; Puthussery et al., 2013). Although the functional role of these channels remains a matter of conjecture, a previous study in homologous cell types in the primate retina has proposed that they may play a role in driving transient signaling to ganglion cells (Puthussery et al., 2013). In t-OFF α cells, TTX reduced the excitatory input at high temporal frequencies, even during GABAergic, glycinergic, and gap junctional blockade, suggesting that the sodium channels are localized to the presynaptic bipolar cells (Figure 4.5). This reduction was even more apparent at low contrast, when Na_V-dependent GABAergic

feedback was apparently silent (Figure 4.12). The reduction in the excitatory input in the presence of TTX resembles that recorded in parasol ganglion cells of the primate retina, which have homologous receptive field properties to alpha cells (Crook et al., 2008), and whose presynaptic bipolar cells express Na_V (Puthussery et al., 2013). These sodium channels boost the excitatory input, particularly at high temporal frequencies (Figure 4.5) and over the full range of contrasts (Figure 4.7, Figure 4.12)—from threshold to saturation. Their strong voltage-dependence and rapid inactivation make TTX-sensitive sodium channels ideal for producing brief depolarizations that could selectively boost transient signals. The results also indicate that the activation of sodium channels advances the phase of the excitatory input (Figures 4.10 and 4.13). This may compensate to some extent for the synaptic delays inherent in bipolar cell transmission, further improving the ability of t-OFF α cells to respond rapidly to motion.

SUPPLEMENTAL FIGURES

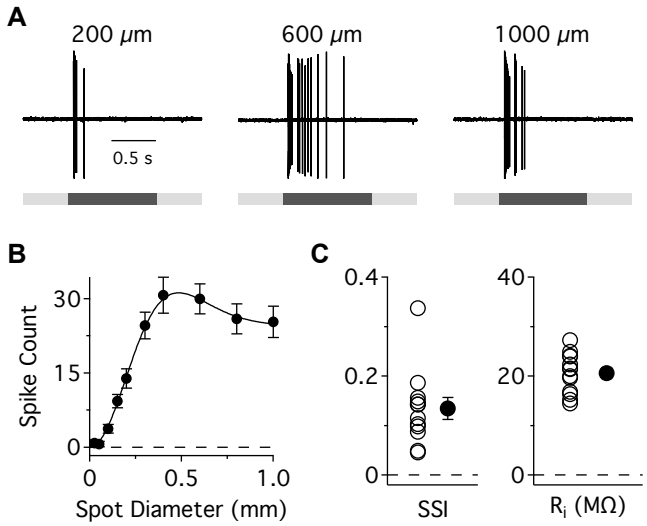

FIGURE 4.9. IDENTIFYING FEATURES OF t-OFF α GANGLION CELLS.

A, Spiking responses to a negative contrast step using a spot of different sizes. **B**, Spike count versus spot diameter (n = 12). Data is fit with a difference of Gaussians function. **C**, Left, Spatial selectivity index (SSI) calculated using the area response curves (n = 12). Right, input resistance measured during voltage clamp recordings (n = 13).

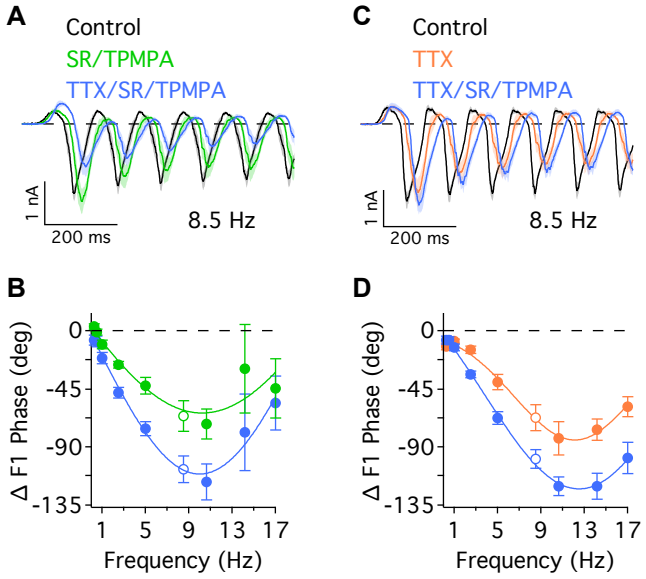

FIGURE 4.10. BOTH Na_V-DEPENDENT AND Na_V-INDEPENDENT MECHANISMS CONTRIBUTE TO PHASE ADVANCE.

A, EPSCs in response to an 8.5 Hz stimulus following GABAR blockade (green) and subsequent Na_V blockade (blue). **B**, Change in phase of the F1 component for the drug applications in (**A**). **C**, Same as in (**A**), but the reverse drug application. **D**, Change in phase of the F1 component for the drug applications in (**C**).

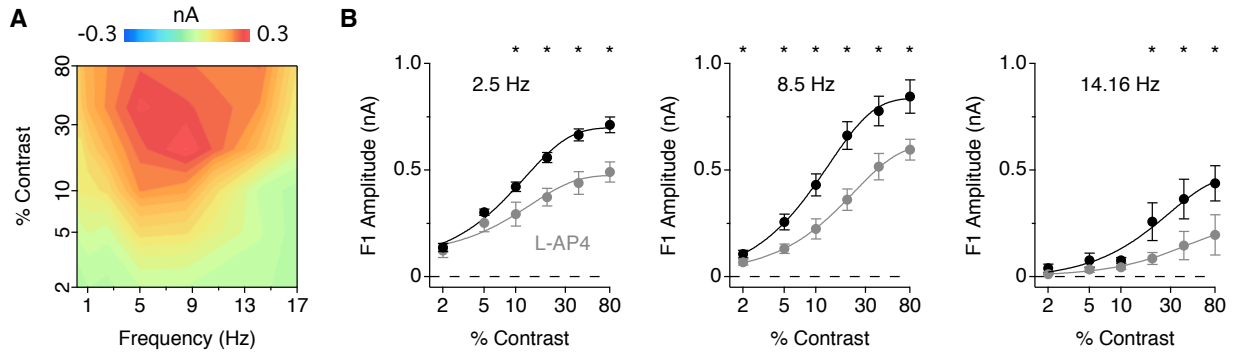

FIGURE 4.11. RELATED TO FIGURE 4.6. CONTRAST DEPENDENCE OF CROSSOVER INHIBITION.

A, Difference contour plot (CTRL minus AP4; 50 µM L-AP4) of F1 amplitude (z-axis, color) versus the contrast (y-axis) and temporal frequency (x-axis) of the visual stimulus. **B**, F1 amplitude versus contrast for a 2.5 Hz, 8.5 Hz, and 14.16 Hz stimulus in the presence of 50 µM L-AP4. **P* < 0.05, Student's *t* test.

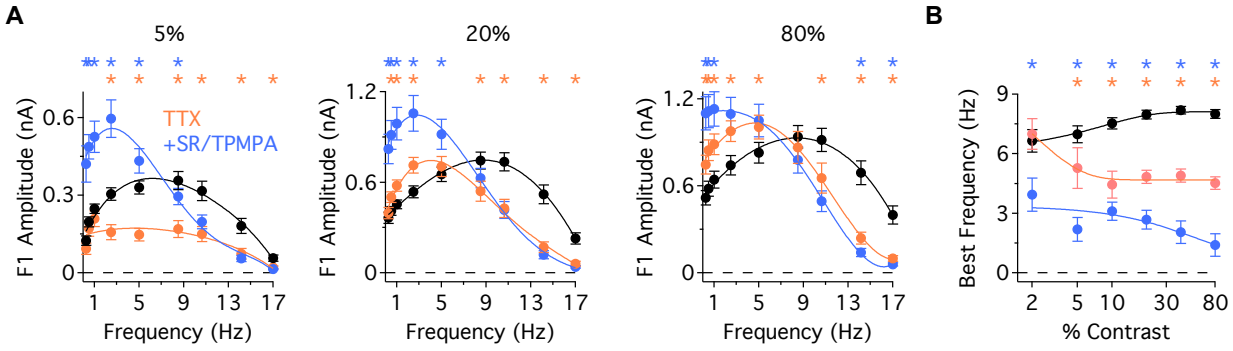

FIGURE 4.12. RELATED TO FIGURE 4.7. MECHANISMS FOR TEMPORAL TUNING ACROSS CONTRAST.

A, F1 amplitude versus temporal frequency for 5%, 20%, and 80% contrast stimuli during sodium channel blockade (orange) followed by subsequent GABAR blockade (blue; $n = 8$). **B**, Stimulus frequency that evoked the largest response for the different pharmacological conditions across all tested contrasts, calculated from the peak of polynomial fits to the data. **P* < 0.05, Student's *t* test.

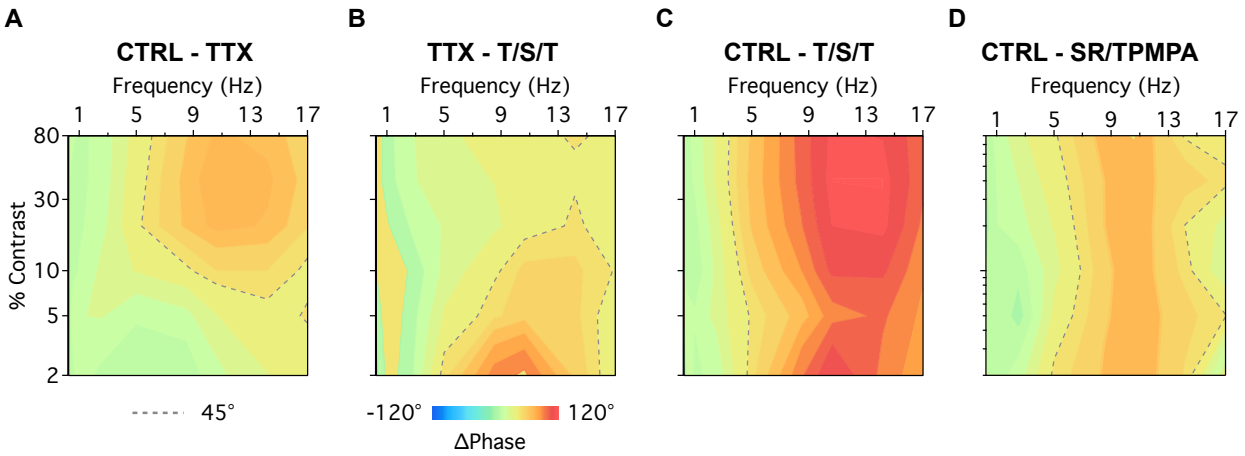

FIGURE 4.13. RELATED TO FIGURE 4.7. CONTRAST SENSITIVITY OF Na_V-DEPENDENT AND GABAERGIC PHASE ADVANCE.

A-C, Difference contour plots of the change in phase (color, z axis) versus the contrast (y axis) and temporal frequency (x axis) of the visual stimulus (n = 8). **A**, Control minus TTX. **B**, TTX minus T/S/T (TTX/SR-95531/ TPMPA). **C**, Control minus T/S/T. Dotted lines are the 45° contour. **D**, Control minus SR/TPMPA from a separate population of cells (n = 6)

ADDITIONAL EXPERIMENTS

Multiple mechanisms contribute to contrast gain control

Contrast gain control comprises several effects on the spiking response of ganglion cells. First, the ganglion cell's response per unit contrast (derivative of response vs. contrast plots) decreases with increasing contrast. This relationship can be seen in the contrast response functions in Figure 4.7A. Second, the temporal tuning is shifted to higher frequencies with increasing contrast. This effect is seen in the best frequency vs. contrast plots in Figure 4.12B, where in control conditions the neuron's best frequency shifts from 6.6 ± 0.64 Hz at 2% contrast to 8.2 ±

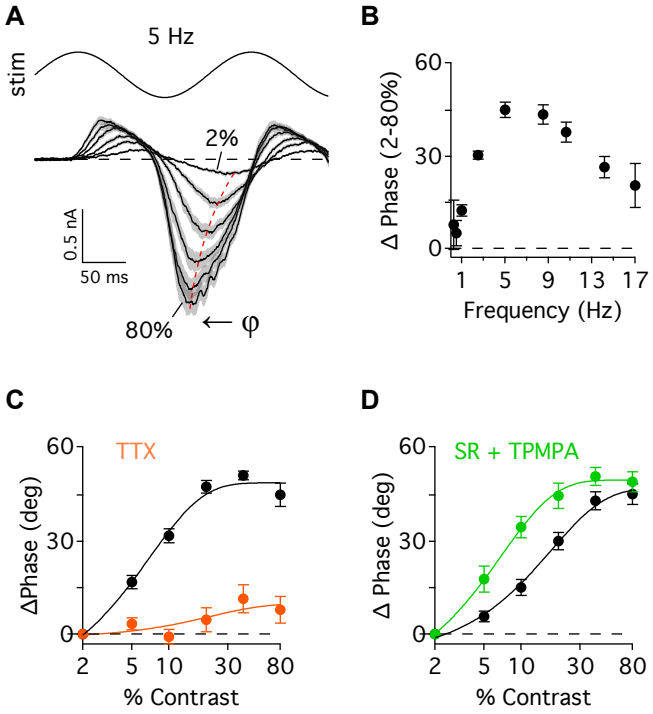

FIGURE 4.14. CONTRAST DEPENDENT PHASE ADVANCE.

A, EPSCs in response to a 5 Hz stimulus at a range of contrasts (2-80%; n = 32). **B**, Total change in phase between 2% and 80% contrast conditions for a range of temporal frequencies (n = 21). **C**, Change in phase from 2% contrast condition in control conditions and after TTX application (n = 8). **D**, As in (**C**), but after GABA receptor blockade (n = 13). Solid lines in (**C**) and (**D**) are exponential fits to the data.

0.30 Hz at 40% contrast (n = 8). Third, the response phase advances with increasing contrast, as shown for a 5 Hz stimulus in Figure 4.14.

In accordance with recent modeling studies (Kim and Rieke, 2001; Ozuysal and Baccus, 2012; Cui et al., 2016), we show that these effects are present in the excitatory input, supporting the hypothesis that contrast gain control originates in the presynaptic bipolar cells. Moreover, many of these effects were eliminated or reduced during our drug applications. For instance, after Na_V blockade, the best frequency did not increase and the phase did not advance with contrast. After GABAR blockade, the best frequency did not increase, but the phase advance remained (Figure 4.14). Importantly, neither Na_V nor GABAR blockade was able to abolish the reduction in gain that occurs with increasing contrast. In fact, the reduction in gain at higher contrasts was even more apparent after GABAR blockade (Figure 4.7). These data suggest that the effects that fall under the umbrella of contrast gain control likely originate from a variety of mechanisms.

Simulating the effects of phase delayed inhibition

In Chapter 4, we blocked GABARs and measured the change in phase and amplitude of the F1 component of the EPSCs. The resulting data was fit by a computational model which output the time delay between excitation and inhibition, as well as the ratio of the inhibitory and excitatory temporal tuning curves, the I:E ratio. This model fit our data well, although it was still conceptually difficult to understand how values for the free parameters in the model contributed to the shape of the phase and amplitude data. To better understand this, we simulated the data by summing two sine waves—one excitatory and one inhibitory—with different relative amplitudes (I:E ratio) and time delays. As in the real data, we calculated the change in phase and amplitude

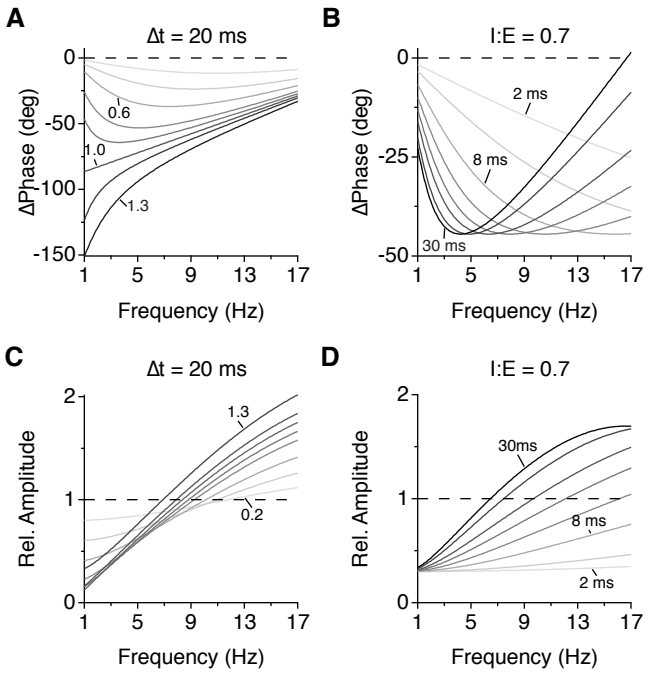

FIGURE 4.15. SIMULATING HOW FEEDBACK INHIBITION CHANGES THE PHASE AND AMPLITUDE OF GANGLION CELL EXCITATORY RESPONSES.

A, With the time delay (Δt) between excitation and inhibition held constant, model fits to the change in phase versus temporal frequency over a range of I:E ratios. **B**, Same as in **(A)**, except I:E ratio is held constant, and Δt is varied. **C**-**D**, Same as in **(A)** and **(B)**, except measuring the relative amplitude between the excitatory and summed sine waves used in the model.

of the summed sine wave (analogous to the EPSCs under control conditions) and the excitatory sine wave (analogous to the EPSCs following GABAR blockade). The resulting data was fit with our model and is presented in Figure 4.15. Note that the I:E ratio (input parameter) and the relative amplitude (y-axis in Figure 4.15C and D) are not the same thing. The I:E ratio is the ratio of the inhibitory and excitatory temporal tuning curves, and the relative amplitude is that between the excitatory sine wave and the summed sine wave of a given frequency. By fixing one parameter (I:E ratio or Δt) and varying the other, these data demonstrate that the relative strength and time delay between excitation and inhibition can have a profound impact on the shape of the phase and amplitude plots.

ON pathway contributes to linear spatial summation under certain visual conditions

The majority of the work presented in Chapter 4 focuses on the temporal properties of t-OFF α ganglion cells. In addition to studies of temporal tuning, alpha cells are a model cell type for studying nonlinear spatial summation in the retina. In a brief series of experiments, we asked whether the temporal frequency of the stimulus affected the nonlinear summation. Nonlinear summation is typically assessed by presenting a ganglion cell with a contrast reversing grating of high spatial frequency. This stimulus drives both positive and negative contrast signals simultaneously, and thus tests how a ganglion cell integrates these opposing inputs. As mentioned earlier, linear summation results in no response because the positive and negative contrast signals cancel. Nonlinear summation results in a response at every contrast reversal; it responds at twice the modulation frequency. This is known as a frequency-doubled response.

We presented t-OFF α cells with a contrast reversing grating over a range of spatial frequencies, each modulated at either a low (0.5 Hz) or high (8.5 Hz) temporal frequency (Figure 4.16). By taking the Fourier transform of the spiking response histograms, we measured the fundamental (F1) and second harmonic (F2) responses. For both modulation frequencies, the F1 amplitude decreased with increasing spatial frequency, approaching zero around 2.5 mm^{-1}, or a bar width of 200 μm. This is slightly less than half the width of the typical alpha cell dendritic arbor (Peichl, 1987). The F2 response, however, behaved differently at low and high temporal frequencies. At 0.5 Hz, there is an intermediate range of spatial frequencies where summation is linear; both the F1 and F2 amplitudes are close to zero (Figure 4.16B). Over this range, the cell doesn't fire any action potentials. At 8.5 Hz, no such range of linearity is present; the F2 amplitude only reaches zero for the highest spatial frequencies, when responses fall out

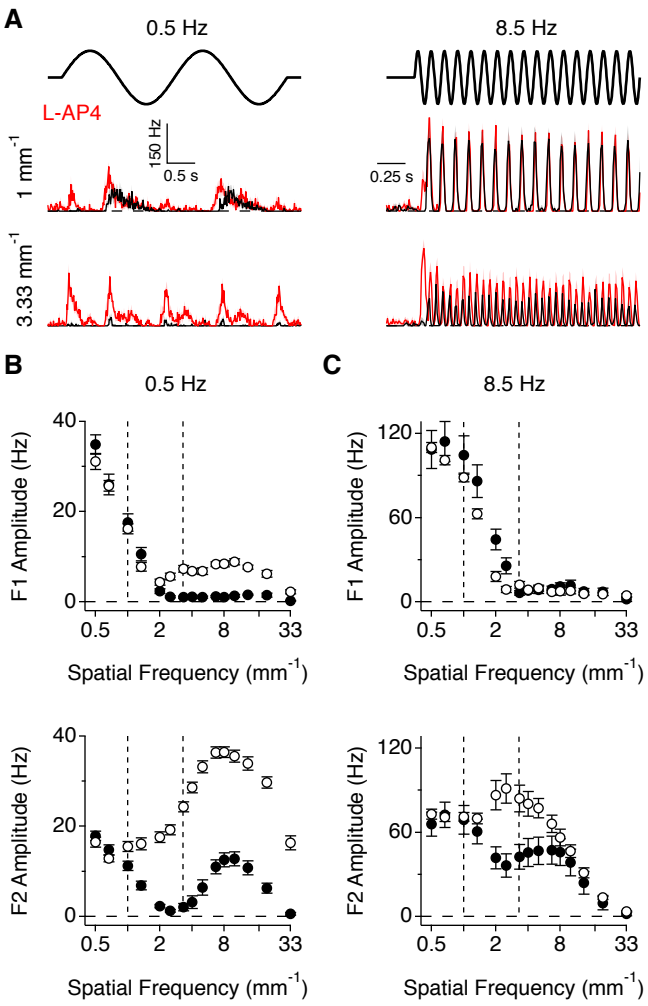

FIGURE 4.16. ON PATHWAY CONTRIBUTES TO LINEAR SPATIAL SUMMATION IN t-OFF α CELLS.

A, Spike histograms of responses to a contrast reversing grating at different spatial and temporal frequencies (n = 9). **B**, F1 (top) and F2 (bottom) amplitudes in response to a 0.5 Hz contrast reversing grating in the presence of 50 µM L-AP4 (n = 9). **C**, Same as in (**B**), but with a 8.5 Hz stimulus (n = 9).

completely. Thus, over the range of linearity observed for the 0.5 Hz stimulus, the 8.5 Hz stimulus evokes a strong frequency-doubled response. These data suggest that there may be a synaptic input that causes t-OFF α cells to integrate linearly over an intermediate range of spatiotemporal frequencies. Since linearity can be caused by crossover inhibition, we blocked the ON pathway with L-AP4 and repeated the contrast reversing grating stimulus. For the 0.5 Hz stimuli, blocking the ON pathway produced robust frequency-doubling over the range of spatial

frequencies that previously produced a null response. At 8.5 Hz, frequency-doubling became stronger than it already was.

These data indicate that t-OFF α cells can integrate contrast linearly or nonlinearly, depending on the presence or absence of crossover inhibition from the ON pathway. The data suggest that the crossover input is more active at low and intermediate spatial frequencies, and at low temporal frequencies. The overall effect is that t-OFF α cells begin frequency-doubling at lower spatial frequencies when the modulation frequency is higher.

Temporal tuning in ON alpha ganglion cells

Our initial experiments on temporal tuning were done in both t-ON α and t-OFF α ganglion cells. Although the two ganglion cell types respond to opposite contrasts, their light-evoked EPSCs had similar kinetics under control conditions and after GABAR blockade (Figure 4.17). As we observed in t-OFF α cells (Figure 4.2), in t-ON α cells GABAergic feedback shifted the temporal

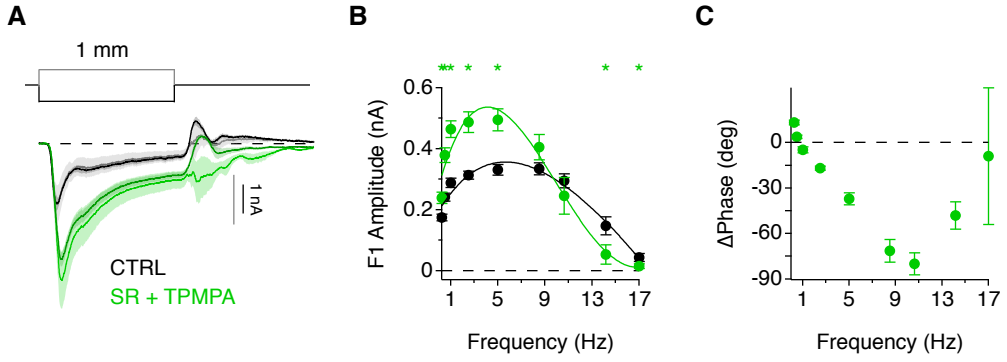

FIGURE 4.17. GABAERGIC FEEDBACK SHAPES TEMPORAL TUNING IN t-ON α CELLS.

A, Comparison of EPSCs in response to a step of positive or negative contrast for t-ON α (n = 10) and t-OFF α (n = 6) ganglion cells, respectively. Stimulus was a 1 mm diameter spot of light at 40% contrast. t-ON α EPSCs are grey and light green; t-OFF α EPSCs are black and dark green. **B**, F1 Amplitude versus temporal frequency after GABAR blockade (n = 6). Data is fit with a polynomial function. **C**, Change in phase after GABAR blockade (n = 6). Asterisks denote $P < 0.05$, paired Student's *t* test. Data in (**A**) is normalized to control t-OFF α EPSCs. Grey scale bar is for t-ON α cells; black scale bar is for t-OFF α cells.

tuning to higher frequencies by suppressing responses at low frequencies, and potentiating them at high frequencies. GABAR blockade also caused phase delays of similar magnitude to those observed in t-OFF α cells. Although more thorough experimentation needs to be done in t-ON α cells, the initial results suggest that similar GABAergic feedback mechanisms play a role in regulating temporal tuning of transient neurons in both the ON and OFF visual pathways.

Interaction of ON and OFF visual pathways in the direction selective circuit

Receptive field coupling is an interesting topic for cells that exhibit complex receptive field properties, such as direction selective ganglion cells. Previous studies have concluded that DSGCs do not have directional-spatial coupling (Hoggarth et al., 2015). However, this study used center-confined gratings to test spatiotemporal coupling, and only tested modulation frequencies up to 8 Hz. It might be useful to revisit these experiments using faster modulation frequencies and wide-field gratings. Wide-field gratings tend to suppress spiking to a significant degree due strong surround inhibition, so these experiments may be difficult to perform. It may be the case that spatiotemporal coupling is masked in ganglion cells that have strong surround receptive fields. In alpha ganglion cells, the surround is relatively weak since wide-field stimulation only moderately reduces the spike output, making spatiotemporal coupling easier to assess. Nowak et al. (2011) concluded that DSGCs do not have directional-temporal coupling either. However, they used moving bars to assess directional-temporal coupling, which might not strongly activate surround inhibitory inputs that affect temporal tuning.

I briefly tested whether ON-OFF DSGCs exhibit directional-temporal coupling by stimulating cells with drifting gratings rather than moving bars. Gratings were drifted over a range of temporal frequencies in both the preferred and null directions. Consistent with earlier work, ON-

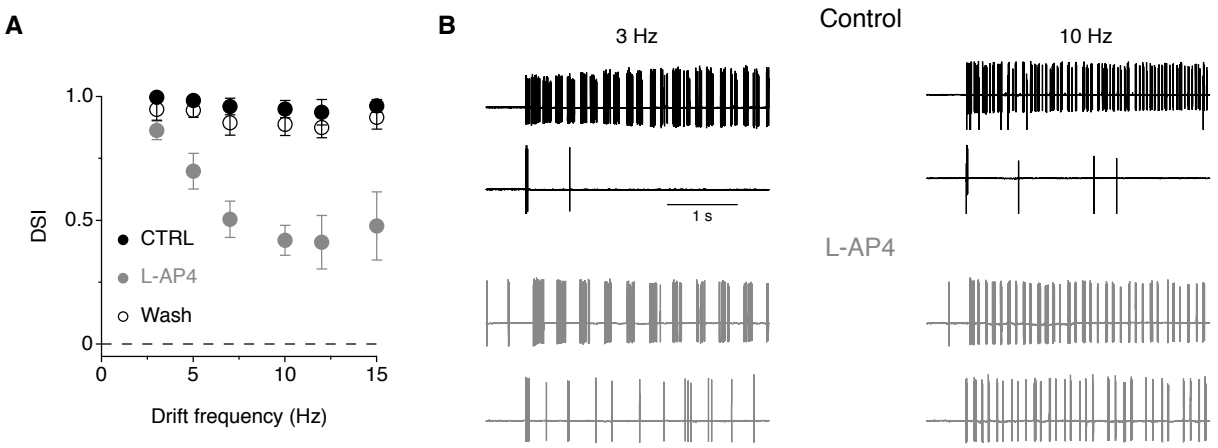

FIGURE 4.18. BLOCKING THE ON PATHWAY REDUCES DIRECTION SELECTIVITY FOR HIGH DRIFT FREQUENCIES IN ON-OFF DSGCS.

A, Direction selective index (DSI; see Methods) versus drift frequency (n = 3). The stimulus was a 2 mm^{-1} sine wave grating that drifted in either the preferred or null direction. Preferred and null directions were determined by recordings spikes in response to drifting gratings in twelve different directions. **B**, Example spike response to a low and high drift frequency grating under control conditions and after ON pathway blockade (50 µM L-AP4).

OFF DSGCs retained strong direction selectivity for all drift frequencies tested (Sivyer et al., 2010; Figure 4.18A). The spatial frequency of the grating was 2 mm^{-1}, where the grating period is about twice the size of the center receptive field. We repeated this experiment while blocking the ON pathway with 50 µM L-AP4, so we might be able to discern whether any changes in direction selectivity originate from the ON or OFF visual pathways. Interestingly, L-AP4 reduced direction selectivity (as measured by direction selective index [DSI], see Methods) only for high drift frequencies (Figure 4.18). On average, spiking responses to the slowest drift speed tested, 3 Hz, were not significantly different between control and L-AP4 conditions. The reduction in DSI at higher frequencies is largely due to increased null direction spiking at higher temporal frequencies. These data suggest that there may be some interaction between the ON and OFF visual pathways in the direction selective circuit. It is unclear whether this interaction takes place in the ganglion cell itself, which receives GABAergic inhibition from both ON and OFF

starburst amacrine cells, or if it takes place in the presynaptic circuitry. This could be an interesting topic for future research.

CHAPTER 5

DISCUSSION

The retina must transmit a massive amount of visual information to the brain at any given moment. All visual signals are encoded in the trains of action potentials fired by retinal ganglion cells. Since a single type of ganglion cell is unable to simultaneously transmit all of the relevant visual information, there exist 30 or more types of ganglion cells that respond to slightly different aspects of the visual scene. This allows the retina to transmit information about many visual features in parallel. What is the underlying cause of feature selectivity in different cell types? The central argument of this dissertation is that although most retinal neurons receive inhibitory inputs—both feedback and feedforward—the neurons that provide that inhibitory input have different morphologies, spatial and temporal receptive field properties, neurotransmitters, and may express different types of voltage-gated channels. These attributes play critical roles in determining the visual features that are detected by specific retinal neurons.

5.1 $PA_{1/3}$ Cells

Orientation selectivity in the visual system

Orientation selectivity has been identified in visual neurons of the cortex (for review, see Priebe, 2016), thalamus (Scholl et al., 2013; Zhao et al., 2013), and retina (Venkataramani and Taylor, 2010, 2016; Nath and Schwartz, 2016). The mechanisms that have been proposed for mediating orientation selectivity in these brain regions are diverse and vary among species. In cat, Hubel and Weisel's (1962) original hypothesis that spatially aligned thalamic neurons converge on neurons in the cortex has stood the test of time. Primates have a similar cortical organization to

cats, and likely employ the same mechanism (Hubel and Weisel, 1968). In rodents, however, neurons of the LGN are also sensitive to orientation. In mice, Scholl et al. (2013) concluded that the sharpness of orientation selectivity is similar in the thalamus and cortex, suggesting that cortical orientation selectivity may be inherited and doesn't require Hubel and Weisel's convergent input model. However, others have claimed the opposite, that orientation selectivity is greatly improved from the LGN to the cortex in mice (Zhao et al., 2013). Thus, it is still controversial how LGN orientation selectivity shapes that found in the cortex.

Orientation selectivity has also been observed in ganglion cells and amacrine cells in rabbit and rodent retinas (Bloomfield, 1994; Venkataramani and Taylor, 2010, 2016; Murphy-Baum and Taylor, 2015; Nath and Schwartz, 2016; Antinucci et al., 2016). Orientation selectivity that arises in retinal ganglion cells is distinct from that originating in the cortex, however, since it requires synaptic inhibition (Venkataramani and Taylor, 2010, 2016; Nath and Schwartz, 2016). Studying the properties of this inhibition is an important step towards understanding how this fundamental feature selectivity first arises in the visual pathway.

In $PA_{1/3}$ cells, orientation selectivity arises only from the excitatory input, and is due to the cell's elongated dendritic arbor. Its dendrites are oriented roughly parallel to the visual streak, meaning that these neurons are selective for stimuli parallel to the horizon in the live animal. Such an amacrine cell is required to explain orientation selectivity in OSGCs, which rely on GABAergic inhibition for their orientation tuning (Venkataramani and Taylor, 2010, 2016). Similar to $PA_{1/3}$ cells, ON OSGCs have orientation-tuned excitatory inputs due to an elongation of their dendritic arbor. However, even though blocking GABARs doesn't eliminate OS

excitatory input in OSGCs, it does prevent OS spiking responses, suggesting that inhibition is the critical factor in generating orientation selectivity.

It is still unclear whether or not $PA_{1/3}$ cells actually mediate OS inhibition in OSGCs. Given that $PA_{1/3}$ cells have long axons, it is reasonable to assume that its inhibition is far-reaching. However, studies of OSGCs have limited their visual stimuli to areas local to the ganglion cell, and conclusions about the spatial extent of OS inhibition cannot be drawn (Venkataramani and Taylor, 2010, 2016; Nath and Schwartz, 2016). Stimulating OSGCs with oriented gratings, which activate more surrounding circuitry than isolated bars, may provide more insight into whether the spatial properties of OS inhibition are consistent with inhibition originating from a PAC. However, future studies involving paired recordings between OSGCs and $PA_{1/3}$ cells may be necessary to determine functional connectivity.

A novel role for linear integration in the retina

High spatial frequency visual inputs—that are finer than the dendritic arbor of the neuron in question—drive both positive and negative contrast signals simultaneously. Retinal neurons must integrate the two signals to form its response. Integration can be carried out linearly, nonlinearly, or somewhere in between. If integration is linear, the positive and negative contrast signals cancel, resulting in no response. If integration is nonlinear, the signals do not cancel. A classic way to test the linearity of integration is to present the neuron with a contrast reversing grating of high spatial frequency (Figure 3.9), where the contrast of the grating is alternated at some temporal frequency. Nonlinear integrators respond at double the modulation frequency, whereas linear integrators don't respond at all. Most previous studies of linear and nonlinear integration have been carried out in X and Y ganglion cells, respectively (Enroth-Cugell and Robson, 1966).

A linear integration of contrast is useful because it reduces distortions of the visual signal, and allows cells to report the average light intensity over their receptive field (Molnar et al., 2009; Werblin, 2010). Neurons that integrate contrast nonlinearly have rectified responses, but they are more effective at detecting moving objects, especially fine textures.

In Chapter 3, we identified a novel role for linear integration in the retina. $PA_{1/3}$ cells respond more linearly than they otherwise would because of a tonic excitatory input from the ON pathway, and crossover inhibition from the OFF pathway. These inputs allow $PA_{1/3}$ cells to hyperpolarize in response to negative contrast nearly as much as they depolarize in response to positive contrast. Thus, if positive and negative contrast signals arrive simultaneously, as they would when presented with a fine texture or grating, $PA_{1/3}$ cells respond very weakly. By integrating opposing contrast signals more linearly, $PA_{1/3}$ cells are able to ignore randomly oriented fine textures that would otherwise drive spiking (Figure 3.9). Although crossover inhibition is known to linearize the summation contrast in retinal neurons (Molnar et al., 2009; Werblin, 2010), this is the first time linear integration has been shown to optimize the detection of a complex feature in the visual input.

Role for $PA_{1/3}$ cells for low spatial frequency inputs

In $PA_{1/3}$ cells, orientation selectivity was most prominent for intermediate spatial frequencies, since its more linear integration precluded strong responses to high spatial frequency inputs of any orientation. However, $PA_{1/3}$ cells also respond strongly to low spatial frequency inputs, which don't necessarily have any orientation information. Under these conditions, $PA_{1/3}$ cells are more likely providing classical surround inhibition to other neurons, rather than OS inhibition. These two functions aren't irreconcilable, since OSGCs in the rabbit have strong surround

receptive fields, and don't respond well to spatially broad inputs (Venkataramani and Taylor, 2010). However, since all previous work in OSGCs used uniform spots (no orientation information) to activate surround inhibition, it remains ambiguous as to whether OSGCs will ignore oriented, low spatial frequency signals. A good experiment would be to stimulate OSGCs with a full field, low spatial frequency grating at different phases. Low spatial frequency gratings are equivalent to a uniform spot unless the phase of the grating is such that an edge crosses the receptive field of the OSGC. Even though individual $PA_{1/3}$ cells respond fairly linearly to this type of stimulus, and are suppressed, the population of $PA_{1/3}$ cells as a whole should be phase-invariant to any grating stimulus. Thus, if $PA_{1/3}$ cells are mediating OS inhibition to OSGCs, the expectation is that OSGCs will not respond to oriented edges at low spatial frequencies. These types of experiments could be useful to better understand how populations of inhibitory neurons interact to form complex receptive field properties in ganglion cells.

Ambiguities in the input circuit to $PA_{1/3}$ cells

In Chapter 3, we applied different pharmacological agents to either stimulate or block specific parts of the $PA_{1/3}$ presynaptic circuit. In doing so, we mapped out the simplest presynaptic circuit that could account for the data. Since only $PA_{1/3}$ cells were recorded from, these experiments are indirect and some ambiguity about the true circuit arrangement remains. For instance, blocking GABARs (both $GABA_A$ and $GABA_C$) increased the inhibitory conductance (Figure 3.7). Since GABA is an inhibitory neurotransmitter, an increase in conductance can only be accounted for if GABA is inhibiting a second source of inhibition that directly inhibits $PA_{1/3}$ cells. This second source is glycinergic, since it is blocked by the GlyR antagonist strychnine (Figure 3.7D). The ambiguity in the circuit arrangement arises because we have no way of knowing whether the

GABARs are located on the glycinergic amacrine cell's dendrites or on its presynaptic bipolar cells. Either situation would produce the same effect on the inhibitory conductance in $PA_{1/3}$ cells. However, the increase in inhibitory conductance is due to blocking $GABA_C$ receptors specifically, since blocking $GABA_A$ receptors alone did not increase it (Figure 3.7A). Since $GABA_C$ receptors are found almost exclusively on bipolar cell terminals, and not on amacrine or ganglion cell dendrites (Wässle et al., 1998), it is likely that GABA release is inhibiting the bipolar cell terminals presynaptic to the glycinergic amacrine cell. This mirrors what was found for the excitatory input to $PA_{1/3}$ cells—the presynaptic bipolar cells receive GABAergic inhibition that is at least partly mediated by $GABA_C$ receptors.

Further ambiguities arise since serial inhibitory circuits are abundant in the retina (Marc and Liu, 2000). For instance, the simplest interpretation of a reduction in inhibitory conductance after blocking GABARs is that $PA_{1/3}$ cells receive direct GABAergic inhibition. However, it is conceivable that a more extensive, multi-neuron inhibitory circuit is responsible, where a complicated series of disinhibitory effects take place to achieve the same end result. In our study, we've rejected these more complicated scenarios in favor of the simplest circuit that can explain the data.

Diverse circuit functions among amacrine cell populations

In order to fully understand a retinal circuit, researchers must study how the inhibitory neurons within the circuit form their own receptive fields. Previous studies have relied upon the morphological differences among amacrine cells to distinguish them and provide an estimate of the total number of functional types (MacNeil and Masland, 1998; Masland, 2001). For example, the level of dendritic stratification determines whether a cell is ON or OFF type, and the size of

the dendritic arbor puts limits on the type of spatial information a neuron can encode. Moreover, most amacrine cells don't have axons, and have output synapses on their dendrites that signal relatively locally. Some amacrine cells, such as $PA_{1/3}$ cells, do have long axons that are probably the sites of their synaptic output, suggesting that they perform a more global function. Thus, cells that have different morphologies are very likely to perform different functions. This is a challenging prospect for researchers, since there are at least 40-60 different morphological types of amacrine cells in the mammalian retina (MacNeil and Masland, 1998; Masland, 2001, 2012). With the study presented in Chapter 3, $PA_{1/3}$ cells join some of the few amacrine cell populations that have been given a thorough functional description. The three well-studied amacrine cell types discussed below—the starburst, AII, and A17 amacrine cells—have vastly different functions from $PA_{1/3}$ cells because of their synaptic inputs, morphology, and channel expression.

First, starburst amacrine cells are GABAergic neurons with radially symmetric dendrites. They allow direction selective ganglion cells (DSGCs) to respond to object motion in one direction, but not in others. In addition to selective wiring with DSGCs (Briggman et al., 2011), the starburst cell produces directional inhibition through reciprocal GABAergic inhibition with neighboring starburst cells (Lee and Zhou, 2006), the clustering of GABA release sites at the dendritic tips (Famiglietti, 1991), electrical isolation of individual dendrites (Ding et al., 2016), and a possible asymmetric distribution of sustained and transient bipolar cell inputs along the dendrites (Greene et al., 2016). Similar to DSGCs and starburst amacrine cells, $PA_{1/3}$ cells also receive dendritic inhibition through $GABA_A$ receptors, but instead of sharpening directional responses, it plays a role in suppressing spiking during negative contrast transitions and linearizing the summation of contrast. The starburst cell is a remarkable demonstration of how

subtle details in morphology, channel expression, inhibition, and synaptic location come together to optimize the detection of a complex feature of the visual scene. Having no reason to suspect that other neurons aren't equally as specialized for their task in visual processing, many fascinating circuit adaptations are likely to be discovered with future research of retinal neurons.

Second, the AII amacrine cell receives excitatory input from rod bipolar cells before channeling it into the cone pathway through electrical synapses with ON cone bipolar cells, and glycinergic synapses with OFF cone bipolar cells and OFF ganglion cells (Marc et al., 2014). Unlike starburst and $PA_{1/3}$ amacrine cells, AII amacrine cells span the retina vertically, and mediate signaling between the ON and OFF visual pathways. Their small dendritic arbors make them receptive to much smaller spatial features than $PA_{1/3}$ cells, which integrate visual inputs over broader regions of space.

Finally, A17 amacrine cells provide GABAergic feedback to rod bipolar cells, thereby regulating glutamate release to AII amacrine cells. One major distinction between $PA_{1/3}$ cells and A17 cells is the location of synaptic integration. $PA_{1/3}$ cells likely integrate synaptic input somewhere near the soma, since they fire somatic action potentials that are sent down its axons. Although A17 neurons have large dendritic arbors like $PA_{1/3}$ cells, they don't have axons and have little sodium channel activity to propagate signals over longer distances. Thus, A17 cells operate using many independent reciprocal feedback circuits along their dendrites, so no centralized integration takes place. Isolated feedback allows individual A17 dendrites to inhibit many rod bipolar cells with little crosstalk between neighboring synapses (Grimes et al., 2014).

One of the defining features of all three of the aforementioned amacrine cell types is that they inhibit specific postsynaptic partners. Starburst cells primarily inhibit DSGCs, A17 cells only

inhibit rod bipolar cells, whereas AII amacrine cells inhibit a wider set of amacrine, ganglion, and bipolar cells in the OFF pathway. Thus, in addition to morphology, channel expression, and synaptic input, synapse specificity plays an important role in defining each cell's function in the retina. As mentioned earlier, one future challenge is to identify the postsynaptic partners for $PA_{1/3}$ cells. Are they like starburst or A17 amacrine cells, only inhibiting a single cell type such as OSGCs or their presynaptic bipolar cells? Or are they more like AII amacrine cells, inhibiting a larger array of cell types? Answering these questions will help build our understanding not only of amacrine cell functionality, but also of how the inhibitory inputs to specific ganglion cell types are generated.

5.2 Alpha Cells

Pharmacological approach tests predictions from modeling studies

The original studies of X and Y ganglion cells were performed by isolating spiking responses from nerve fibers in the optic tract that had certain receptive field properties. Y cells, identified functionally (Enroth-Cugell and Robson, 1966), eventually became synonymous with the anatomically identified alpha cells (Boycott and Wässle, 1974). Since their discovery, they have been used as a model cell type for studies of contrast gain control, spatial summation, and temporal tuning. While the first studies characterized the spatial and temporal properties of Y cell receptive fields, others began to use computational models to predict their responses. These models were initially used to explain the effects of contrast on the temporal receptive field properties of Y cells. Namely, increasing contrast shifts the temporal tuning to higher frequencies in the visual input and speeds up spiking response kinetics (Shapley and Victor, 1978, 1979a,

1979b; Enroth-Cugell et al., 1987). Along with a reduction in gain at higher contrasts, these effects were termed contrast gain control.

One of the first models of contrast gain control was proposed by Shapley and Victor (1978, 1979a, 1979b), and was designed to account for the temporal frequency-dependent changes in response amplitude and phase that occur with increasing contrast. This model comprised a linear center-surround input to the ganglion cell, and a second nonlinear input that accounts for the effects of contrast on the response. Subsequent modeling proposed that the nonlinear contrast mechanism is spread over a wide area, and may involve inhibitory feedback (Shapley and Victor, 1979b, 1980, 1981). This developed into the more complicated linear-nonlinear-linear sandwich model that accurately predicts alpha cell spiking responses to changes in contrast and spatiotemporal frequency (Victor and Shapley, 1988). These initial models form the basis of linear-nonlinear (LN) models used today that are designed to predict ganglion cell responses to arbitrary stimuli. They typically pass the visual stimulus through a linear filter, followed by a static (time-invariant) nonlinearity, in order to predict ganglion cell responses (Kim and Rieke, 2001; Baccus and Meister, 2002; Ozuysal and Baccus, 2012; Cui et al., 2016).

Other models, rather than predicting responses to arbitrary stimuli, have focused on predicting the amplitude and phase of Y cell responses to stimuli with different spatiotemporal frequencies and contrasts (Enroth-Cugell et al., 1983; Frishman et al., 1987). These latter models are similar to that employed in Chapter 4 to fit the phase and amplitude data after GABAR blockade (Figure 4.4). Despite their differences, all of these models include some element of feedback that is localized to the surround receptive field, and is delayed relative to excitation. A major gap in knowledge of this system stems from the fact that no studies have actually tested these models

using pharmacology that blocks specific inhibitory receptors. That is one of the primary functions of our study of alpha cells: to use a pharmacological approach to test how feedback inhibition affects the temporal tuning and response kinetics of alpha cells, and to determine whether these changes reflect predictions made from these modeling studies.

Indeed, we found that GABAergic feedback from the surround receptive field plays an important role in shifting temporal tuning to higher frequencies, and speeding up response kinetics. The delayed GABAergic feedback that we observed in t-OFF α cells resembles that identified using modeling by Cui et al. (2016) in ON alpha ganglion cells. Moreover, Cui et al. localized this inhibition to the surround receptive field, similar to the wide-field Na_V-dependent GABAergic feedback identified in our study. However, contrary to their model, our data requires some additional mechanism to account for every aspect of contrast adaptation, since neither GABAR blockade nor Na_V blockade was able to prevent a reduction in gain with increasing contrast (Figure 4.7). In accordance with a suggestion made by Cui et al. (2016), intrinsic mechanisms such as synaptic depression (Jarsky et al., 2011) may play a larger role in producing contrast adaptation in cells that receive lower rates of tonic glutamate release than the ON alpha ganglion cells used in their study. In summary, the work in Chapter 4 is important step towards relating the numerous computational models of contrast gain control and temporal tuning back to a biophysical mechanism.

Mechanisms generating temporal tuning in the retina

Beyond the series of papers on X and Y cells discussed above, more recent studies of temporal tuning have focused on bipolar cells rather than ganglion cells. DeVries (2000) and Puthussery et al. (2014) described how the expression of different types of dendritic glutamate receptors and

their auxiliary proteins can change the kinetics of bipolar cell responses. The expression of voltage-gated sodium channels can cause further kinetic regulation by selectively boosting transient signals in bipolar cells (Ichinose et al., 2005; Puthussery et al., 2013). Moreover, it has been routinely observed that blocking GABARs can make ganglion cell EPSCs and spiking responses more sustained, suggesting that GABAergic inhibition plays a role in shaping bipolar cell kinetics (Caldwell and Daw, 1978b; Dong and Werblin, 1998; Flores-Herr et al., 2001). These types of studies are useful for identifying the set of mechanisms that alter bipolar cell response kinetics, but it is unclear how kinetic properties generalize to temporal tuning. Perhaps most relevant to our study, Ichinose et al. (2014) showed that the temporal tuning of bipolar cells in the mouse retina are diverse, but they didn't explore the underlying mechanisms. Decades of work suggests that the dominant mechanism is wide-field inhibitory feedback, since wide-field stimulation shifts ganglion cell temporal tuning to higher frequencies (Shapley and Victor, 1978), and without wide-field stimulation bipolar cell responses have more homogeneous temporal properties (Franke et al., 2017).

Our work builds upon these studies by providing the much needed pharmacological evidence for the mechanisms that shape temporal tuning in the presynaptic bipolar cells. In doing so, we found that GABAergic feedback contributes to temporal tuning in a more complex way than previously appreciated. For instance, although both local and wide-field GABAergic feedback contribute to temporal tuning, wide-field Na_V-dependent GABAergic feedback is only active at higher contrasts, whereas local Na_V-independent GABAergic feedback is more active at lower contrasts. At high contrast, GABAergic feedback also switches from suppressing the excitatory response to potentiating it as temporal frequency rises. This phenomenon still may occur at low

contrast, although it is less apparent, suggesting that it originates from wide-field, Na_V-dependent GABAergic feedback.

Feedback is not the only synaptic mechanism that shapes ganglion cell temporal tuning. In local edge detector (LED) ganglion cells, for instance, direct feedforward inhibition onto the ganglion cell plays a larger role. LEDs are sustained neurons, and are temporally tuned to low frequencies; they don't fire spikes to visual inputs that are modulated faster than 1 Hz (van Wyk et al., 2006). Their low-pass temporal properties are formed by both excitatory and inhibitory inputs. The excitatory inputs are tuned to low frequencies, whereas the direct glycinergic inhibitory inputs are tuned to higher frequencies (Venkataramani et al., 2014). This comes in contrast to t-OFF α cells, whose excitatory inputs are tuned to high frequencies. Since t-OFF α cells receive direct glycinergic inhibition, it will be interesting to determine how inhibition contributes to temporal tuning. Although the excitatory inputs closely resemble the spiking response (Figure 4.1), there still may be a role for feedforward inhibition in maintaining temporal tuning.

Ambiguities in pharmacological data

The study in Chapter 4 relies on pharmacology to dissect the different circuit components that contribute to temporal tuning. Most of the experiments involved the sequential application of a Na_V channel blocker and GABAR antagonists, in either order. Forward and reverse drug applications resolve some ambiguities in the data. For instance, Na_V activity may be present in both bipolar cells and GABAergic amacrine cells. By measuring how TTX affects the EPSCs both before and after GABAR blockade, we can narrow down the true source of sodium channel activity. Some ambiguities remain, however, since blocking GABARs could depolarize the

presynaptic bipolar cells and inactivate populations of Na_V channels that reside therein. This is a possibility, since we observed increased spontaneous EPSCs while washing in the GABAR antagonists, suggesting that the presynaptic bipolar cells are more depolarized. However, if the GABAR antagonists are inactivating bipolar-expressed Na_V channels, it will only cause us to underestimate the effect that those channels have in boosting high frequency signals. The fact that after adding the GABAR antagonists, Na_V blockade still significantly reduced the EPSC rising phase and amplitude suggests that it plays a prominent role in temporal tuning.

Sodium channels in horizontal cells

The study in Chapter 4 did not address the possibility that horizontal cells are contributing to temporal tuning. Horizontal cells are inhibitory neurons found in the inner nuclear layer (INL) that receive excitatory input from photoreceptors. Horizontal cells are GABAergic neurons, although they use other mechanisms to provide feedback inhibition to photoreceptors and affect glutamate release to downstream bipolar cells (Kamermans and Sprekreijse, 1999). Importantly, GABAR blockade has no effect on horizontal cell feedback (Thoreson and Burkhardt, 1990). Thus our experiments involving GABAR blockade should only be affecting inner retinal circuits.

There is some evidence in cell culture that rabbit horizontal cells express voltage-gated sodium channels (Löhrke and Hofmann, 1994). Although horizontal cells don't fire action potentials, Na_V could be boosting depolarizing signals, which occur during negative contrast transitions. This could account for the increase in excitatory input that we observed during Na_V blockade. However, this TTX-driven increase in the EPSC was occluded by GABAR blockade. Since GABAR blockade doesn't eliminate horizontal cell feedback, we can conclude that Na_V activity in horizontal cells are unlikely to be suppressing the excitatory input to t-OFF α cells.

Receptive field coupling

Receptive field coupling describes the phenomenon where one property of the visual input affects a ganglion cell's sensitivity to another. Coupling can be an important feature of retinal circuits, because it can optimize a ganglion cell's response to the dominant feature of the visual input. When presented with a spatially broad input, for instance, t-OFF α cells are less interested in fine spatial detail, and instead become more capable of responding to faster temporal modulation. Similarly, in response to a low temporal frequency input, t-OFF α cells are more sensitive to smaller spatial features (Figure 4.4).

Previous studies have attributed spatiotemporal coupling in alpha cells to a temporal delay between excitation and inhibition (Ratliff et al., 1969; Derrington and Lennie, 1982; Enroth-Cugell et al., 1983; Dawis et al., 1984; Frishman et al., 1987). Similar conclusions have been drawn from studies of parasol ganglion cells (Kaplan and Benardete, 2001). Our work supports this hypothesis, but takes it further by demonstrating not only that spatiotemporal coupling is present in the excitatory input (previous studies only recorded spiking responses), but that it can be significantly reduced by blocking GABARs (Figure 4.4). Moreover, the temporal delay between excitation and GABAergic feedback inhibition that we identified (~20 ms) is similar to that calculated in previous studies. Two important conclusions can be drawn from our data: GABAergic inhibition contributes to spatiotemporal coupling, and that inhibition is localized to the presynaptic bipolar cells. Although others have produced models where feedback inhibition contributes to spatiotemporal coupling (Enroth-Cugell et al., 1983; Dawis et al., 1984; Frishman et al., 1987), ours is the first study to pharmacologically demonstrate it.

Besides spatiotemporal coupling, one of the first descriptions of receptive field coupling comes from color-opponent ganglion cells of the primate retina. In 1979, Gouras and Zrenner showed that midget ganglion cells lose their color-opponent receptive fields in response to visual inputs with higher temporal frequencies. As in our study, they hypothesized that a temporal delay between the spectrally different center and surround causes red-green color opponency to weaken at high temporal frequencies, since the excitatory (red) and inhibitory (green) inputs fall out of phase. Barring any compensatory mechanisms, any retinal circuit that has inhibitory inputs that are delayed relative to the excitatory inputs should exhibit some level of temporal dependence.

However, a recent study of the direction selective circuit indicates that temporal coupling may not be a general property of ganglion cells. Not only are DSGCs not spatiotemporally coupled, but the spatial frequency of the stimulus had no bearing on the directional response (Hoggarth et al., 2015). This may be because directional tuning and spatial tuning are accomplished by inhibitory inputs from two separate populations of amacrine cells. Starburst amacrine cells handle directional information by inhibiting DSGC dendrites, while wide-field amacrine cells handle broad spatial information by inhibiting the presynaptic bipolar cells. Receptive field properties that are coupled may suggest that both properties are controlled by the same population of amacrine cells, or that the inhibition acts on the same synaptic site.

Similar to the spatial properties, the temporal frequency or speed of a moving object doesn't affect direction selectivity (Sivyer et al., 2010; Nowak et al., 2011). It is possible that higher temporal frequencies are needed to reveal coupling, or that the stimulus did not properly engage the surround receptive field. Wide-field stimulation, and not just low spatial frequency

stimulation, may be necessary to reveal spatiotemporal coupling, since GABAergic inhibition from the surround receptive field is likely involved (Figure 4.4). However, since the surround receptive field is so strong in ON-OFF DSGCs, and responses to wide-field stimuli are mostly absent, it is possible that any temporal coupling that might otherwise be apparent is masked. Finally, the result in Chapter 4, that blocking the ON pathway reveals directional-temporal coupling in ON-OFF DSGCs, suggests that future research of temporal coupling in the direction selective circuit is merited.

Complexity of retinal circuits

The study presented in Chapter 4, along with the series of experiments investigating the spatial properties of t-OFF α cells (Figure 4.16), demonstrate the complexity of retinal circuits, and the difficulty in speculating as to what a ganglion cell's 'function' is. Although others have used alpha ganglion cells as model cell types for studies of nonlinear spatial summation, we show that under certain visual conditions (low temporal frequency, and intermediate spatial frequency), t-OFF α cells employ linear spatial summation. It is unclear what effect linear summation has on the overall function of t-OFF α cells. However, the data support the notion that fully understanding a circuit requires exploring a very large region of stimulus space. Certain circuit elements, due to their receptive field properties, will be invisible in response to certain visual stimuli, and their contributions to a ganglion cell's light response will go unnoticed. For instance, in our experiments in Chapter 4, the crossover input that linearizes the spatial summation is not apparent because our stimulus is a uniform spot, and does not drive positive and negative contrast signals simultaneously. If we were to repeat experiments using a contrast reversing grating at different spatial frequencies, our results would undoubtedly be affected. Thus, it is

important to note that our data is only applicable when considering t-OFF α cell responses to low spatial frequency inputs. It is clear that bipolar cells receive multiple inhibitory inputs from different cell types. Since each input has its own receptive field properties, the collective impact of these inputs on a ganglion cell's function is difficult to reveal.

Concluding remarks and contributions to the field

To conclude, this dissertation presents data from an orientation selective amacrine cell and a ganglion cell that is selective for high temporal frequency inputs. Using electrophysiological and pharmacological techniques, we mapped different aspects of each neuron's presynaptic circuitry. By using visual stimuli with different attributes—such as orientation, contrast, and spatiotemporal frequency—we were able to determine how specific presynaptic circuit elements contribute to the emergent feature selectivities of the neurons. These studies are important steps forward in their respective subfields.

The study in Chapter 3 was the first comprehensive functional analysis of the presynaptic circuit of a wide-field, polyaxonal amacrine cell in any retina. This is an important step towards understanding how the many different types of amacrine cells in the retina handle visual information. Along with its possible role in mediating orientation selectivity in ganglion cells, polyaxonal amacrine cells have been implicated in mediating surround inhibition in general. Thus, our study provides important insight into the workings of one of the most well-established circuit functions in the retina.

The study in Chapter 4 was the first pharmacological analysis of temporal tuning in alpha ganglion cells. As mentioned earlier, modeling studies have predicted the types of circuit elements we might expect to be influencing temporal tuning in alpha cells, but ours is the first

study to specifically show how the temporal properties of excitation from bipolar cells are affected by blocking GABAergic feedback. This study identified multiple instances of feedback inhibition that influence temporal tuning and kinetics, and suggests that Na_V activity in the presynaptic bipolar cells may contribute as well. One of the more important findings in the study is that these multiple inputs have different receptive field properties, and thus are active for different visual conditions. Thus, this study is an important demonstration of how multiple circuit elements come together to maintain feature selectivity over a wide range of visual conditions.

Future Directions

The experiments described in this dissertation suggest several avenues of future research. First, as more amacrine cell types are identified and characterized, a major challenge for researchers will be to identify the postsynaptic partners. This is especially challenging for studies of wide-field amacrine cells, whose postsynaptic partners may be very far away, making paired recordings extremely difficult and impractical. Some groups have approached this problem by using multi-electrode arrays, which can record spiking activity from many ganglion cell types at once. By injecting current into a single cell of choice, changes in ganglion cell spiking activity can be observed through the array recording, and some connectivity can be deduced. Instead of using an electrode array, similar experiments can be done by imaging the fluorescence of genetically encoded calcium indicators in large populations of ganglion cells. As calcium and voltage imaging become more common techniques in retinal physiology labs, it will be interesting to see what circuit connectivity can be uncovered.

In Chapter 4, we studied how the excitatory inputs to t-OFF α cells acquire their temporal tuning. Our study made no attempt to study how the direct inhibitory inputs contribute to

temporal tuning. Since spiking can be driven by strong glycinergic disinhibition in OFF alpha cells (Manookin et al., 2008), especially at low contrast, it is possible that inhibition also helps maintain temporal tuning. If so, is the temporal tuning of excitation and inhibition the same? If inhibition is tuned to lower temporal frequencies than excitation, it could bias t-OFF α cell spiking responses to higher temporal frequencies. This is a feasible mechanism, since the spiking responses were tuned to slightly higher frequencies than the excitatory input, suggesting that inhibition may play a supportive role in temporal tuning.

Our experiments investigating the role of phase-delayed GABAergic inhibition in receptive field coupling have kindled my interest in understanding how retinal circuits can change their function under different visual conditions. For instance, center-surround organization is one of the most well-recognized circuit arrangements in the retina, but its conventional function is inactive under certain visual conditions, such as low background luminance or high temporal frequencies. Further studies on circuits that change functionality depending on the properties of the visual input will help us understand the full breadth of their role in visual processing.

One of my major interests going forward is understanding how excitatory and inhibitory inputs are integrated in a neuron, how those inputs are compartmentalized, and how that effects the neuron's output. Bipolar cells are obvious targets for this type of work, since they receive both excitatory and inhibitory inputs, and provide output to ganglion cells with diverse functionality. Since there are many more functional types of ganglion and amacrine cells than bipolar cells, it is interesting to consider whether or not single bipolar cell types multiplex, or provide differential output to their postsynaptic neurons (Asari and Meister, 2012, 2014). For instance, in Chapter 4 we found that inhibitory feedback is important for shifting temporal tuning

of a ganglion cell's excitatory input (i.e. from bipolar cells) to higher frequencies. Does inhibition only affect the temporal tuning of glutamatergic output from the terminal boutons that receive inhibition? This hypothesis requires that individual boutons in a single bipolar cell are electrically isolated, and that the boutons receive differential inhibition. Studies involving calcium and voltage imaging of the terminal boutons in single bipolar cells could be a way to test this hypothesis. Calcium imaging is a good indicator for synaptic output at each terminal, whereas voltage imaging allows more insight into the interplay of excitation and inhibition at each terminal. Indeed, 2-photon imaging is a powerful tool for investigating neural activity over large populations of neurons as well as in small regions of interest in single neurons, and will be critical for understanding the subtleties of neural circuit function.

REFERENCES

Antinucci, P., Suleyman, O., Monfries, C., and Hindges, R. (2016). Neural Mechanisms Generating Orientation Selectivity in the Retina. Current Biology *26*, 1-14.

Ariel, M., and Daw, N.W. (1982). Pharmacological analysis of directionally sensitive rabbit retinal ganglion cells. J. Physiol. *324*, 161–185.

Asari, H., and Meister, M. (2012). Divergence of visual channels in the inner retina. Nat. Neurosci. *15*, 1581-1589.

Asari, H., and Meister, M. (2014). The Projective Field of Retinal Bipolar Cells and Its Modulation by Visual Context. Neuron *81*, 641-652.

Awatramani, G.B., and Slaughter, M.M. (2000). Origin of Transient and Sustained Responses in Ganglion Cells of the Retina. J Neurosci. *20*, 7087–7095.

Babai, N., and Thoreson, W.B. (2009). Horizontal cell feedback regulates calcium currents and intracellular calcium levels in rod photoreceptors of salamander and mouse retina. J. Physiol. *587*, 2353-64.

Baccus, S., Ölveczky, B.P., Manu, M., Meister, M. (2008). A retinal circuit that computes object motion. J. Neurosci. *28*, 6807–17.

Baccus, S.A., and Meister, M. (2002). Fast and Slow Adaptation in Retinal Circuitry. Neuron *36*, 909-919.

Baden, T., Berens, P., Franke, K., Román Rosón, M., Bethge, M., Euler, T., (2016). The functional diversity of retinal ganglion cells in the mouse. Nature *529*, 345–50.

Baden, T., Nikolaev, A., Esposti, F., Dreosti, E., Odermatt, B., and Lagnado, L. (2014). A Synaptic Mechanism for Temporal Filtering of Visual Signals. PLoS Biol. *12*, 1-16.

Barlow, H.B., Hill, R.M., and Levick, W.R. (1964). Retinal Ganglion Cells Responding Selectively to Direction and Speed of Image Motion in the Rabbit. J. Physiol. *173*, 377-407.

Benardete, E.A., and Kaplan, E. (1997). The receptive field of the primate P retinal ganglion cell, I: Linear dynamics. Vis. Neurosci. *14*, 169–185.

Benardete, E.A., and Kaplan, E. (1999). The dynamics of primate M retinal ganglion cells. Vis. Neurosci. *16*, 355–368.

Berntson, A., and Taylor, W.R (2000). Response characteristics and receptive field widths of on-bipolar cells in the mouse retina. J. Physiol. *524*, 879-889.

Bieda, M.C., and Copenhagen, D.R. (1999). Sodium action potentials are not required for light-evoked release of GABA or glycine from retinal amacrine cells. J. Neurophysiol. *81*, 3092–3095.

Bloomfield, S.A., Völgyi, B. (2009). The diverse functional roles and regulation of neuronal gap junctions in the retina. Nature Reviews Neuroscience *10*, 495-506.

Bloomfield, S. (1994). Orientation-Sensitive Amacrine and Ganglion Cells in the Rabbit Retina. J. Neurophysiol. *71*, 1672–91.

Bloomfield, S.A., and Xin D. (2000). Surround Inhibition of mammalian AII amacrine cells is generated in the proximal retina. J. Physiol. *523*, 771-783.

Boos, R., Schneider, H., and Wässle, H. (1993). Voltage- and transmitter-gated currents of all-amacrine cells in a slice preparation of the rat retina. J Neurosci *13*, 2874–2888.

Boycott, B.B., and Wässle, H. (1974). The Morphological Types of Ganglion Cells of the Domestic Cat's Retina. J. Physiol. *240*, 397-419.

Brigmann, K.L., Helmstaedter, M., and Denk, W. (2011). Wiring specificity in the direction-seelectivity circuit of the retina. Nature *471*, 183-188.

Buldyrev, I., and Taylor, W.R. (2013). Inhibitory mechanisms that generate centre and surround properties in ON and OFF brisk-sustained ganglion cells in the rabbit retina. J. Physiol. *591*, 303–25.

Caldwell, J.H., Daw, N.W., and Wyattt, H.J. (1978). Effects of picrotoxin and strychnine on rabbit retinal ganglion cells: lateral interactions for cells with more complex receptive fields. J. Physiol. *276*, 277–298.

Caldwell, J.H., and Daw, N.W. (1978). New Properties of Rabbit Retinal Ganglion Cells. J. Physiol. *276*, 257-276.

Capaday, C., and Van Vreeswijk, C. (2006). Direct control of firing rate gain by dendritic shunting inhibition. Journal of Int. Neuroscience *5*, 199-222.

Chávez, A.E., Grimes, W.N., and Diamond, J.S. (2010). Mechanisms Underlying Lateral GABAergic Feedback onto Rod Bipolar Cells in Rat Retina. J. Neurosci. 30, 2330-2339.

Chen, X., Hsueh, H.A., and Werblin, F.S. (2011). Amacrine-to-amacrine cell inhibition: Spatiotemporal properties of GABA and glycine pathways. Visual Neuroscience *28*, 193-204.

Chun, M.H., and Wässle, H. (1989). GABA-like Immunoreactivity in the Cat Retina: Electron Microscopy. J. Comp. Neuro. 279:55-67.

Cleland, B.G., Dubin, M.W., and Levick, W.R. (1971). Sustained and Transient Neurones in the Cat's Retina and Lateral Geniculate Nucleus. J. Physiol. 217, 473-496.

Cook, P.B., and McReynolds, J.S. (1998). Lateral inhibition in the inner retina is important for spatial tuning of ganglion cells. Nat. Neurosci. 1, 714–719.

Crook, J.D., Peterson, B.B., Packer, O.S., Robinson, F.R., Troy, J.B., and Dacey, D.M. (2008). Y-Cell Receptive Field and Collicular Projection of Parasol Ganglion Cells in Macaque Monkey Retina. J. Neurosci. 28, 11277-11291.

Cui, Y., Yanbin, W. V, Park, S.J.H., Demb, J., and Butts, D.A. (2016). Divisive suppression explains high-precision firing and contrast adaptation in retinal ganglion. eLife *5*, e19460.

Dacey, D. (1989). Axon-Bearing Amacrine Cells of the Macaque Monkey Retina. J. Comp. Neuro. *284*, 275-93.

Dacey, D. (2004). Origins of perception: retinal ganglion cell diversity and the creation of parallel visual pathways. In: The cognitive neurosciences (Gazzaniga, M., ed.), pp 281-301. Cambridge, MA: MIT.

Dacey, D., Packer, O.S., Diller, L., Brainard, D., Peterson, B., and Lee, B. (2000). Center surround receptive field structure of cone bipolar cells in primate retina. Vision Research *40*, 1801-11.

Davenport, C.M., Detwiler, P.B., and Dacey D.M. (2008). Effects of pH Buffering on Horizontal and Ganglion Cell Light Responses in Primate Retina: Evidence for the Proton Hypothesis of Surround Formation. J. Neurosci. *28*, 456-464.

Dawis, S., Shapley, R., Kaplan, E., and Tranchina, D. (1984). The Receptive Field Organization of X-Cells in the Cat: Spatiotemporal Coupling and Asymmetry. Vision Res. 24, 549-564.

Demb, J.B. (2007). Cellular Mechanisms for Direction Selectivity in the Retina. Neuron *55*, 179-186.

Demb, J.B., Zaghloul, K.A., Haarsma, L., and Sterling, P. (2001). Bipolar cells contribute to nonlinear spatial summation in the brisk-transient (Y) ganglion cell in mammalian retina. J. Neurosci. 21, 7447–7454.

Derrington, A.M., Lennie, P., and Wright, M.J. (1979). The mechanism of peripherally evoked responses in retinal ganglion cells. J. Physiol. *289*, 299-310.

Derrington, A.M., and Lennie, P. (1982). The influence of temporal frequency and adaptation level on receptive field organization of retinal ganglion cells in cat. J. Physiol. 333, 343-366.

DeVries, S.H., Qi, X., Smith, R., Makous, W., and Sterling, P. (2002). Electrical Coupling between Mammalian Cones. Current Biology *12*, 1900-07.

DeVries, S.H. (2000). Bipolar cells use kainate and AMPA receptors to filter visual information into separate channels. Neuron 28, 847–856.

Ding, H., Smith, R.G., Poleg-Polsky, A., and Diamond, J.S. (2016). Species-specific wiring for direction selectivity in the mammalian retina. Nature *0*, 1-6.

Dong, C.-J., and Werblin, F.S. (1998). Temporal Contrast Enhancement via GABA C Feedback at Bipolar Terminals in the Tiger Salamander Retina. J. Neurophysiol. 79, 2171–2180.

Dowling, J.E. (1968). Synaptic Organization of the Frog Retina: An Electron Microscopic Analysis Comparing the Retinas of Frogs and Primates. Proc. R. Soc. Longd. *170*, 205-228.

Dowling, J.E., and Boycott, B.B. (1966). Organization of the Primate Retina: Electron Microscopy. Proc. R. Soc. Lond. *166*, 80-111.

Eggers, E.D., and Lukasiewicz, P.D. (2006). Receptor and Transmitter Release Properties Set the Time Course of Retinal Inhibition. J. Neurosci. *26*, 9413-25.

Eggers, E.D., and Lukasiewicz, P.D. (2010). Interneuron Circuits Tune Inhibition in Retinal Bipolar Cells. J. Neurophysiol. *103*, 25-37.

Eggers, E.D., Lukasiewicz, P.D. (2011). Multiple pathways of inhibition shape bipolar cell responses in the retina. Visual Neuroscience *28*, 95-108.

Eggers, E.D., McCall, M.A., and Lukasiewicz, P.D. (2007). Presynaptic inhibition differentially shapes transmission in distinct circuits in the mouse retina. J. Physiol. *582*, 569–582.

Enroth-Cugell, C., and Robson, J.G. (1966). The contrast sensitivity of retinal ganglion cells of the cat. J. Physiol. *187*, 517-52.

Enroth-Cugell, C., and Freeman, A.W. (1987). The receptive field spatial structure of cat retinal Y cells. J. Physiol. *384*, 49-79.

Enroth-Cugell, C., Robson, J.G., Schweitzer-Tong, D.E., and Watson, A.B. (1983). Spatiotemporal interactions in cat retinal ganglion cells showing linear spatial summation. J. Physiol. *341*, 279-307.

Euler, T., and Wässle, H. (1998). Different Contributions of GABAA and GABAC Receptors to Rod and Cone Bipolar Cells in a Rat Retinal Slice Preparation. J. Neurophys. 79, 1384-1395.

Euler, T., Detwiler, P.B., and Denk, W. (2002). Directionally selective calcium signals in dendrites of starburst amacrine cells. Nature *418*, 845-852.

Famiglietti, E.V. (1981) Functional Architecture of Cone Bipolar Cells in Mammalian Retina. Vision Research *21*, 1559-63.

Famiglietti, E.V. (1991). Synaptic Organization of Starburst Amacrine Cells in Rabbit Retina: Analysis of Serial Thin Sections by Electron Microscopy and Graphic Representation. J. Comp. Neuro. *309*, 40-70.

Famiglietti, E.V. (1992a). Polyaxonal amacrine cells of rabbit retina: morphology and stratification of PA1 cells. J. Comp. Neuro. *316*, 391–405.

Famiglietti, E.V. (1992b). Polyaxonal amacrine cells of rabbit retina: size and distribution of PA1 cells. J. Comp. Neuro. *316*, 406–21.

Famiglietti, E.V. (1992c). Polyaxonal amacrine cells of rabbit retina: PA2, PA3, and PA4 cells. Light and electron microscopic studies with a functional interpretation. J. Comp. Neuro. *316*, 422–46.

Feigenspan, A., Wässle, H., and Bormann, J. (1993). Pharmacology of GABA receptor Cl- channels in rat retinal bipolar cells. Nature *361*, 159-161.

Flores-Herr, N., Protti, D.A., and Wässle, H. (2001). Synaptic currents generating the inhibitory surround of ganglion cells in the mammalian retina. J. Neurosci. 21, 4852–4863.

Franke, K., Berens, P., Schubert, T., Bethge, M., Euler, T., and Baden, T. (2017). Inhibition decorrelates visual feature representations in the inner retina. Nature *0*, 1-6.

Frishman, L.J., Freeman, A.W., Troy, J.B., Schweitzer-Tong, D.E., and Enroth-Cugell, C. (1987). Spatiotemporal Frequency Responses of Cat Retinal Ganglion Cells. J. Gen. Physiol. 89, 599-628.

Galizia, C.G., and Rössler, W. (2010). Parallel olfactory systems in insects: anatomy and function. Annual Review of Entomology 55, 399–420.

Gouras, P., and Zrenner, E. (2016). Enchancement of Luminance Flicker by Color-Opponent Mechanisms. Science 205, 587–589.

Greene, M.J., Kim, J.S., Seung, H.S., and the EyeWirers (2016). Analogous Convergence of Sustained and Transient Inputs in Parallel On and Off Pathways for Retinal Motion Computation. Cell Reports *14*, 1892-1900.

Greschner, M., Field, G.D., Li, P.H., Schiff, M.L., Gauthier, J.L., Ahn, D., Sher, A., Litke, A.M., and Chichilnisky, E.J. (2014). A polyaxonal amacrine cell population in the primate retina. J. Neurosci. *34*, 3597–606.

Grimes, W.N., Schwartz, G.W., and Rieke, F. (2014). The Synaptic and Circuit Mechanisms Underlying a Change in Spatial Encoding in the Retina. Neuron *82*, 460-473.

Grimes, W.N., Zhang, J., Graydon, C.W., Kachar, B., and Diamond, J.S. (2010). Retinal Parallel Processors: More than 100 Independent Microcircuits Operate within a Single Interneuron. Neuron *65*, 873-885.

Grünert, U., and Wässle, H. (1996). Glycine receptors in the rod pathway of the macaque monkey retina. Visual Neuroscience *13*, 101–115.

Hartveit, E. (1999). Reciprocal synaptic interactions between rod bipolar cells and amacrine cells in the rat retina. J. Neurophysiol. *81*, 2923–2936.

Hochstein, S., and Shapley, R.M. (1976). The linear and nonlinear spatial subunits in Y cat retinal ganglion cells. J. Physiol. *262*, 265-84.

Hoggarth, A., McLaughlin, A.J., Ronellenfitch, K., Trenholm, S., Vasandani, R., Sethuramanujam, S., Schwab, D., Briggman, K.L., and Awatramani, G.B. (2015). Specific Wiring of Distinct Amacrine Cells in the Directionally Selective Retinal Circuit Permits Independent Coding of Direction and Size. Neuron *86*, 1-16.

Ichinose, T., and Lukasiewicz, P.D. (2005). Inner and outer retinal pathways both contribute to surround inhibition of salamander ganglion cells. J. Physiol. *565*, 517–35.

Ichinose, T., Shields, C.R., and Lukasiewicz, P.D. (2005). Sodium Channels in Transient Retinal Bipolar Cells Enhance Visual Responses in Ganglion Cells. J. Neurosci. *25*, 1856–1865.

Ichinose, T., Fyk-Kolodziej, B., and Cohn, J. (2014). Roles of ON Cone Bipolar Cell Subtypes in Temporal Coding in the Mouse Retina. J. Neurosci. *34*, 8761-8771.

Isaacson, J.S., and Scanziani, M. (2011). How Inhibition Shapes Cortical Activity. Neuron *72*, 231-243.

Jarsky, T., Cembrowski, M., Logan, S.M., Kath, W.L, Riecke, H., Demb, J.B., and Singer, J.H. (2011). A Synaptic Mechanism for Retinal Adaptation to Luminance and Contrast. J. Neurosci. *31*, 11003-11015.

Kamermans, M., and Spekreijse, H. (1999). The feedback pathway from horizontal cells to cones: A mini review with a look ahead. Vision Research *39*, 2449-2468.

Kamermans, M., Fahrenfort, I., Schultz, K., Janssen-Bienhold, U., Sjoerdsma, T., and Weiler, R. (2001). Hemichannel-Mediated Inhibition in the Outer Retina. Science *292*, 1178-80.

Kaplan, E., and Benardete, E. (2001). The dynamics of primate retinal ganglion cells. Prog. Brain Res. *134*, 17–34.

Kim, K.J., and Rieke, F. (2001). Temporal Contrast Adaptation in the Input and Output Signals of Salamander Retinal Ganglion Cells. J. Neurosci. *21*, 287-299.

Kittila, C., and Massey, S.C. (1997). Pharmacology of directionally selective ganglion cells in the rabbit retina. J. Neurophysiol. *77*, 675-689.

Koontz, M.A., and Hendrickson, A.E. (1990). Distribution of GABA-immunoreactive amacrine cell synapses in the inner plexiform layer of macaque monkey retina. Visual Neuroscience *5*, 17-28.

Kuffler, S.E. (1953). Discharge Patterns and Functional Organization of Mammalian Retina. J. Neurophys. *16*, 37-68.

Lamb, T.D., and Simon, E.J. (1976). The relation between intercellular coupling and electrical noise in turtle photoreceptors. J. Physiol. *263*, 257-286.

Levick, W.R. (1967). Receptive fields and trigger features of ganglion cells in the visual streak of the rabbit's retina. J. Physiol. *188*, 285-307.

Lee, S., Zhou, Z.J. (2006). The Synaptic Mechanism of Direction Selectivity in Distal Processes of Starburst Amacrine Cells. Neuron *51*, 787-799.

Li, Z. (1992). Different Retinal Ganglion Cells Have Different Functional Goals. International Journal of Neural Systems *3*, 237-248.

Lin, B., and Masland, R.H. (2006). Populations of Wide-Field Amacrine Cells in the Mouse Retina. J. Comp. Neuro. *499*, 797-809.

Liu, Z.Q. (1991). Scale space approach to directional analysis of images. Applied Optics *30*, 1369-1373.

Löhrke, S., and Hofmann, H-D. (1994). Voltage-gated currents of rabbit A- and B-type horizontal cells in retinal monolayer cultures. Visual Neuroscience *11*, 369-378.

Lukasiewicz, P.D., and Shields, C.R. (1998). Different combinations of GABAA and GABAC receptors confer distinct temporal properties to retinal synaptic responses. J. Neurophysiol. *79*, 3157–3167.

Lukasiewicz, P.D., and Werblin, F.S. (1994). A Novel GABA Receptor Modulates Synaptic Transmission from Bipolar to Ganglion and Amacrine Cells in the Tiger Salamander Retina. J. Neurosci. *14*, 1213-23.

Lukasiewicz, P.D., and Wong, R.O. (1997). GABAC receptors on ferret retinal bipolar cells: A diversity of subtypes in mammals? Visual Neuroscience *14*, 989-94.

Ma, Y.-P., Cui, J., and Pan, Z.-H. (2005). Heterogeneous expression of voltage-dependent Na+ and K+ channels in mammalian retinal bipolar cells. Vis. Neuro. *22*, 119-133.

MacNeil, M.A., Heussy, J.K., Dacheux, R.F., Raviola, E., and Masland, R.H. (2004). The Population of Bipolar Cells in the Rabbit Retina. J. Comp. Neuro. *472*, 73-86.

MacNeil, M.A., Heussy, J.K., Dacheux, R.F., Raviola, E., and Masland, R.H. (1999). The shapes and numbers of amacrine cells: matching of photofilled with Golgi-stained cells in the rabbit retina and comparison with other mammalian species. J. Comp. Neuro., *413*, 305–326.

MacNeil, M.A., and Masland, R.H. (1998). Extreme Diversity among Amacrine Cells: Implications for Function. Neuron *20*, 971-82.

Mangel, S.C. (1991). Analysis of the horizontal cell contribution to the receptive field surround of ganglion cells in the rabbit retina. J. Physiol. *442*, 211–234.

Manookin, M.B., Beaudoin, D.L., Ernst, Z.R., Flagel, L.J., and Demb, J.B. (2008). Disinhibition Combines with Excitation to Extend the Operating Range of the OFF Visual Pathway in Daylight. J. Neurosci. *28*, 4136-4150.

Maple, B.R., and Wu, S.M. (1998). Glycinergic synaptic inputs to bipolar cells in the salamander retina. J. Physiol. *506*, 731-744.

Marc, R.E., and Liu, W.L.S. (2000). Fundamental GABAergic Amacrine Cell Circuitries in the Retina: Nested Feedback, Concatenated Inhibition, and Axosomatic Synapses. J. Comp. Neuro. *425*, 560-82.

Marc, R.E., Anderson, J.R., Jones, B.W., Sigulinsky, C.L., and Lauritzen, J.S. (2014). The AII amacrine cell connectome: a dense network hub. Front. Neural Circuits *8*, 1–13.

McMahon, M.J., Packer, O.S., and Dacey, D.M. (2004). The Classical Receptive Field Surround of Primate Parasol Ganglion Cells Is Mediated Primarily by a Non-GABAergic Pathway. J. Neurosci. *24*, 3736-45.

Menger, N., Pow, D.V., and Wässle, H. (1998). Glycinergic Amacrine Cells of the Rat Retina. J. Comp. Neuro. *401*, 34-46.

Merigan, W.H., Byrne C.E., Maunsell, J.H.R. (1991). Does Primate Motion Perception Depend on the Magnocellular Pathway? J. Neurosci. *11*, 3422-3429.

Mills, S.L., and Massey, S.C. (1992). Morphology of Bipolar Cells Labelled by DAPI in the Rabbit Retina. J. Comp. Neuro. *321*, 133-149.

Mitchell, S.J., and Silver, R.A. (2003). Shunting Inhibition Modulates Neuronal Gain during Synaptic Excitation. Neuron *38*, 433-445.

Molnar, A., Hsueh, H.-A., Roska, B., and Werblin F.S. (2009). Crossover inhibition in the retina: circuitry that compensates for nonlinear rectifying synaptic transmission. J. Comput. Neurosci. *27*, 569-590.

Molnar, A., and Werblin, F.S. (2007). Inhibitory Feedback Shapes Bipolar Cell Responses in the Rabbit Retina. J. Neurophysiol. *98*, 3423–3435.

Murphy, G.J., and Rieke, F. (2006). Network Variability Limits Stimulus-Evoked Spike Timing Precision in Retinal Ganglion Cells. Neuron 52, 511-524.

Murphy-Baum, B.L., and Taylor, W.R. (2015). The Synaptic and Morphological Basis of Orientation Selectivity in a Polyaxonal Amacrine Cell of the Rabbit Retina. J. Neurosci. *35*, 13336–13350.

Myatt, D.R., Hadlington, T., Ascoli, G.A., and Nasuto, S.J. (2012). Neuromantic – from semi-manual to semi-automatic reconstruction of neuron morphology. Frontiers in Neuroinformatics *6*, 1-14.

Nirenberg, S., and Meister, M. (1997). The light response of retinal ganglion cells is truncated by a displaced amacrine circuit. Neuron 18, 637–650.

Nowak, P., Dobbins, A.C., Gawne, T.J., Grzywacz, N.M., and Amthor, F.R. (2011). Separability of stimulus parameter encoding by on-off directionally selective rabbit retinal ganglion cells. J. Neurophysiol. *105*, 2083-2099.

Ohki, K., Chung, S., Ch'ng, Y.H., Kara, P., and Reid, R.C. (2005). Functional imaging with cellular resolution reveals precise micro-architecture in visual cortex. Nature *433*, 597-603.

Ölveczky, B.P., Baccus, S.A., and Meister, M. (2003). Segregation of object and background motion in the retina. Nature *423*, 401–408.

Ölveczky, B.P., Baccus, S.A., Meister, M. (2007). Retinal Adaptation to Object Motion. Neuron *56*, 689-700.

Ozuysal, Y., and Baccus, S.A. (2012). Linking the Computational Structure of Variance Adaptation to Biophysical Mechanisms. Neuron 73, 1002-1015.

Pan, Z.H., and Hu, H.J. (2000). Voltage-dependent Na(+) currents in mammalian retinal cone bipolar cells. J. Neurophysiol. 84, 2564–2571.

Pang, J-J., Gao, F., Wu, S.M. (2003). Light-evoked Excitatory and Inhibitory Synaptic Inputs to ON and OFF α Ganglion Cells in the Mouse Retina. J Neurosci 23, 6063-6073.

Petrusca, D., Grivich, M.I., Sher, A., Field, G.D., Gauthier, J.L., Greschner, M., Shlens, J., Chichilnisky, E.J., and Litke, A.M. (2007). Identification and Characterization of a Y-Like Primate Retinal ganglion Cell Type. J. Neurosci. 27, 11019-11027.

Pourcho, R.G., and Goebel, D.J. (1983). Neuronal subpopulations in cat retina which accumulate the GABA agonist, (3H)muscimol: a combined Golgi and autoradiographic study. J. Comp. Neuro. *219*, 25–35.

Pourcho, R.G., and Goebel, D.J. (1985). A combined Golgi and autoradiographic study of (3H)glycine-accumulating amacrine cells in the cat retina. J. Comp. Neuro. *233*, 473-80.

Pourcho, R.G., and Owczarzak, M.T. (1989). Distribution of GABA immunoreactivity in the cat retina: A light- and electron-microscopic study. Visual Neuroscience *2*, 425-435.

Puller, C., Ivanova, E., Euler, T., Haverkamp, S., and Schubert, T. (2013). OFF bipolar cells express distinct types of dendritic glutamate receptors in the mouse retina. Neuroscience *243*, 136–148.

Puthussery, T., Percival, K.A., Venkataramani, S., Gayet-Primo, J., Grünert, U., Grunert, U., and Taylor, W.R. (2014). Kainate Receptors Mediate Synaptic Input to Transient and Sustained OFF Visual Pathways in Primate Retina. J. Neurosci. *34*, 7611–7621.

Puthussery, T., Venkataramani, S., Gayet-Primo, J., Smith, R.G., and Taylor, W.R. (2013). NaV1.1 channels in axon initial segments of bipolar cells augment input to magnocellular visual pathways in the primate retina. J. Neurosci. *33*, 16045–16059.

Ratliff, F., Knight, B.W., and Graham, N. (1969) On Tuning and Amplification by Lateral Inhibition. PNAS *62*, 733-740.

Ratliff, F., Knight, B.W., Toyoda, J.-I., and Hartline, H.K. (1967). Enhancement of Flicker by Lateral Inhibition. Science *158*, 392–393.

Raviola, E., and Gilula, N.B. (1973). Gap Junctions between Photoreceptor Cells in the Vertebrate Retina. PNAS *70*, 1677-1681.

Saszik, S., and DeVries, S.H. (2012). A mammalian retinal bipolar cell uses both graded changes in membrane voltage and all-or-nothing Na+ spikes to encode light. J. Neurosci. 32, 297–307.

Schindelin, J., Arganda-Carreras, I., Frise, E., Kaynig, V., Longair, M., Pietzsch, T., Preibisch, S., Rueden, C., Saalfeld, S., Schmid, B., Tinevez, J.Y., White, D.J., Hartenstein, V., Eliceiri, K., Tomancak, P., and Cardona, A. (2012). Fiji: an open-source platform for biological-image analysis. Nature Methods *9*, 676-82.

Schreiner, C.E., Read, H.L., and Mitchell S.L. (2000). Modular Organization of Frequency Integration in Primary Auditory Cortex. Annu. Rev. Neurosci. *23*, 501-529.

Schubert, T., Degen, J., Willecke, K., Hormuzdi, S.G., Monyer, H., and Weiler, R. (2005). Connexin36 Mediates Gap Junctional Coupling of Alpha-Ganglion Cells in Mouse Retina. J. Comp. Neurol. *485*, 191–201.

Schwartz, G.W., Okawa, H., Dunn, F.A., Morgan, J.L, Kerschensteiner, D., Wong, R.O., Rieke, F. (2012). The Spatial Structure of a nonlinear receptive field. Nat. Neurosci. *15*, 1572-1580.

Shapley, R.M., and Victor, J.D. (1978). The Effect of Contrast on the Transfer Properties of Cat Retinal Ganglion Cells. J Physiol *285*, 275–298.

Shapley, R.M., and Victor, J.D. (1979a). Nonlinear spatial summation and the contrast gain control of cat retinal ganglion cells. J. Physiol. *290*, 141–161.

Shapley, R.M., and Victor, J.D. (1979b). The contrast gain control of the cat retina. Vision Res. *19*, 431–434.

Shapley, R.M., and Victor, J.D. (1980). The effect of contrast on the non-linear response of the Y cell. J. Physiol. *302*, 535-547.

Shapley, R.M., and Victor, J.D. (1981). How the Contrast Gain Control Modifies the Frequency Responses of Cat Retinal Ganglion Cells. J. Physiol. *318*, 161-179.

Shields, C.R., and Lukasiewicz, P.D. (2003). Spike-dependent GABA inputs to bipolar cell axon terminals contribute to lateral inhibition of retinal ganglion cells. J. Neurophysiol. *89*, 2449–2458.

Shields, C.R., Tran, M.N., Wong, R.O., and Lukasiewicz, P.D. (2000). Distinct ionotropic GABA receptors mediate presynaptic and postsynaptic inhibition in retinal bipolar cells. J. Neurosci. *20*, 2673–82.

Slaughter, M.M., and Miller, R.F. (1981). 2-amino-4-phosphonobutyric acid: a new pharmacological tool for retina research. Science *211*, 182-185.

Smith, R.G., and Vardi, N. (1995). Simulation of the AII amacrine cell of mammalian retina: Functional consequences of electrical coupling and regenerative membrane properties. Visual Neuroscience *12*, 851-860.

Stafford, D.K., and Dacey, D.M. (1997). Physiology of the A1 amacrine: A spiking, axon-bearing interneuron of the macaque monkey retina. Visual Neuroscience *14*, 507-22.

Tamalu, F., and Watanabe, S. (2007). Glutamatergic input is coded by spike frequency at the soma and proximal dendrite of AII amacrine cells in the mouse retina. Eur. J. Neurosci. *25*, 3243–3252.

Taylor, W.R. (1999). TTX attenuates surround inhibition in rabbit retinal ganglion cells. Vis. Neurosci. *16*, 285–290.

Thoreson, W.B., and Burkhardt, D.A. (1990). Effects of synaptic blocking agents on the depolarizing responses of turtle cones evoked by surround illumination. Visual Neuroscience *5*, 571-583.

Tian, M., Jarsky, T., Murphy, G.J., Rieke, F., and Singer, J.H. (2010). Voltage-gated Na channels in AII amacrine cells accelerate scotopic light responses mediated by the rod bipolar cell pathway. J. Neurosci. *30*, 4650–4659.

Tikidji-Hamburyan, A., Reinhard, K., Seitter, H., Hovhannisyan, A., Procyk, C.A., Allen, A.E., Schenk, M., Lucas, R.J., and Münch, T.A. (2015). Retinal output changes qualitatively with every change in ambient illuminance. Nat. Neurosci. *18*, 66-74.

Tomchik, S.M., Berg, S., Kim, J.W., Chaudhari, N., and Roper, S.D. (2007). Breadth of Tuning and Taste Coding in Mammalian Taste Buds. J Neurosci. *27*, 10840–10848.

Trenholm, S., Borowska, J., Zhang, J., Hoggarth, A., Johnson, K., Barnes, S., Lewis, T.J., and Awatramani, G.B. (2012). Intrinsic oscillatory activity arising within the electrically coupled AII amacrine – ON cone bipolar cell network is driven by voltage-gated Na + channels. J. Physiol. *10*, 2501–2517.

Troy, J.B., Einstein, G., Schuurmans, R.P., Robson, J.G., and Enroth-Cugell, C. (1989). Responses to sinusoidal gratings of two types of very nonlinear retinal ganglion cells of cat. Visual Neuroscience *3*, 213-23.

van Wyk, M., Taylor, W.R., and Vaney, D.I. (2006). Local edge detectors: a substrate for fine spatial vision at low temporal frequencies in rabbit retina. J. Neurosci. *26*, 13250–63.

van Wyk, M., Wässle, H., and Taylor, W.R. (2009). Receptive field properties of ON- and OFF-ganglion cells in the mouse retina. Vis. Neurosci. *26*, 297-308.

Vaney, D.I., and Taylor, W.R. (2002). Diverse synaptic mechanisms generate direction selectivity in the rabbit retina. J. Neurosci. *22*, 7712-7720.

Vardi, N., and Smith, R.G. (1996). The AII Amacrine Network: Coupling can Increase Correlated Activity. Vision Research *36*, 3743-3757.

Venkataramani, S., and Taylor, W.R. (2010). Orientation Selectivity in Rabbit Retinal Ganglion Cells Is Mediated by Presynaptic Inhibition. The J. Neurosci. *30*, 15664–76.

Venkataramani, S., van Wyk, M., Buldyrev, I., Sivyer, B., Vaney, D.I., and Taylor, W.R. (2014). Distinct Roles for Inhibition in Spatial and Temporal Tuning of Local Edge Detectors in the Rabbit Retina. PLOS One *9*, e88560.

Venkataramani, S., and Taylor, W.R. (2016). Synaptic Mechanisms Generating Orientation Selectivity in the ON Pathway of the Rabbit Retina. J. Neurosci. *36*, 3336-3349.

Veruki, M.L., and Hartveit, E. (2009). Meclofenamic Acid Blocks Electrical Synapses of Retinal AII Amacrine and ON -Cone Bipolar Cells. J. Neurophysiol. *101*, 2339–2347.

Victor, J.D., and Shapley, J.D. (1988). The Dynamics of the Cat Retinal Y Cell Subunit. J. Physiol. *405*, 289-320.

Vigh, J., Vickers, E., and von Gersdorff, H. (2011). Light-evoked lateral GABAergic inhibition at single bipolar cell synaptic terminals is driven by distinct retinal microcircuits. J. Neurosci. *31*, 15884–93.

Vigh, J., and von Gersdorff, H. (2005). Prolonged Reciprocal Signaling via NMDA and GABA receptors at a Retinal Ribbon Synapse. J. Neurosci. *25*, 11412-11423.

Völgyi, B., Abrams, J., Paul, D.L., and Bloomfield, S.A. (2005). Morphology and tracer coupling pattern of alpha ganglion cells in the mouse retina. J. Comp. Neurol. *492*, 66–77.

Völgyi, B., Xin, D., Amarillo, Y., and Bloomfield, S.A. (2001). Morphology and Physiology of the Polyaxonal Amacrine Cells in the Rabbit Retina. J. Comp. Neuro. *125*, 109–125.

Völgyi, B., Xin, D., Bloomfield, S.A. (2002). Feedback inhibition in the inner plexiform layer underlies the surround-mediated responses of AII amacrine cells in the mammalian retina. J. Physiol. *539*, 603-614.

Wässle, H., Koulen, P., Brandstätter, J.H., Fletcher, E.L., and Becker, C-M. (1998). Glycine and GABA receptors in the mammalian retina. Vision Research *38*, 1411-30.

Wässle, H., Peichl, L., and Boycott, B.B. (1983). A spatial analysis of ON- and OFF-ganglion cells in the cat retina. Vision Research *23*, 1151-1160.

Werblin, F.S. (2010). Six different roles for crossover inhibition in the retina: Correcting the nonlinearities of synaptic transmission. Visual Neuroscience *27*, 1–8.

Winters, R.W., and Hamasaki, D.I. (1976). Temporal Characteristics of Peripheral Inhibition of Sustained and Transient Ganglion Cells in Cat Retina. Vision Research *16*, 37-45.

Wright, L.L., Vaney, D.I. (2004). The type 1 polyaxonal amacrine cells of the rabbit retina: A tracer coupling study. Visual Neuroscience *21*, 145-155.

Xin, D., and Bloomfield, S.A. (1997). Tracer Coupling Pattern of Amacrine and Ganglion Cells in the Rabbit Retina. J. Comp. Neurol. *528*, 512–528.

Zaghloul, K.A., Boahen, K., and Demb, J.B. (2005). Contrast Adaptation in Subthreshold and Spiking Responses of Mammalian Y-Type Retinal Ganglion Cells. J. Neurosci. *25*, 860–868.

Zenisek, D., Henry, D., Studhome, K., Yazulla, S., and Matthews, G. (2001). Voltage-dependent Sodium Channels Are Expressed in Nonspiking Retinal Bipolar Neurons. J. Neurosci. *21*, 4543-4550.

Zhang, J., Jung, C.S., and Slaughter, M.M. (1997). Serial inhibitory synapses in retina. Visual Neuroscience *14*, 553-63.

Zhang, J., and Slaughter, M.M. (1995). Preferential Suppression of the ON Pathway by GABAC Receptors in the Amphibian Retina. J. Neurophysiol. *74*, 1583-92.

Zhao, X., Chen, H., Liu, X., and Cang, J. (2013). Orientation-selective responses in the mouse lateral geniculate nucleus. J. Neurosci. *33*, 12751–12763.